SURFACE MODIFICATION OF INNER WALLS OF POLYETHYLENE TUBING GENERATED BY DIELECTRIC BARRIER DISCHARGE PLASMAS

by

Lee Organski

A Thesis

Submitted to the Faculty of Purdue University

In Partial Fulfillment of the Requirements for the degree of

Master of Science in Aeronautics and Astronautics

School of Aeronautics and Astronautics

West Lafayette, Indiana

July 2021

THE PURDUE UNIVERSITY GRADUATE SCHOOL
STATEMENT OF COMMITTEE APPROVAL

Dr. Alexey Shashurin, Chair
School of Aeronautics and Astronautics

Dr. Yoon Yeo
School of Pharmacy

Dr. Alina Alexeenko
School of Aeronautics and Astronautics

Dr. Coralie Richard
Eli Lilly & Co

Approved by:
Dr. Gregory A. Blaisdell

Dedicated to my wife, Anna, who pushes me to be better than I ever hoped to be.

ACKNOWLEDGMENTS

Being of predominant importance in my success and development as a graduate researcher. Both in the classroom and in the lab, Dr. Alexey Shashurin has been a deeply involved and dedicated advisor and teacher, working hard to introduce physical principles while always grounding scientific work in practical applications. I am very grateful to him for his dedication to my development in his lab and look forward to growing further under his advisement as I continue in my doctoral education.

I would also like to thank my thesis committee members, Dr. Yeo Yoon, Dr. Alina Alexeenko, and Dr. Coralie Richard, for their time and commitment to my thesis work, and continued involvement in the progression of my research. I would further like to thank Dr. Kinam Park, Dr. Hugh Lee, and Dr. Sarena Horava for the opportunity to work and collaborate with them on my project and the broader work related to it.

I would like to acknowledge the help and friendship shared by fellow graduate students in APPL, including Xingxing Wang and Andrew Myers, who have been directly involved in my research and have provided a great deal of assistance throughout my thesis work, as well as Adam Patel, Glynn Smith, Apoorv Ranjan, and Yunping Zhang, who have all contributed to my development as a researcher. I would also like to thank Xingtao Liu and Dr. Rosa Diaz for their assistance with me in learning microscopy techniques in SEM, EDX and FIB.

Further, I would like to thank Dr. Alexey Shashurin, Dr. Sally Bane, Purdue University, NSF, and Eli Lilly & Co. for providing support in my education through the provision of research assistant and teaching assistant positions. The opportunities have been highly educational both academically and professionally.

TABLE OF CONTENTS

LIST OF TABLES

LIST OF FIGURES

ABSTRACT

Plasma treatment of polymers has been a rapidly growing area of research due to its broad applications, homogenous and repeatable surface properties, low cost, and environmental friendliness when compared to alternative techniques. Only recently have significant developments been made in the application of atmospheric pressure plasma in polymer surface treatment. The use of atmospheric pressure plasma enables further reductions in cost and mechanical complexity. Of particular interest in this work is the application of atmospheric pressure plasma for the isolated modification of the inner surfaces of small diameter polymer tubing to improve the wetting and adhesion characteristics compared to untreated polymer.

This work focuses on the development, characterization, and implementation of an atmospheric pressure dielectric barrier discharge (DBD) plasma apparatus for the treatment of the inner surface of polymer tubes. The iterative process of the development of this system is detailed, with two finalized designs established and defined. These two designs are then applied to low density polyethylene (LDPE) tubing of $0.38\,mm$ inner diameter (ID), and characteristics for surface morphology and wettability are analyzed.

Investigation of the relationship between plasma power and treatment time with morphology characteristics of protrusion density and size and surface roughness parameter, R_a is presented. Treatment times of 5, 10, 15, 30 and 45 minutes are performed on tubing samples at a power level of $35\,mW$. From 5 to 15 minutes, protusion density increases rapidly, from $n_p = 4 * 10^4 - 10^7\,\frac{protrusions}{mm^2}$, and small variation in protrusion size, with $0.1 < A_p < 0.2\,\mu m^2$. At treatment times of 30 and 45 minutes, coalescence of protrusions was observed, resulting in a decrease in protrusion density, down to $n \approx 4 * 10^4\,\frac{protrusions}{mm^2}$, and substantial increases in mean

protrusion size, up to $A_P = 5 - 9\ \mu m^2$. Plasma powers of 9, 12, 16, 25, 35, and 45 mW were also investigated, at a treatment time of 15 minutes. As power level was increased, protrusion density was observed to increase, with an inverse relationship with mean protrusion size. Protrusion density was observed to increase from $n_p = 2 * 10^5 - 10^7 \frac{protrusion}{mm^2}$, with diminishing increases in density observed between power levels of 35 and 45 mW. Protrusion mean size was observed to decrease from $A_p = .25 - 0.025\ \mu m^2$, with similar diminishing reductions observed at 35 and 45 mW. Surface roughness, R_a, was observed to vary from $.01 - 0.3\ \mu m$, or ISO roughness grades N1 to N5, in the treated samples.

Wettability characteristics were measured and characterized relative to plasma power and linear feed rate. Wettability was measured by measurement of contact angles of the meniscus formed from water introduced into the tubing volume by capillary action. On all samples treated, a duality of mechanisms for surface wetting were observed. After initial treatment, samples were observed to have a lower contact angle, indicating higher wettability, but after 12 hours samples were observed to have reduced wetting characteristics, indicating a transient mechanism for surface wetting in addition to permanent effects induced my surface morphology. Samples were treated at plasma powers of 7, 10, 15, 20, and 40 mW. At all power levels, initial contact angle was generally consistent, with $20^o < \theta_0 < 30^o$. Permanent wetting features measured on these samples indicated almost complete reversing of wettability at 7 and 10 mW, with θ_{SS} measured at $\sim 75^o$, comparable to the average measurement of an untreated sample of $\sim 80^o$. Conversely, at higher powers of 15, 20 and 40 mW, significant retention of wettability was observed, with $45^o < \theta_{SS} < 55^o$ for those samples.

1. INTRODUCTION

1.1 Importance of Surface Modification

Often, in industry, surface properties of a material with desirable bulk properties are ill-suited for specific applications. The scope of applications of surface modification span a huge cross-section of industries. Novel machining techniques using electrical discharge machining have been applied to develop methods for machining metal components in ways that traditional practices cannot achieve, as well as applying specialized surface treatments, enhancing desirable characteristics of the surface for specific applications [1]. Titanium components designed for implantation in human tissue have seen varied surface modification techniques intended to inhibit the formation of biofilms that can promote bacterial growth leading to infections and potential implant failures [2]. Various techniques of surface modification have been applied to natural fibers to inhibit their natural qualities of absorptivity and enhance their adhesive properties as replacements for artificially-produced fibers as a green and replenishable alternative [3].

Perhaps one of the most varied fields of surface modification research is in the treatment of polymers. Polymers have played a substantial role in a broad range of industries, due to their widespread and desirable mechanical, thermal, and electrical characteristics. The many different characteristics of polymers has led to their use in nearly every facet of human life, from packaging, textiles, and toys to advanced technologies such as membranes, microelectronics, and biomedical devices [4]. Despite the high versatility and functionality of polymers, it is often the case that the bulk characteristics of the material are not suitable for the surface characteristics needed for an intended application. As a result, the field of polymer surface modification has consistently grown in the past several decades, and trends indicate continued growth and interest in this research as topics of study continue to branch out [5].

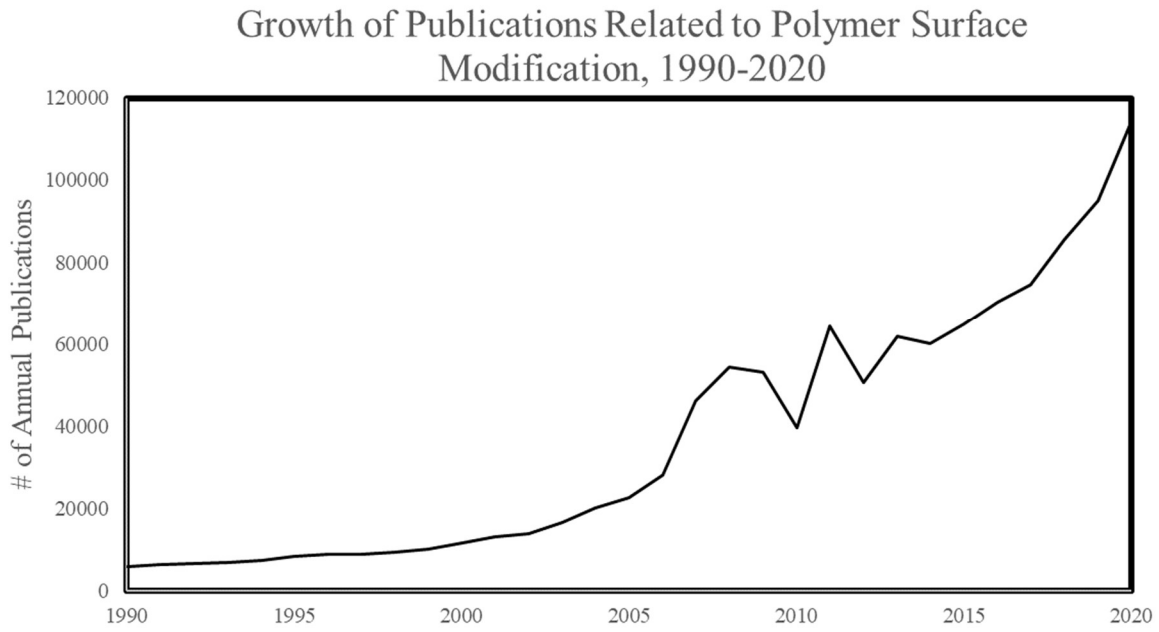

Figure 1.1 30-year publication trends for polymer surface modification. Growth trends indicate that a saturation point has not yet been reached, and that growth in the volume and diversity of research will continue in coming years (from [5]).

1.2 Polymer Surface Modification Methods and Applications

While there are numerous methods of polymer surface modification, some key techniques can be categorized as follows: wet chemical, physical, and plasma [6]. Surface modification by these approaches is often referred to as a "top-down" approach as the surface is modified from the outer surface of the material and penetrates into the surface layer by layer [7].

1.2.1 Wet Chemical Surface Modification

Chemical (or Wet) etching is a process by which a surface, in our case a polymer surface, is modified by the application of a reactive chemical, such as sodium hydroxide, sulfuric acid, or fluorine. These chemicals can be either to apply a film on the polymer surface or alternatively to

chemically and physically alter the surface for its intended purpose, such as wettability modification, bacterial/chemical/wear resistance, antistatic characteristics, etc [8].

While chemical surface modification has been a broadly developed technique, it has several drawbacks. Due to the wide variety of polymers used in industry, there is necessity for many different reagents, both for selective reactivity with the polymer of choice and to achieve the desired modifications [6]. Additionally, chemical etching is becoming more undesirable as a practice due to the large volume of chemical and water waste produced as a byproduct. Finally, polymer bulk crystalline characteristics can be altered by strong reagents, which can negatively change the bulk mechanical properties of the material and render them undesirable for their intended application.

1.2.2 Physical Surface Modification

Physical surface modification is arguably the simplest form of surface modification. Modification through these techniques is purely mechanical, and can be performed by any number of methods which can involve a sophisticated developed process or simple abrasive surface texturing. One of the most common approaches is by the production of template molds on metal foils via conventional CNC machining or high-precision micro-milling [9]. Using these techniques, micron-scale surface features can be patterned on a mold and then transferred onto a polymer film in an in-line manufacturing process with high repeatability and precision. A similar method of generating regular patterns on the surface of a polymer is photolithography, an approach by which a light-resistant mask is placed on a surface and irradiated with a photoresist, producing the desired etched patterns [7].

Surface textures developed through these means are often part of bio-inspired surface patterning, such as lotus leaves, and have applications in the productions of surfaces with superhydrophobic and/or high adhesion properties. Micro-molding and patterning technologies have been able to generate surfaces with complex 3 dimensional features, such as the T-shaped structures and micropillars for biomimetic applications, as well as "icephobic" surfaces to reduce performance loss in electrical systems and prevent failures caused by ice buildup [10]–[12]. However, templates can be costly to machine, and new templates are required to create new surfaces, a tradeoff for repeatability that limits the efficacy of a single system to a broad range of applications.

1.3 Plasma Surface Modification

1.3.1 Plasma Basics

Plasma, often considered the fourth state of matter, has been a linchpin medium for advancements in industrial processes for decades. Of particular interest, cold plasma (or non-equilibrium plasma) has garnered particular interest in a broad sweep of industries, including lighting, electric displays, semiconductor manufacturing, pollution control, food processing, and surface etching/functionalization [13]–[15]. Plasma as it pertains to physical sciences is regularly confused with blood plasma, particularly in research pertaining to biological and medical sciences. Plasma, in the context of this thesis, is a state of matter in which a gaseous medium has at least a small fraction of atoms or molecules that have lost an electron, leaving positive ions and free electrons [16]. Additionally, for a medium to be considered a plasma, it must also have collective behavior indicative of a plasma, meaning that local conditions within a body of plasma can be affected by conditions of the same body in remote regions, without any direct collisional interactions. Applications in plasma research is far-reaching, including fusion, atmospheric

science, magnetohydrodynamic energy conversion, electric propulsion and, with relevance to this research, surface modification.

In plasma surface modification, non-thermal (or non-equilibrium plasmas) are functionally exclusively used [17]. These plasma types are considered "non-equilibrium," because the electron temperatures are much higher (~10,000 K) than their respective ions, which are typically around room temperature. Due to the huge mass disparity, collisions between electrons and ions/neutrals transfer very little energy. A common metaphor is the act of throwing a ping-pong ball at the side of a building; the ball may bounce off, preserving it's kinetic energy, or stick to the wall, but regardless there is no substantial change to the building. These types of plasmas are relatively ubiquitous in everyday life. However, these types of plasmas behave in unique ways relative to thermal plasmas, and as such are more complex, garnering increasing interest in recent years. Surface modification via a non-equilibrium plasma medium has chiefly been performed via three methods: corona discharge, plasma jet, and DBD.

1.3.2 Advantages of Plasma vs Wet Chemical Treatment

Plasma surface modification has gained interest as an alternative to other more traditional modification methods, in particular chemical etching, one of the most common methods used in industry. A key disadvantage of wet chemical modification compared to plasma is the nonspecific nature of the treatment, introducing unpredictable or unrepeatable functionalization [18]–[20]. Additionally, it has been observed that chemical treatments often leave a layer of organic contamination, or can affect the bulk characteristics of the material under treatment, weakening the necessary properties of the material and potentially impairing its original functional purpose. Further, wet chemical treatments have been criticized in recent years due to growing environmental and safety concerns in dealing with highly reactive acids and solvents.

As an alternative, plasma treatments are advantageous over other applications for a variety of reasons. Plasma surface treatments are typically highly uniform and repeatable, regardless of geometry, and functionalization can be carefully controlled by manipulation of the plasma gas composition and other plasma parameters [21], [22]. Additionally, surface modification only affects the surface, and does not penetrate very deeply, leaving the bulk characteristics unaffected, and can safely be applied to biological tissues [23]–[26]. Plasma treatment also is clean, requiring no additional cleaning measures, and producing no environmentally hazardous byproducts [27]–[29].

1.3.3 Methods and Applications of Plasma Surface Modification

Corona discharge plasma treatment has seen wide interest in treatment applications within the fields of plasma treatment due to their ability to modify surfaces in relatively short time scales compared to other treatments, in addition to the benefits previously outlined for plasma treatment in general. One unique element of corona plasma treatment is that the high voltage electrodes are often adapted to unique geometries, with some unique shapes being chosen to induce specific effects, from simple conical tips to complex needle-plate electrodes [6], [30]. Corona treatments have been demonstrated with high adaptability, with treatments performed in pulsed and continuous charge profiles, and a broad range of materials being treated, including LDPE, vulcanized rubber and polyolefins with air, nitrogen, oxygen, bromine, etc. [30]–[35]. While corona plasma treatments have shown great interest and have high adaptability, the physical properties associated with the mechanisms of the discharge prevent application of this treatment method for scalable surface treatment on tubing IDs.

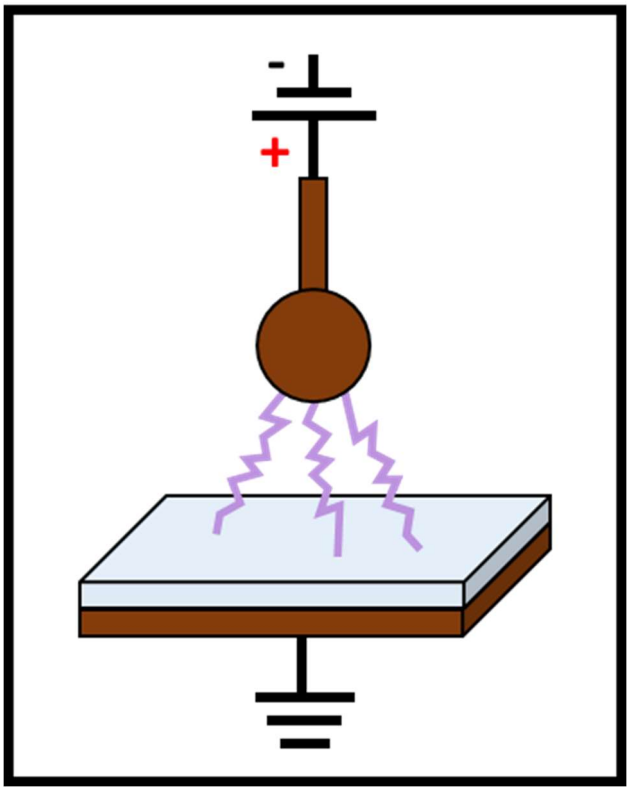

Figure 1.2 General schematic of a corona discharge plasma treatment apparatus, though there are many different arrangements in use. The discharge is induced by and electric field induced by a high frequency voltage supply, usually in the RF frequency regime. Polymer surfaces are typically mounted on a grounding electrode coated in a special dielectric. Plasma discharge can either present as an arc or as a more homogenous glow.

A more recent development in plasma treatment techniques, the plasma jet, or "pencil" as it is sometimes termed, is a unique arrangement of electrodes and power frequency regimes that enables the generation of plasma at atmospheric pressure, using certain gas compositions. Atmospheric Pressure Plasma Jets (APPJs) can be used for a broad range of applications in polymers, including adhesion, cleaning, wetting modification, and surface etching [36]–[39]. APPJ offers a low cost, robust and mechanically simple approach to polymer surface treatment. However, despite efforts to perform APPJ surface treatments on the inner surface of tubing, the scalability of said treatment will always be inexorably tied to the maximum penetration depth

achievable by the treatment process, and the natural gradient of plasma intensity will inevitably result in some degree of heterogeneity in the surface treatment induced [40], [41].

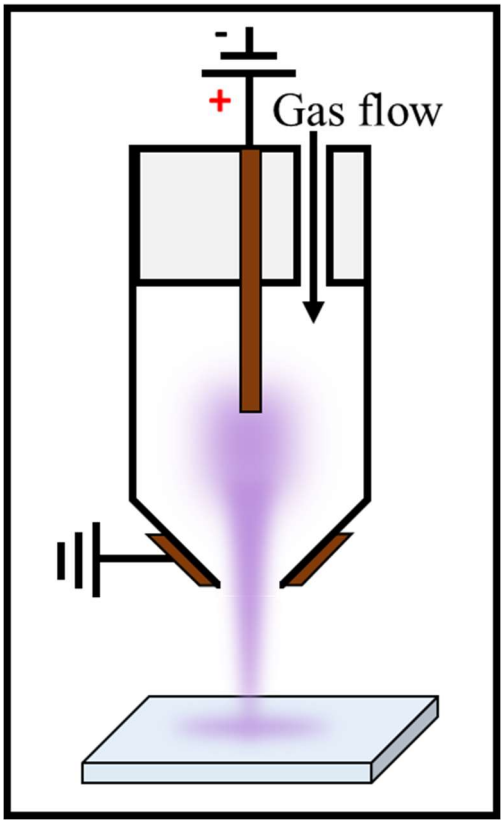

Figure 1.3 General schematic of a plasma jet (or "pencil") treatment apparatus as it would be used to treat polymer surfaces, though there are many numerous arrangements. Depending on the arrangement, a plasma jet could be classified as a corona discharge or a dielectric barrier discharge and can be operated in AC or DC voltage regimes.

DBD is a common technique for producing plasma discharge with homogenous characteristics, is perhaps the original methodology of polymer surface modification with plasma. DBD plasma treatment, in its simplest form, consists of a high voltage electrode and a ground electrode insulated from the plasma medium by a dielectric material. The dielectric functionally "softens" the intensity of the plasma discharges at a given voltage, preventing unwanted arcing at breakdown, and allows for a highly uniform discharge of plasma in a fixed volume as compared

to other treatment methods [42]. DBD surface modification has been demonstrated at low, medium and atmospheric pressure using a variety of gas mediums on a wide array of polymer substrates such as polyethylene, polymide films, polypropylene, polycaprolactone, and Teflon [43]–[48]. These treatments, as with other plasma treatments, work extremely well for adhesion improvement, wetting, cleaning, biocompatibility, and film deposition [49]–[52]. DBD plasma treatments can be modified to adapt to unique morphologies, and can easily be applied to in line processing.

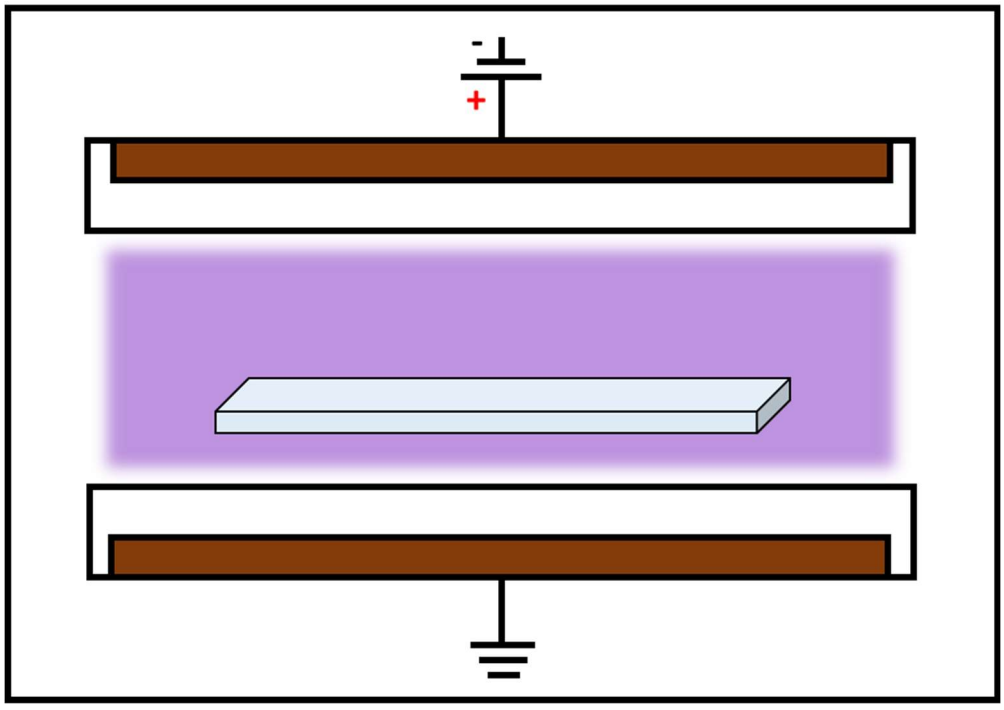

Figure 1.4 General schematic of a DBD plasma treatment apparatus. The system comprises of a high voltage electrode, coated in a dielectric material, with a ground electrode. Typically, DBD is in a parallel-plate arrangement, though variations exist. DBD can be performed in vacuum or, in some cases, at atmospheric pressure, depending on the composition of the plasma medium.

1.4 Motivation

The motivation of this thesis work is to close a research gap in plasma treatment techniques applied to dielectric tubing of small diameters. It can be argued that wet chemical surface

modification methods can be used in lieu of plasma modification for this problem. However, as has been indicated in previous sections, wet chemical treatments are undesirable relative to plasma treatments due to their non-uniformity, uncontrollable chemistry, bulk material effects, and hazardousness to humans and the environment.

Thus far, plasma treatment techniques have largely been applied to simplified, planar geometries. As a result, little capacity for applying useful plasma treatments more broadly to unique geometries has been developed. Of particular interest is the application of plasma treatments for enhanced wettability and surface adhesion to the inner surface of small diameter dielectric polymeric tubing. Due to the geometry of typical parallel-plate DBD treatment methods which limit their ability to uniformly treat non-planar surfaces, and the low penetration depth that can be achieved by plasma jet treatment techniques, it is readily evident that a novel apparatus for uniform and scalable treatment of small diameter tubing needs to be developed, and modalities of plasma parameters to achieve specific morphological change and wetting effect need to be identified.

1.5 Objectives

The objectives of this research can be divided into two major parts: the design and development of a novel apparatus for the plasma surface treatment of small-diameter dielectric tubing, and the demonstration of said system's capabilities to induce key material characteristics on select dielectric tubing. The plasma treatment system must be capable of isolated treatment on the inner surface of the tubing while inducing homogenous surface changes in reasonable time scales. Additionally, the system must be developed such that it can be practically adapted to scalable implementation as an inline process.

The second objective can be further subdivided into separate goals, centered around surface morphology and wetting. Surface morphologies induced by the plasma treatment needs to be characterized using practical definitions to define scope of capabilities of the system as a function of plasma power and treatment time. Additionally, demonstration of the adhesive capability of the tubing as a result of treatment must be performed. Further, wetting characteristics induced on the tubing from the plasma treatment process must be characterized by similar parameters of time and power, and the time-dependent decay of these effects must be investigated.

1.6 Outline

The body of this paper will begin with a detailed discussion of the prototyping and development of the plasma treatment apparatus, outlining the stages of development, and the rationale for varied alterations and modifications. Detailed characterization of the electrical behavior of the system will be provided, along with substantive documentation of design specifications. The paper will then discuss the definitions of key experimental parameters used for characterizing the plasma treatment process, and the experimental procedures designed for characterization of the treatment of the polymer surfaces under inspection.

Treatment characterization, making the body of results and discussion, will be broken up into several subsections. Direct observations of surface morphological changes will be described, reporting effects of key controls such as plasma power, exposure time, and electrode proximity on physical characteristics such as protrusion density, size distributions, and roughness. Similar parameters of plasma power and feed rate, a comparator to exposure time, will be reported for their effects on surface wetting. Additionally, temporal decay and transience of wetting characteristics will be reported for several key treatment regimes.

As a supplement, observations on general trends of surface modification characteristics will be shared, comparing trends of protrusion density vs. size, roughness etc. Finally, qualitative observations of micro- and nano-scale surface features will be reported, as well as observations of mechanical adhesion of a polymer compound to the surface of a treated segment of tubing.

In supplemental discussions, an outline will be made for plans for future modifications and the development of a more robust plasma treatment apparatus. Additionally, justifications will be made for potential additional capabilities of the system for surface modification practices, as well as a plan of action for future works in the development and characterization of novel applications.

2. METHODS AND APPARATUS

2.1 Peripheral Systems and Materials

2.1.1 Oscilloscope

For the bulk of voltage and current monitoring, a Teledyne Lecroy HDO9304 High Definition Oscilloscope was employed. The HDO9304 Oscilloscope is a 4-channel device with a 3 GHz bandwidth at 50 Ω termination and 1 GHz at 1 $M\Omega$ termination. In a two-channel arrangement, the system is capable of sampling at 40 GS/s, and is equipped with a variety of internal functions for the real-time interpretation of direct voltage and current readings. The oscilloscope was used to directly convert real-time signals of voltage and current measured from the DBD plasma system and convert them into interpretable power consumption measurements.

These measurements, taken in 2 ms time steps, captured 20 waveforms from the 10 kHz in each trigger, and averaged those waveforms to extract an approximate value of the total power draw from the system. These measurements were further used to generate a 1000 sample normally distributed histogram that reflected the variance and average power consumption in the plasma setup. The differential between the averages of the power consumption histograms with and without plasma discharge (with and without LDPE tubing present in the treatment area), was taken to decouple the power draw from capacitive sources and the true power draw from the plasma discharge withing the tubing.

Figure 2.1 Display of typical readout of the Teledyne Lecroy HDO9304 High Definition Oscilloscope. The pink trace represents the voltage, the yellow represents the current, the small red trace represents the computed power, and the histogram is the cumulation of net sums of power generated in 20 cycles. The range of +/- 10 mW about the mean is typical.

2.1.2 Voltage and Current Monitoring

For all samples produced in the DBD plasma system, voltage and current in the system were always directly measured. The current in the system was measured by a Pearson Current Monitor, Model 2100. This monitor has a sensitivity returning a 1:1 ratio of Volt/Ampere, 50 Ω output resistance and frequency bandwidth of 125 Hz – 20 MHz. The system also has a usable rise time of 20 nanoseconds, comfortably capturing the millisecond scale of the plasma discharge events. The current monitor is mounted in the plasma treatment system around the high voltage cable coming directly out of the power supply, ahead of the voltage probe and plasma discharge.

The voltage is monitored by a Tektronix P6015A voltage probe. The probe is rated to operate between 1.5 kV to 20 kV DC + peak AC, with a 75 MHz bandwidth and a rise time less than 5 ns. The probe has attenuation factor 1000:1 (1 kV reads as 1 V on the oscilloscope) when loaded with high-impedance oscilloscope input. The voltage probe is connected at a point on the high voltage line via an alligator clip where a small amount of conductive material is exposed for the express purpose of connecting the probe and is grounded to a large optical table. For

consistency, these probes are never removed from the apparatus and are always used to directly measure the electrical properties of the plasma discharge and latent electrical phenomena.

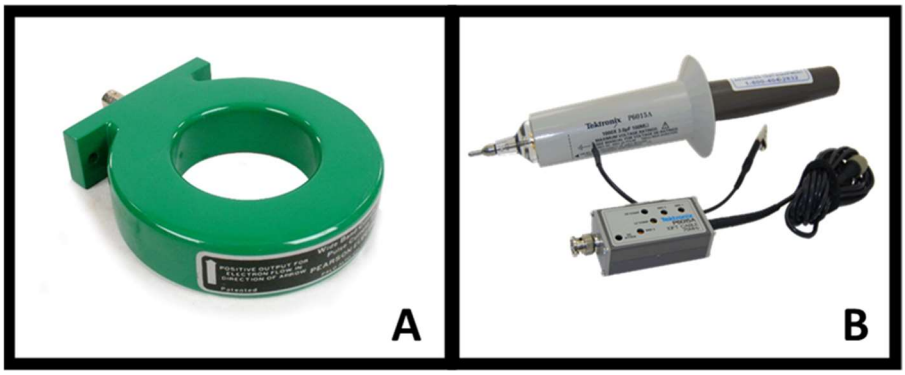

Figure 2.2 A) Pearson Current Monitor, Model 2100, and B) Tektronix P6015A voltage probe

2.1.3 Power Supplies

Two power supplies were used throughout the development of this system. The first power supply was CHT-1309A High Voltage Power supply, produced by Chirk Industry Co., Ltd. The power supply has limited documentation and is no longer produced by the manufacturer. It has a fixed operating frequency of approximately 10 kHz, with limited voltage control that could be driven by varying the voltage of the low voltage power input. This control was very limited and caused some fluctuation in the waveform that warranted concerns about repeatability.

The power supply that was implemented for the final developments of the DBD plasma system was the Coronalab CTP-2000K Plasma Generator. The generator, specifically designed for applications in DBD and arc discharges with applications in surface treatments, has an operating output voltage ranging from 0 – 30 kV, and a peak power output of 500 W. The frequency ranges that this system operates in are at least 10 – 30 kHz (These are the only frequencies that this system has been operated under for this work), and has generally been fixed at 10 kHz.

Figure 2.3 Coronalab CTP-2000K Plasma Generator

2.1.4 Other Lab Materials/Equipment

As previously mentioned, this apparatus makes use of two Alicat MC-200SCCM flow controllers, connected to their supply tanks (Helium working gas, O_2, N_2, or air seed gasses) via a network of Tygon tubing and connectors. The Helium mass flow controller is always fixed at 0.25 cubic centimeters per minute, with the other controller free to vary as a ratio of the Helium flow, generally less than 5%. For most work in this study, the only gas supplied to the system is pure helium.

The gasses used in this study are supplied by Purdue university, and are laboratory-grade with purities of at least 99.997%. The dry air supply is taken directly from the central gas line in Armstrong Hall on Purdue University's main campus.

The tubing used in this study is a PTFE catheter tube, BTPE-20, produced by Instech. The tubing is supplied in 30 meter lengths with an outer diameter of 1.09 mm (+/- 10% extruder variance) and an outer diameter of 0.38 mm (+/- 10% extruder variance). This tubing was connected to the upstream gas sufficiently far downstream of the mixing point to be confident of good mixing by a 27 gauge (~0.41 mm OD) needle. The tubing was allowed to flush impurities at

the start of treatment or in between gas composition adjustments for at least 30 minutes prior to any active treatment.

For some low-magnification imaging, a simple USB-enabled hand-held microscope was used to image meniscus' from wettability studies and general microscopic features that did not need electron microscopy to image but could not be readily viewed with the naked eye. The microscope is enabled with a 40x – 1000x magnification range and is equipped for plug-and-play interfacing with any computer.

Figure 2.4 Sunnywoo USB Microscope, with accompanying stand

2.2 Analytical Apparatus and Techniques

2.2.1 Sample Preparation Techniques

As the primary motivation of this work is to isolate surface treatments on the internal surface of polymer tubing, it was necessary to develop novel techniques for sample preparation. Traditional techniques for plasma treatment are performed on flat surfaces, and as a result the samples require very little preparation for microscopy analysis. The 0.38 mm ID LDPE tubing, after treatment, goes through a regular procedure for scanning electron microscopy (SEM) analysis. The sample is observed by eye and under a low low-magnification is segmented and cross-sectioned by hand using scalpels with a sterilized #15 and #12 scalpel blade, respectively.

These blades were specifically chosen for their unique shapes and sizes. The #12 blade, having an extremely sharp, curved tip allowed for easier longitudinal bisection due to the easy penetration into the tube and decreased frictional resistance of the blade as it was drawn through the length of the tubing. The #15 blade was selected for sectioning mainly due to its small size, making it easier to use when manipulating extremely small sections of tubing.

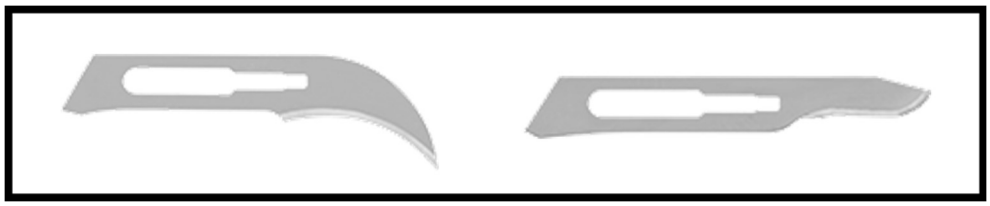

Figure 2.5 Left) #12 scalpel blade; Right) #15 scalpel blade

After segmenting and bisecting, the samples were mounted onto Ted Pella 12.7 mm sample stubs with carbon tape. The samples are then sputter-coated using an SPI Sputter Coater, located in Birck Nanotechnology Center. The SPI-Module sputter coater uses a 60:40 Au/Pd target to coat samples using an Argon plasma medium. Coatings of 10s of nanometers are applied to the surface of the tubing to allow for conductive pathways on the otherwise non-conductive surface, allowing for clear imaging under a SEM.

Figure 2.6 SPI-module sputter-coater for SEM analysis

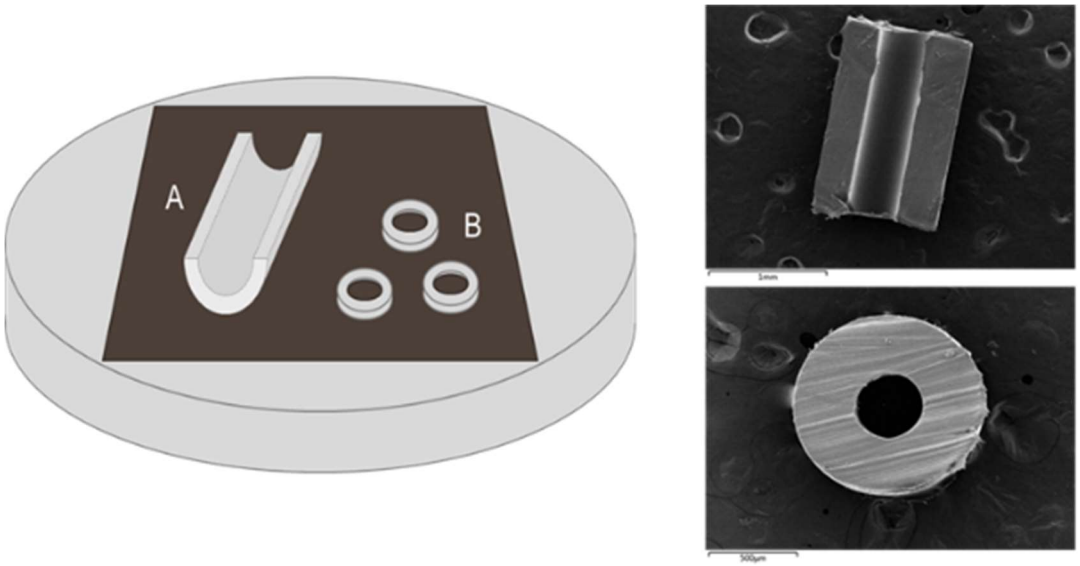

Figure 2.7 Left: Schematic of sample preparation on SEM stub for longitudinal and axial cross-sections. Right: SEM Images of prepared samples.

2.2.2 Microscopy

Microscopy analysis was largely performed on two critical machines. Initial analytical work was performed on a Hitachi S-4800 Field Emission SEM with energy-dispersive X-Ray spectroscopy (EDS) capabilities with an Oxford X-Max 80 Silicon Drift Detector. The SEM has a

maximum resolution of 2 nm and acceleration voltages of 0.5 – 30 kV. The EDS equipment is equipped with a peak resolution of 127 eV at 5.8keV.

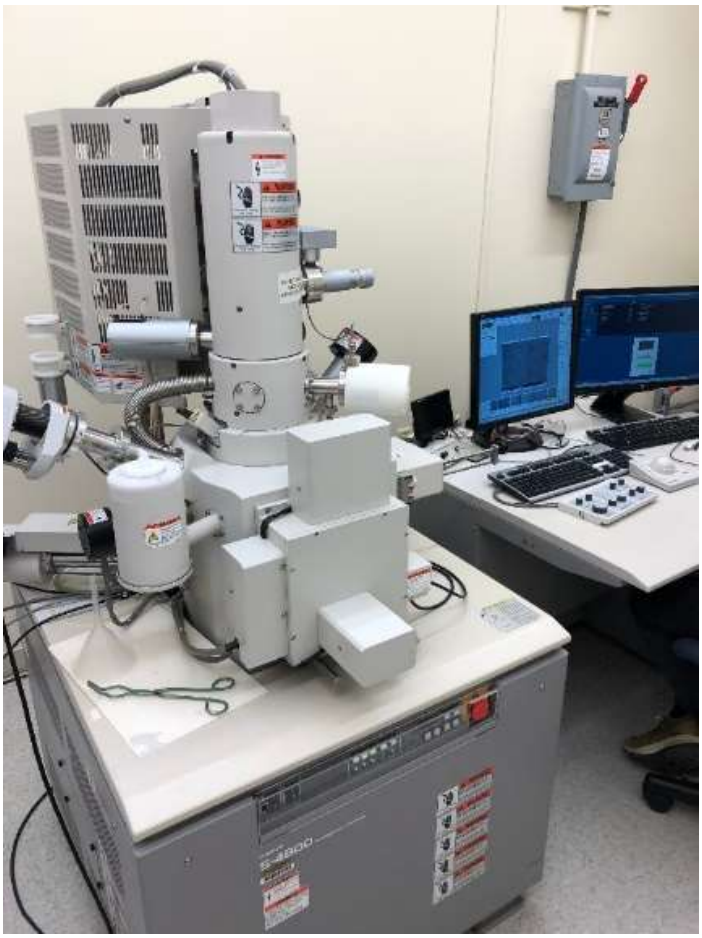

Figure 2.8 SPI-module sputter-coater for SEM analysis

For higher performance analysis, a Thermo Scientific Helios G4 UX Dual Beam SEM/EDX/FIB was employed. The Helios SEM has a peak resolution of 0.7 nm at operating voltages of 5 – 10 kV in the electron beam, allowing for superb resolution at magnifications greater than 10,000X. The Helios is also equipped with an excellent EDX for chemical composition analysis and an FIB for cross-sectional analysis should it be needed.

Figure 2.9 Thermo Scientific Helios G4 UX Dual Beam SEM/EDX/FIB

2.2.3 Surface Morphology Analysis

For surface morphology analysis, samples were collected after plasma treatment to include 1 cm of tubing from the outside edge of both ground electrodes to include all regions of the tubing where plasma discharge was visible. For each treatment profile, triplicate samples were prepared. The full length of the samples, approximately $5\ cm$ of tubing, was prepared on SEM stubs, and sample prep and analysis was performed on the Helios SEM device housed in Birck Nanotechnology Center at Purdue University. Images were collected in $\frac{1}{2}\ mm$ increments longitudinally for all samples within the regions of peak roughening.

SEM analysis is performed to enable observations of the physical morphology of treated tubing, particularly special protrusions that are generated from surface treatment. A convenient

characteristic of electron microscopy, sharp edges appear more brightly than smooth surfaces. Protrusions on the surface of treated tubing appear substantially brighter that the background surface so, by adjusting the contrast and brightness of the SEM image, the photos taken can be processed via an image processing app, such as ImageJ. By doing particle analysis on the images after careful processing, several key surface morphology characteristics, including protrusion density, mean size, and size distribution.

The protrusion size distribution function $F(D)$ was defined as follows:

$$F(D) = \frac{\Delta N}{\Delta D \Delta A}$$

With N being the number of protrusions in a given area, A and protrusion diameters in the range between D and $D + \Delta D$. The protrusion number density per unit area was determined then as a 0^{th} moment of the distribution function:

$$n_p = \int F(D) dD = \frac{\Delta N}{\Delta A}$$

An average protrusion diameter $\overline{D_p}$ was determined as a 1^{st} moment of the distribution:

$$\overline{D_p} = \frac{\int F(D) D dD}{\int F(D) dD}$$

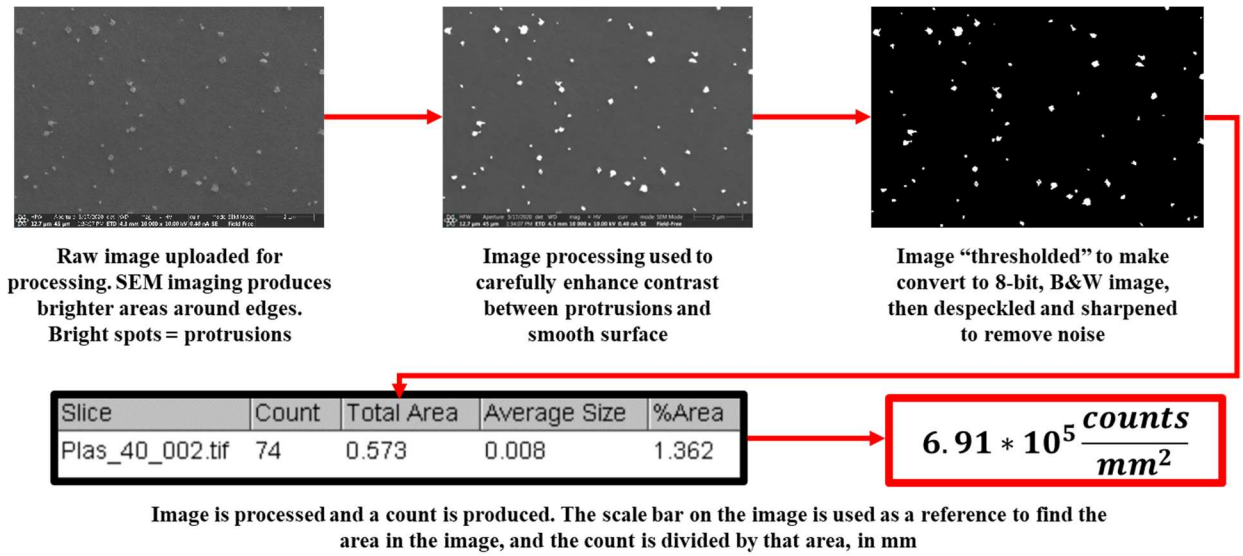

Figure 2.10 Diagram describing the process of interpreting the micro-scale surface morphology features, including density, mean protrusion size, and size distributions using ImageJ

Surface roughness can further be quantified by approximating the height of individual protrusions from the mean diameter of the protrusions based on the observed average aspect ratio of width to weight from a selection of cross-sectional images. A standard metric of surface roughness, R_a, is typically calculated by the surface integral

$$R_a = \frac{1}{A}\oiint |z(x,y)|\, dy\, dx$$

where A is the surface area under observation, and $z(x,y)$ is the discreet height f the surface at a given point. With approximations based on the given aspect ratio, and assuming that no significant roughness is contributed by the interstitial space between protrusions, this equation can be transformed into a numerical summation approximation given by

$$R_a \approx \frac{1}{A}\sum_{i=1}^{n} V_n$$

where V_n is the approximated volume of individual protrusion, n, in the area under inspection. R_a values are further correlated to industrial standards for roughness, providing practical comparisons to standard definitions for surface finishes. Table 1 shows the ISO-defined roughness grades with matching SI and imperial values of R_a.

Table 1: ISO standards for roughness; ISO Roughness grades with corresponding R_a values in SI and imperial units [53].

ISO Roughness Grade	$\boldsymbol{R_a, \mu m}$	$\boldsymbol{R_a, \mu in}$
N12	*50*	*2000*
N11	*25*	*1000*
N10	*12.5*	*500*
N9	*6.3*	*250*
N8	*3.2*	*125*
N7	*1.6*	*63*
N6	*0.8*	*32*
N5	*0.4*	*16*
N4	*0.2*	*8*
N3	*0.1*	*4*
N2	*0.05*	*2*
N1	*0.025*	*1*

2.2.4 Contact Angle Techniques

A key metric for the measurement of surface modification is surface wettability. There are many conventional means by which wettability is measured. One of the most common means of measurement of wettability is water contact angle. Conventionally, water contact angle is measured via a droplet test on a flat surface. Unfortunately, due to the highly confined volume of the small-diameter tubing under investigation in this study, conventional droplet tests were not

feasible, and as an alternative, a series of alternative investigations were performed, including initial qualitative measurements confirming the wettability changes induced by plasma treatment relative to an untreated sample, and then more in depth studies into the effects of plasma parameters on wettability as well as the retention of wettability effects as a function of time after treatment.

The measurement of wettability induced by plasma treatment is performed by measuring the contact angle on the inner surface of the tubing. After tubing treatment, 1-5 μL of DI water was introduced to the open face of the tubing using a low volume insulin syringe, producing small droplets on the needle which is then drawn into the tubing via capillary action. DI water is not forced into the tubing using the syringe due to potential variation induced by induced pressure gradients from manual injection. Because of the narrow diameter of the tubing, the optical distortion near the inner walls of the tubing is difficult to accurately image. To approximate the true contact angle, images are taken of the tubing, and a "best fit" of the arc of the meniscus is drawn, approximated as a section of an ellipse. The image is then translated to a droplet drawn from the flat lower line of the imaged meniscus, and the droplet contact angle is directly extrapolated via an ImageJ plug-in. The value returned from ImageJ is then converted to the true contact angle of the meniscus by the simple equation:

$$\theta = \theta_{men} = \theta_{drop} - 90^{o}$$

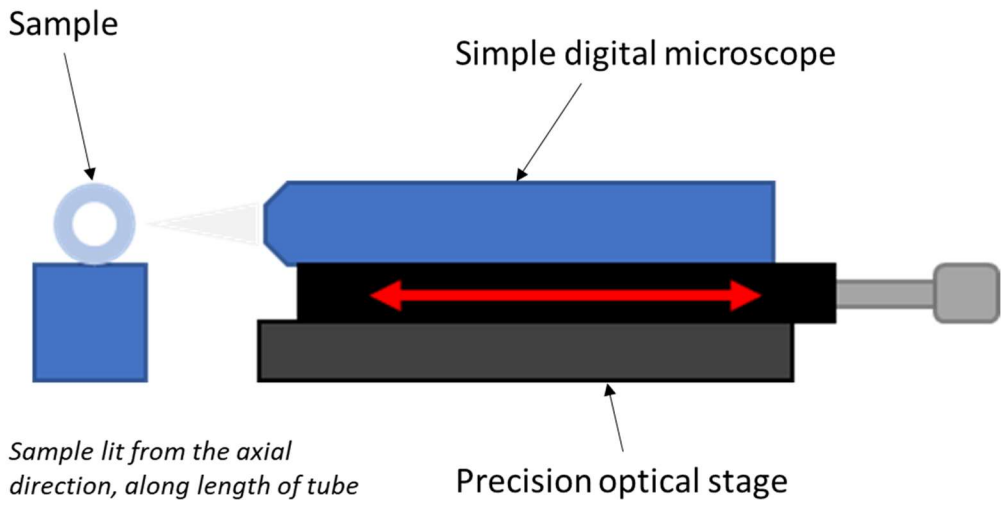

Figure 2.11 Diagram of experimental setup for microscopy analysis of wettability of tubing ID via meniscus imaging

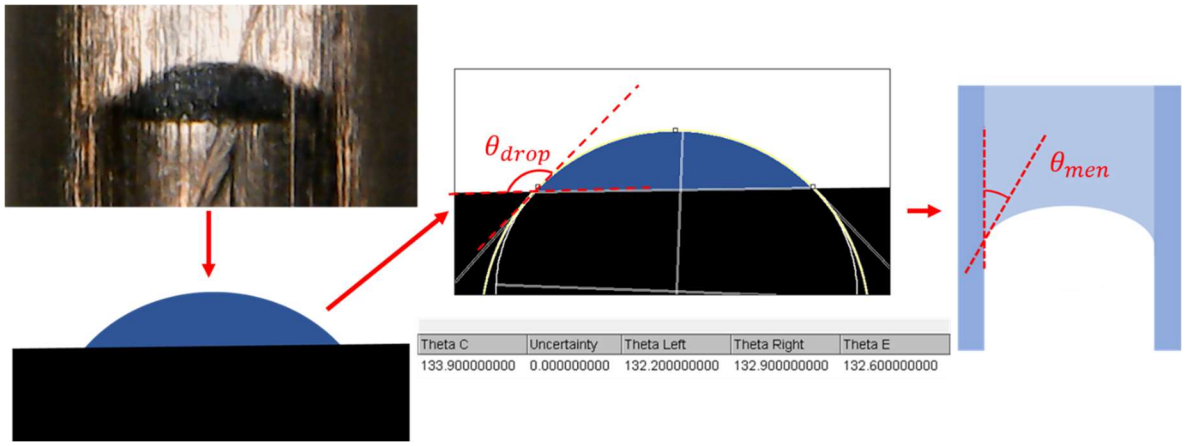

Figure 2.12 Diagram describing the process of determining the contact angle of the meniscus imaged on the inside of LDPE tubing using ImageJ

3. RESULTS

3.1 Development of Atmospheric-Pressure DBD Plasma Treatment System for the Inner Surface of Polymer Tubing

3.1.1 Plasma Jet Treatment Apparatus

At the onset of the design of the plasma apparatus, it was originally conceived that an existing plasma jet could be adapted to operate as a staging element to test the feasibility of the plasma system. The original system consisted of a segment of PTFE (Teflon) round bar of approximately 1" diameter by 2" length with a thru-hole bored to allow for a single HV 10 kHz electrode to pass into an enclosure created by a quartz glass converging nozzle, as well as a secondary hole for a working gas to pass through. The quartz glass nozzle was designed to act as a containing volume for a plasma discharge to initiate in and eject a "streamer" of plasma into free air. The plasma was generated using a CHT-1309A High Voltage Power supply, with a simple 10 kHz output. In the original setup, a section of Teflon or LDPE tubing was positioned a few centimeters from the outlet of the quartz nozzle, and the plasma streamer was permitted to penetrate the end of the tubing.

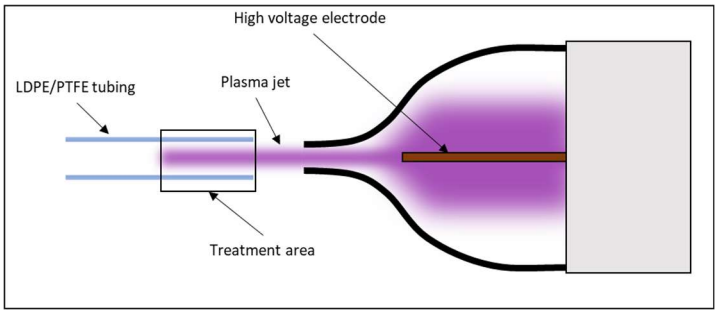

Figure 3.1: Basic diagram of the helium plasma jet arrangement for PTFE and LDPE treatment. As is readily apparent, the treatment area is functionally limited by the length that the streamer will extend before it dissipates.

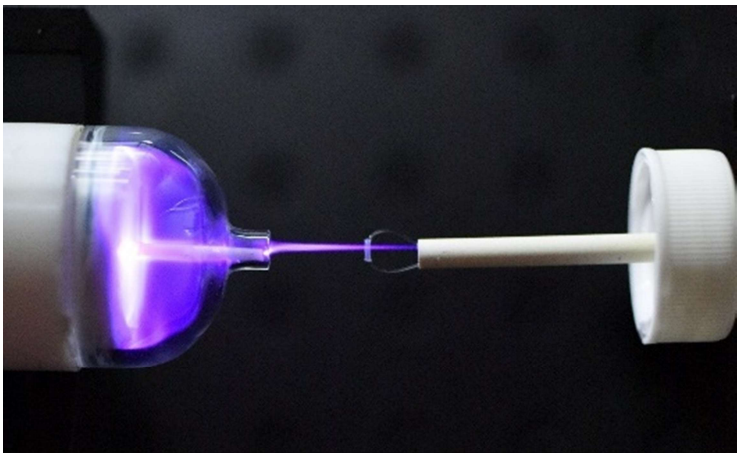

Figure 3.2 Early iteration of plasma treatment apparatus via plasma jet, used for troubleshooting and analysis of plasma effects. Here, a small (~3 mm) section of tubing is suspended by nylon wire and an APPJ is impinged on the outer surface of the tubing.

While initial testing was beginning to generate promising results, it quickly became apparent that any efforts at homogeneous treatments over lengths of tubing greater than a few centimeters would be functionally impossible. Additionally, our plasma jet (or pencil, as it is sometimes called) was unable to adequately penetrate tubing of moderately small internal diameter. As a result, effort in the development of an entirely new system was necessary to eliminate anticipated issues with heterogeneity and surface treatment control.

3.1.2 Dielectric Barrier Discharge Treatment Apparatus

In the process of developing an apparatus capable of performing treatments of reasonable homogeneity, several design schemes were considered. The final design that was selected was chosen for its simplicity and robustness as well as to take advantage of convenient material properties of the tubing in use, namely, its characteristics as a dielectric. An apparatus was developed that would operate as a modified dielectric barrier discharge (DBD).

DBD plasma has been regularly employed in polymer surface modification processes, but typically in parallel plate arrangements and usually in low pressure/vacuum conditions. In this

system, the working gas, usually helium, is flowed into the tubing from a tank, and the tubing material is used as the dielectric through which the electric fields generated by special ring electrodes penetrate. The result is a totally enclosed helium plasma discharge. Along with the 1 cm long, Teflon insulated high voltage electrode, additional ring electrodes were added on either side of the system to act as additional control points to increase the functional range of the plasma and intensify the plasma in the treatment area.

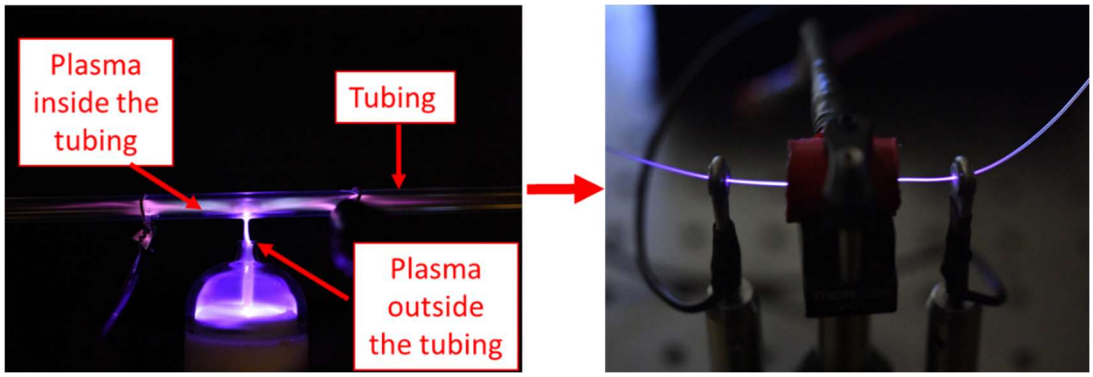

Figure 3.3 Left: Initial test of DBD tubing by APPJ impingement on a quartz glass tube with He gas flow. Right: Modified arrangement of atmospheric pressure DBD treatment apparatus, simplified by the removal of the APPJ with a HV electrode operating at 10 kHz.

Several iterations of this design were implemented. From the start, the system used the same power supply as the helium plasma jet (CHT-1309A High Voltage Power supply), but after some considerations regarding the repeatability and reliability of such a simple power supply, it was later determined that the system would benefit from a more robust power supply, and a laboratory-grade system, the Coronalab CTP-2000K Plasma Generator, was implemented. The system was capable of generating identical 10 kHz waveforms, but with much better precision and accuracy in peak-to-peak voltage outputs through the use of a dedicated transformer as opposed to simple voltage inputs in the previous system.

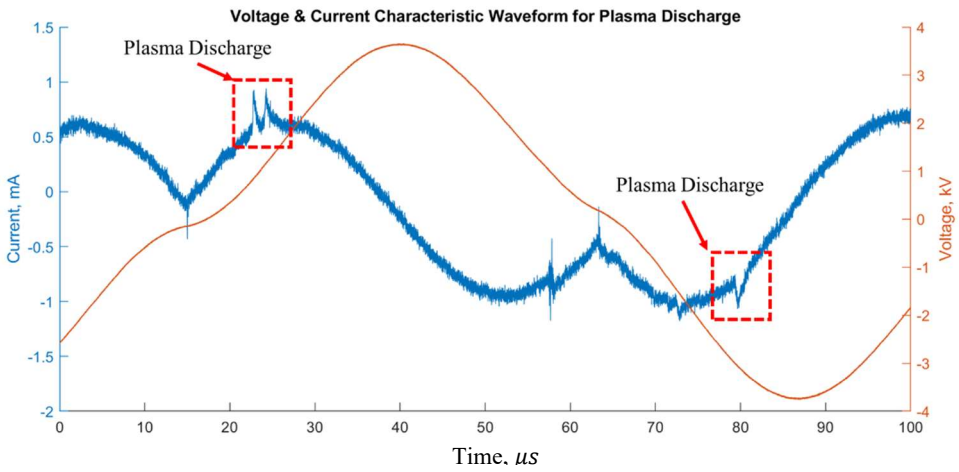

Figure 3.4 Characteristic voltage and current waveforms for DBD plasma apparatus under operation. Plasma discharge events are boxed in red. Other spikes are noise from other sources.

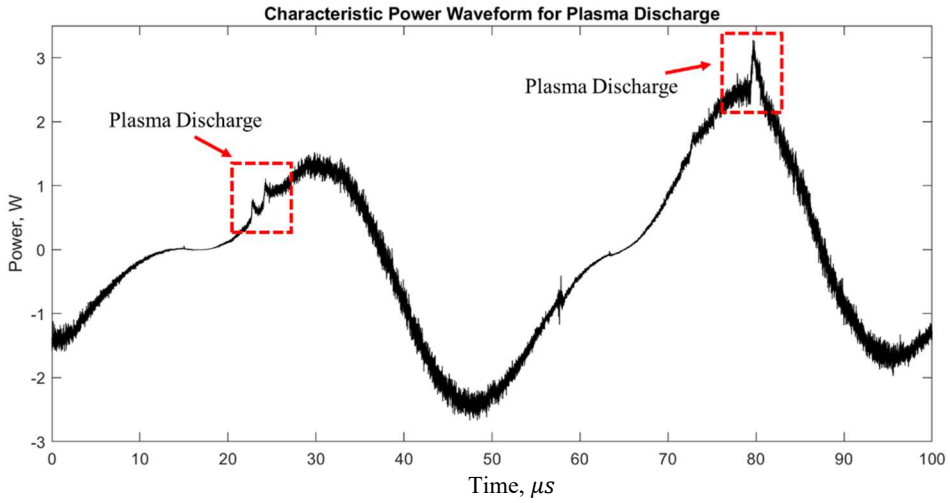

Figure 3.5 Characteristic power consumption waveforms for DBD plasma apparatus under operation. Plasma discharge events are boxed in red. Other spikes are noise from other sources.

3.1.3 Experimental Observations from Pin Electrode and Electrode Contact

Early testing with the DBD apparatus showed promising results in terms of demonstrating control over surface morphology and wetting characteristics, in particular the variety of characteristics achievable by one treatment platform. However, concerns arose over the time-scale necessary to achieve desired morphologies, as well as the capability of the system to produce more

densely roughened surface features, and efforts were made to determine modifications to the system that could accelerate the treatment process and densify the resulting morphologies.

It had already been determined that a simple increase in voltage was not sufficient to decrease treatment time for equivalent results or increase roughness, but rather that a specific regime of voltage parameters was necessary to produce the certain morphologies. In fact, voltages above a certain threshold or exposure time were at times observed to either remove morphologies already present or failed to produce morphologies at all.

As an alternative, ground electrode geometry and contact were explored as a means to expedite and intensify the formation of desired surface features, and two experiments were performed to investigate the impacts of these factors. To explore the impacts of the total contact, or sharpness, of the ground electrode, a simple copper pin was fabricated in the lab, and positioned in direct contact with the tubing 1 cm away from the high voltage (HV) electrode in the longitudinal direction of the tubing. This test was intended to identify how the intensification and concentration of electric field lines would impact the surface morphology of the tubing in the region of contact.

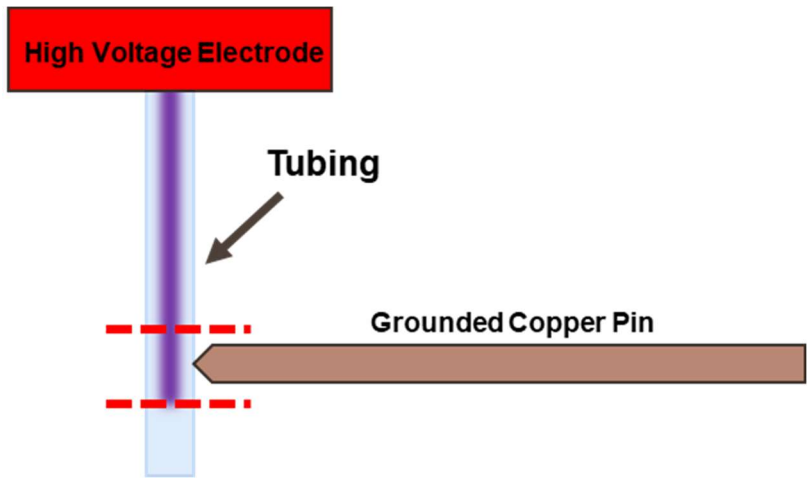

Figure 3.6 Schematic of the pin electrode experiment for the analysis of surface morphology impacts from the concentration of electric field lines to a discreet point on the tubing.

Tubing was treated in this special arrangement for 60 seconds, an exposure period 30x less than the standard treatment profile of 30 minutes, at voltage levels commensurate with the standard treatment profile. During treatment, plasma discharge about the pin electrode was observed to be noticeably brighter than that of the standard ring-shaped ground electrodes. After the treatment, at the interface of the pin electrode and the tubing, a small, $\sim 200\ \mu m$ opaque spot was clearly visible on the inner surface of the tubing, and the peripheral area around the point of contact was observed to be slightly more opaque than an untreated sample of tubing. After the treatment, qualitative surface morphology analysis was performed via SEM for several samples.

SEM analysis showed extreme morphological changes on the inner surface of the tubing about the point of contact of the ground electrode. Large raised features, $\sim 4\ \mu m$ in height, were observed, forming a circular patter about the contact point of the pin. There surface features were unique to previously observed "protrusion" morphologies characteristic of the ring-electrode treatment, demonstrating much larger ratios of height to top-down surface area and, interestingly, were extremely flat, forming plateau-like structures rather than the more random, jagged morphologies of other treatment profiles. Further, the space between these plateaux presented as canyon-like. The surface height of these canyons was observed to be at the same apparent height of the surrounding tubing, indicating that these morphologies may be emergence events rather than surface etching.

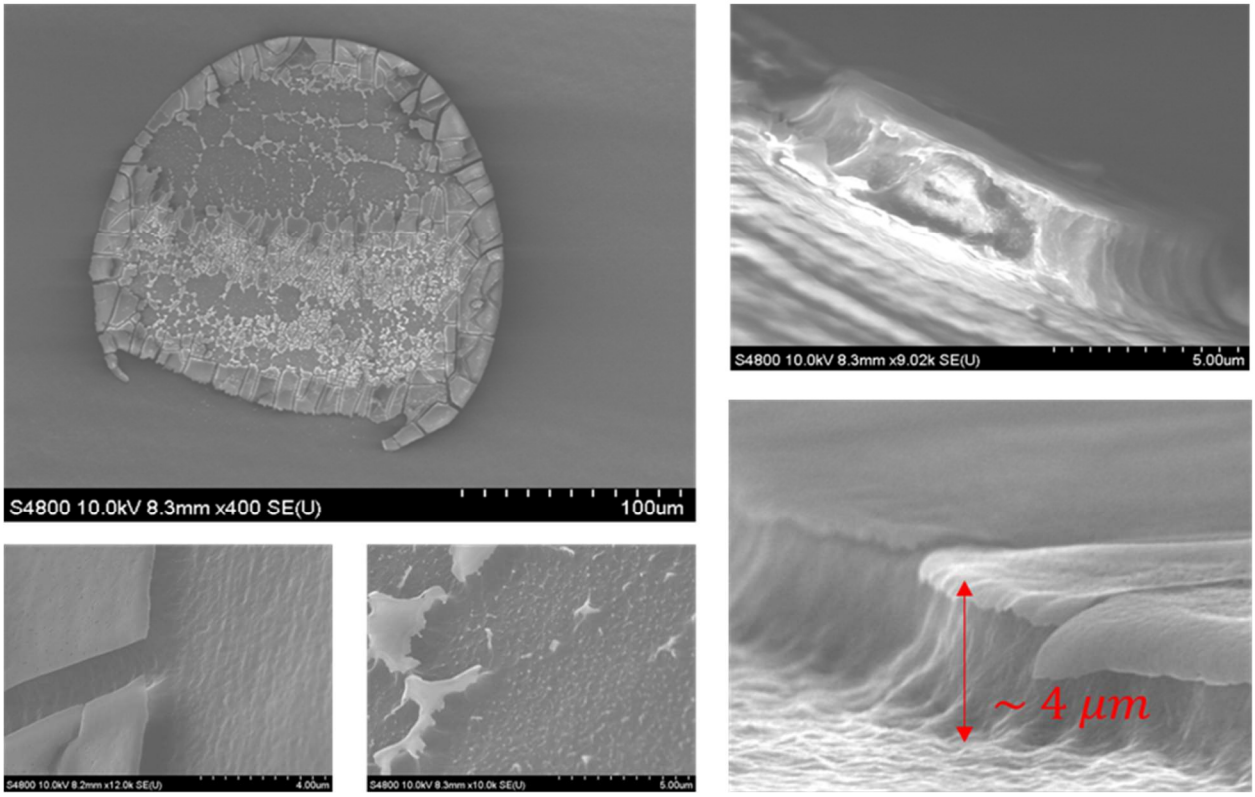

Figure 3.7 Resulting morphology about the point of contact of the pin electrodes. $\sim 4\ \mu m$ plateau-like features were observed, with distinct canyon-like valleys between the features that were observed to be at the same heigh as the surrounding surface further away from the point of contact.

In the regions more distant from the point of contact of the ground electrode, but not in the far-field region, less than a few millimeters longitudinally from the pin contact point, additional morphologies were observed that were observed to be more consistent protrusion morphologies that have been observed in other treatment profiles and are similarly assumed to be emergences rather than features formed from etching. The protrusions were measured in heights ranging from $50 - 500\ \mu m$, with roughly proportional widths.

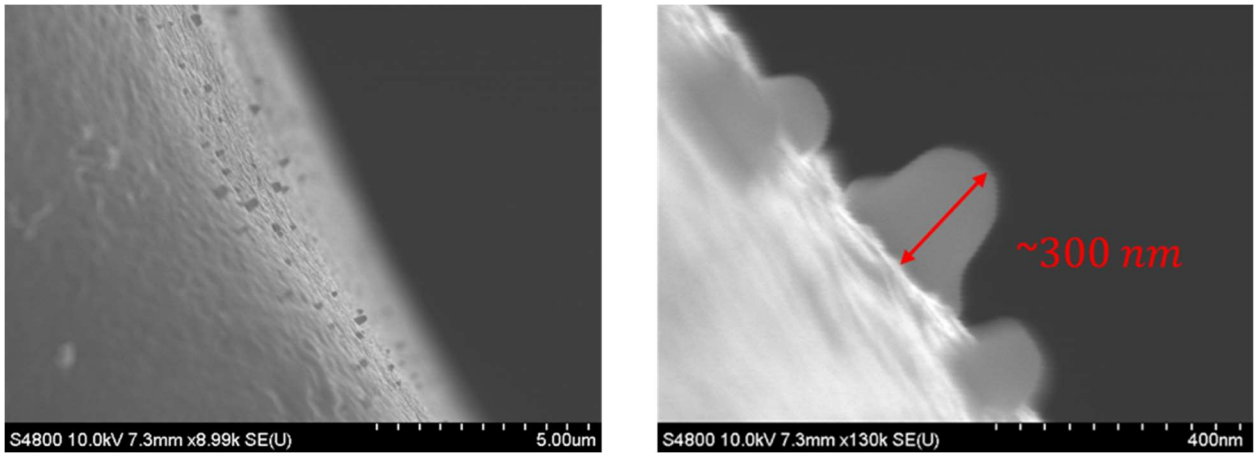

Figure 3.8 Other morphologies observed in the distal regions of the tubing about the point of contact. These protrusions were observed to be similar to other morphologies observed in the standard treatment profiles.

The results from the pin electrode test confirmed that extreme morphologies could be generated and that treatment times could be reduced by narrowing the ground electrodes. However, the results of these treatments were highly heterogeneous, and required further development for adaptation into the apparatus for practical applications.

In addition to the pin electrode treatment, a further test was performed to analyze the effect of electrode contact on surface morphology. In this test, an electrode was fabricated with identical thickness of the standard electrode apparatus, but with a $\frac{3}{64}$" thru hole for the tubing to pass though. This permitted almost zero clearance for the tubing, allowing for uniform tight contact of the ground electrodes to the tubing, while keeping all other parameters of the electrode geometry constant. Samples were treated in identical fashion, with voltage and treatment time being kept constant.

Similar to the pin electrode test, plasma discharge about the ground electrodes were observed to be noticeably brighter than the loose electrode arrangement, and the tubing from the tight electrode arrangement was notably more opaque than the loose arrangement, though the

opacity presented over a shorter length of tubing, indicating that the region of treatment had been tightened about the electrode. After treatment, samples from both arrangements were prepared and analyzed under SEM.

SEM analysis showed that the treatment from the tight electrode produced a substantially more densely roughened surface. Rather than protrusions of roughly $0.5\,\mu m$ presenting with substantial interstitial space as observed in the loose hole arrangement, the morphology of the tightly fitted electrode was substantially more heterogeneous on the micron-scale.

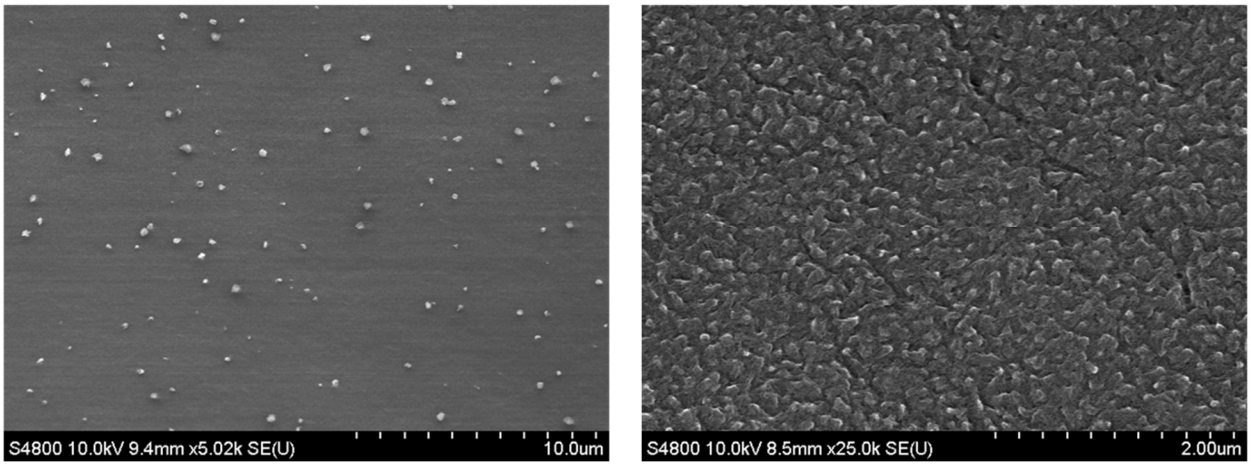

Figure 3.9 Left: Characteristic morphology of the plasma treatment in the loose-fit arrangement. Right: Characteristic morphology of samples produced from the tight-fit arrangement. Increasing electrode contact results in a much more substantially densified surface profile.

The results of these two tests were used to inform further modifications to the plasma treatment apparatus. By improving the consistency of the contact of the ground electrodes radially on the tubing, and reducing the total contact of the electrodes on the tubing, it was supposed that more extreme, dense morphologies could be produced on a shorter time-scale than previously possible. This capability would allow for a spool-fed tubing treatment capability to produce homogeneous morphologies on arbitrary lengths of tubing, enhancing the scalability and applicability of the treatment apparatus.

3.1.4 Modifications to System

To widen the capabilities of the system and further enhance the homogeneity of the treated tubing, several additional modifications were made. To implement more capability in gas control, a second Alicat MC-200SCCM flow controller was added, operating with 20 psi of upstream pressure, and specially tuned for each type of working gas. The addition of a second flow controller provides capabilities to inject seed gas as a partial flow fraction of the working gas, Helium. Several working gasses were considered for use in this system, including oxygen, nitrogen, ammonia, and dry air. In practice, there is functionally no limit to the gas type or the variety of mixtures that can be used as a seed gas in the working gas. The only limitation is the dampening of the plasma discharge induced by gasses that have greater breakdown thresholds, such as oxygen. For example, it was observed that arcing between the high voltage electrode and the ground electrodes occurred before DBD breakdown inside of the tubing at oxygen flow ratios greater than 5% of the helium flow.

Observations were made that sharper ground electrodes and consistent contact between the outside walls of the tubing and inside walls of the electrodes significantly impacted surface morphology. Simple changes in electrode geometry produced more substantial morphological changes on the inner surface of the tubing and reduced the treatment time necessary to produce equivalent surface morphologies observed in the previous setup, which used loose, wider ground electrodes. As a result, implementations were made to modify the ground electrodes to improve their performance. The electrodes were replaced with thin sheets of copper with carefully drilled thru-holes using a 3/64” drill bit to most closely match the OD of the tubing in use. The results of these modifications will be more closely discussed in following sections.

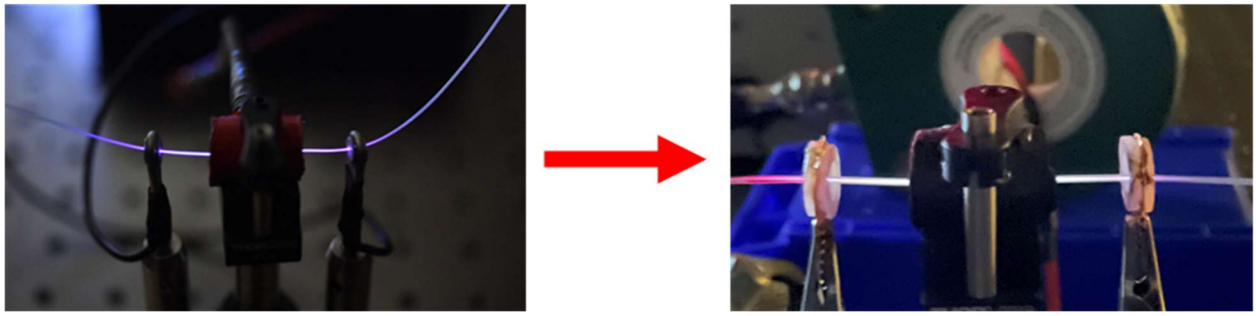

Figure 3.10 Modifications made to the ground electrode to intensify and expedite the formation of morphologies of interest, and allow for implementation of a spool fed treatment profile for improved homogeneity of surface morphology. Left: Treatment arrangement “A” Right: Treatment arrangement “B”

The final major modification to the system was the capacity for linear translation of the tubing through the working section of the apparatus. The initial intended solution was the implementation of two bobbins (one to feed and one for uptake). Due to space constraints and to remove unnecessary mechanical complexity, it was instead decided that a linear actuator would be used. The “feed” system is comprised of a gantry with a counterweight to provide tension in the tubing, and a carriage mounted on a worm gear, driven by a stepper motor, with a clip for the tubing to attach to. The stepper motor is operated by a 12 volt power supply connected to a timer relay to provide step control. Because the treatment time necessary for the production of desirable surface effects was long relative to the continuous feed speed of the developed system, the motor was instead programed to make discreet steps of approximately 1 mm, and the time between steps was programmatically controlled to define the feed rate of the system. The results of these modifications and their effects on homogeneity will be discussed in more detail in later chapters.

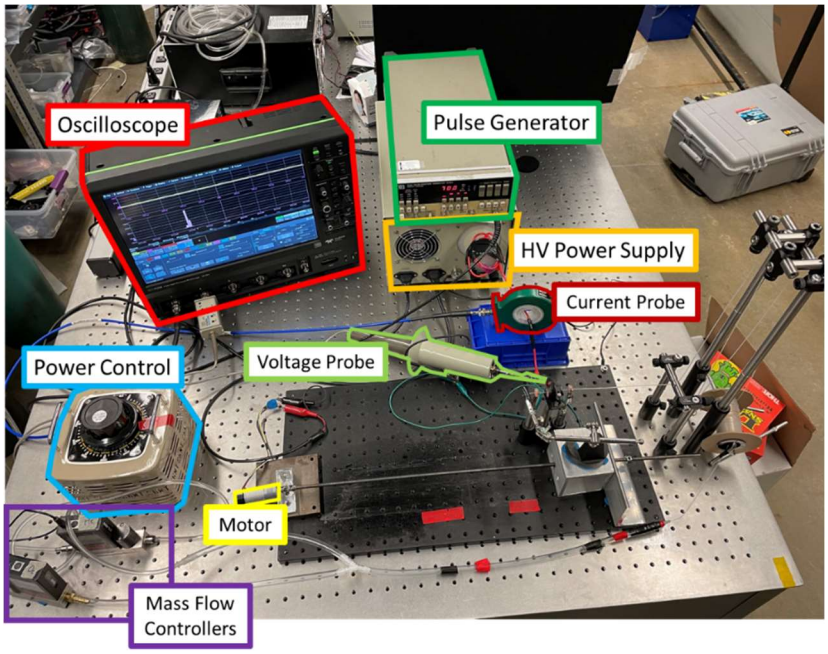

Figure 3.11 Macroscopic view of total system, complete with oscilloscope, voltage and current probes, signal generator, stepper motor, mass flow controllers, variable transformer, power supply, and electrodes. The signal generator was later replaced with a more versatile relay switch.

3.1.5 Measurement of Latent Power Draw

To streamline the process of measuring the power draw from the plasma discharge only, an effort was made to identify and characterize the power draw from latent sources in the plasma treatment apparatus. The intention was to use this system characterization, should it be correlated to a simple function with a reasonable fit, to directly calculate plasma discharge power by subtracting the theoretical latent power draw from the total measurements in real-time. This modification to the measurement process would greatly expedite the process of measuring plasma discharge power and reduce changeover time between treatment regimes.

To identify and characterize the power draw from sources outside of the plasma discharge, a series of tests was performed to measure the power draw from the plasma system without plasma discharge. To achieve this, the tubing was removed from the electrode system, and total power

measurements were taken using the standard techniques used for power measurements. Measurements were taken at various peak-to-peak voltage values consistent with the range of voltages characteristic of the operational ranges under investigation for plasma treatment. Due to the analog nature of the voltage transformer, it was not possible to achieve uniform step sizes from measurement to measurement, but a best effort was made to make the step sizes small enough to capture the macroscopic characteristics of the evolution of the power draw with respect to voltage. Average power measurements were recorded after an averaging of 1000 samples on the oscilloscope and was recorded in the plot below.

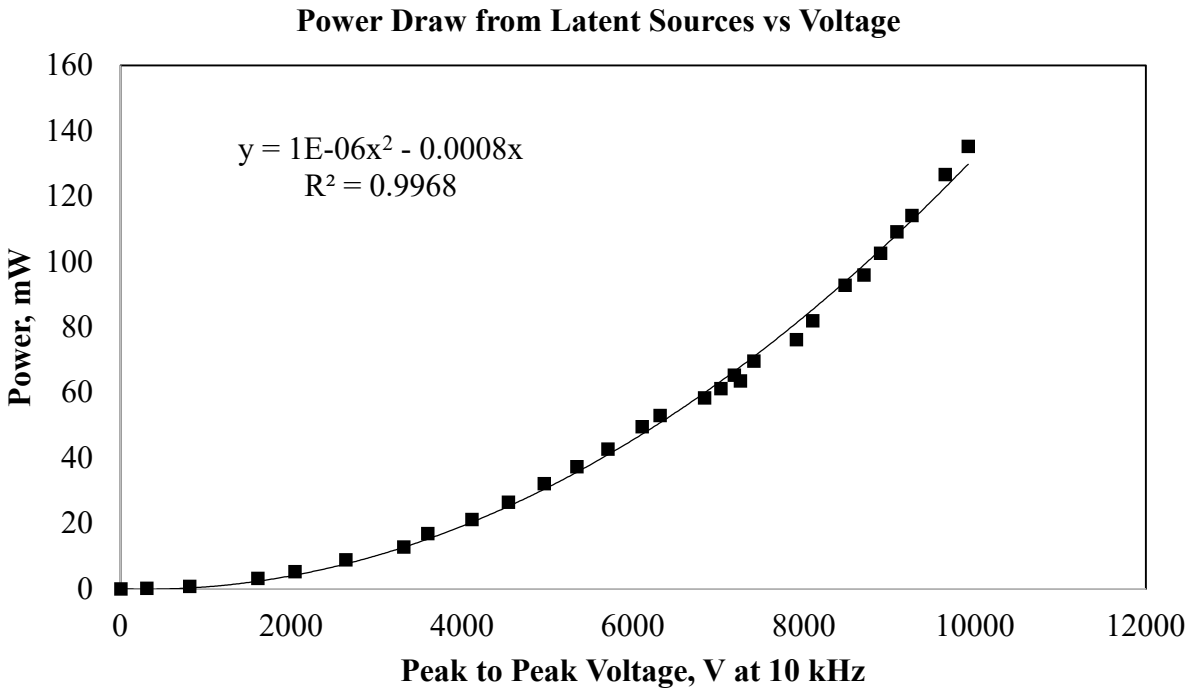

Figure 3.12 Measurements of latent power draw from sources other than the plasma discharge. The trend of power consumption closely follows a 2nd-order polynomial trend.

The trend of power dissipation from latent power sources as a function of voltage closely follows a 2nd-order polynomial form. The results of this investigation were not surprising, and

indicates that the dominant source of latent power draw comes from capacitive sources, following the below modified equation for power draw from a capacitor take from the characteristic equation for stored energy of a capacitor:

$$P = \frac{CV^2}{2t}$$

where we can assume the capacitance, C, of the latent system to be constant, and the energy is directly proportional to power as the measurements were all taken over fixed time steps. This investigation was useful in identifying the dominant sources of latent power draw. The correlation was successful in predicting plasma discharge power draw directly from the total power draw measured, but only on the day the correlation was made. Ultimately this correlation was not useful due to unpredictable variation in system capacitance due to changes in atmospheric composition, introduction of additional capacitive sources from other experiments in the laboratory environment, etc. As a result, isolating the power from the plasma discharge was performed by direct sampling of discharge power with and without plasma present at a fixed voltage, and calculating plasma power as the difference of the means of those sample sets.

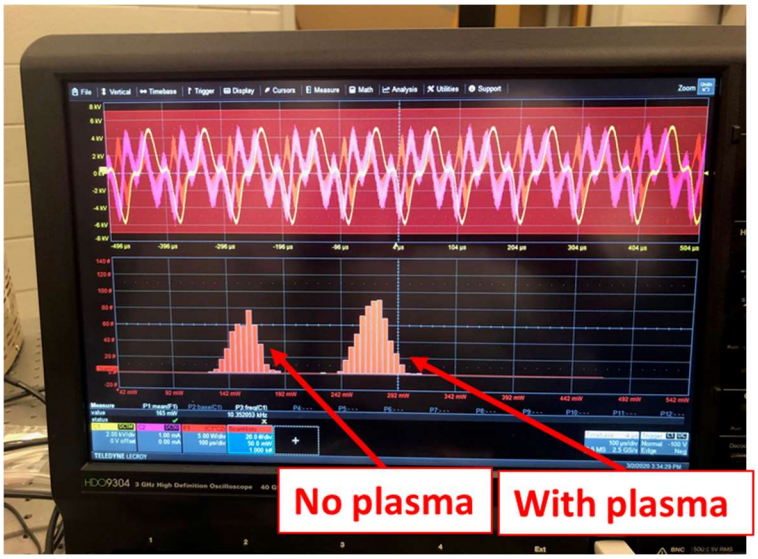

Figure 3.13 Visualization of the normal distribution of power measurements, with and without plasma discharge at a fixed voltage.

3.1.6 Summary of Plasma System and Experimental Conditions

The final treatment apparatus was oriented in two arrangements. Both arrangements are consistent in geometry in all aspects but the ground electrodes that were used. The central high voltage electrode is 2.2 cm in length, with a 1 mm ID copper tube encased in Teflon insulation. The spacing between the edges of the high voltage electrode and the ground electrodes is maintained at 1 cm. The first arrangement, called arrangement "A," has loose ground electrodes, $\frac{1}{4}$ cm thick, and 5.3 mm diameter thru-holes. Arrangement "A" was used for stationary treatment profiles used for morphology analysis and quantification. Arrangement "B" had ground electrodes fabricated from 0.1 mm thick copper sheet, with a 1 mm thru-hole for a tight fit of the LDPE tubing. This arrangement was used with a linear actuator to produce homogenous treatments over longer lengths of tubing for wettability studies.

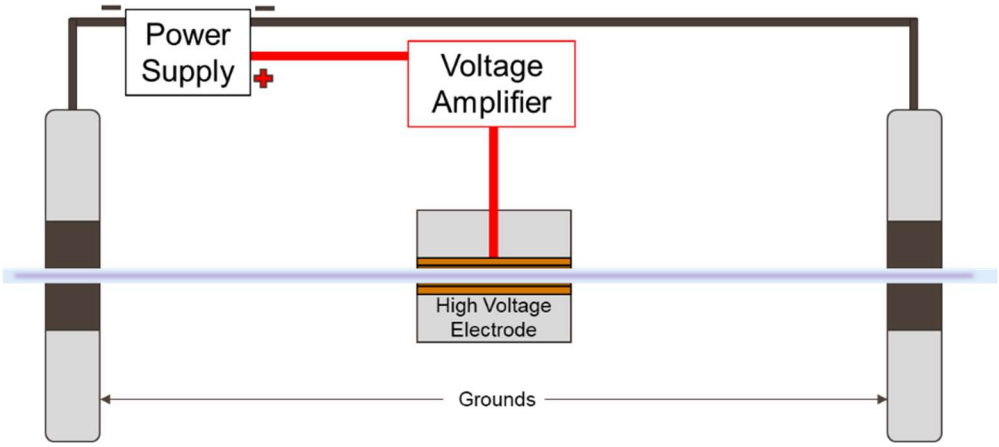

Figure 3.14 Basic diagram of the DBD plasma treatment apparatus. The system was implemented with two ground electrodes set equidistant from the centerline of the high voltage electrode for symmetry. The ground electrodes were changed for arrangement "A" and "B" for different analyses of plasma treatment.

3.2 Plasma Induced Surface Morphology

This section outlines the qualitative and quantitative analysis performed on LDPE tubing treated by the atmospheric pressure DBD plasma treatment apparatus. Included in this analysis is a comprehensive analysis and discussion on the presentation of different morphologies produced by SEM analysis. Additionally, presentation and discussion of three key metrics of the surface morphology and how they correlate to plasma power, treatment time and total dose, as well as discussion on the positional impacts of surface morphology relative to the electrode geometry.

3.2.1 Qualitative Observations of Polymer Morphology

A critical, though imprecise methodology for determining the effect of different plasma treatment profiles was qualitative analysis via SEM. By observing characteristic morphologies from different plasma parameters and electrode arrangements, we can illustrate meaningfully the wide variety of surface features that can be generated from this novel treatment apparatus.

Baseline analysis was performed on untreated LDPE tubing. SEM imaging of the inner surface of the tubing via longitudinally and axially bisected samples showed little morphological variation and almost no topographical variance. The surface of the tubing, aside from some small defects, either from the extrusion process of possible from the preparation of the sample, the tubing had virtually no observable roughness at 1,000x magnification, and was observed to have mild "rippling" at a sub-micron scale when imaged at 10,000x. Numerous observations of untreated samples over the course of this thesis work showed consistent characteristics.

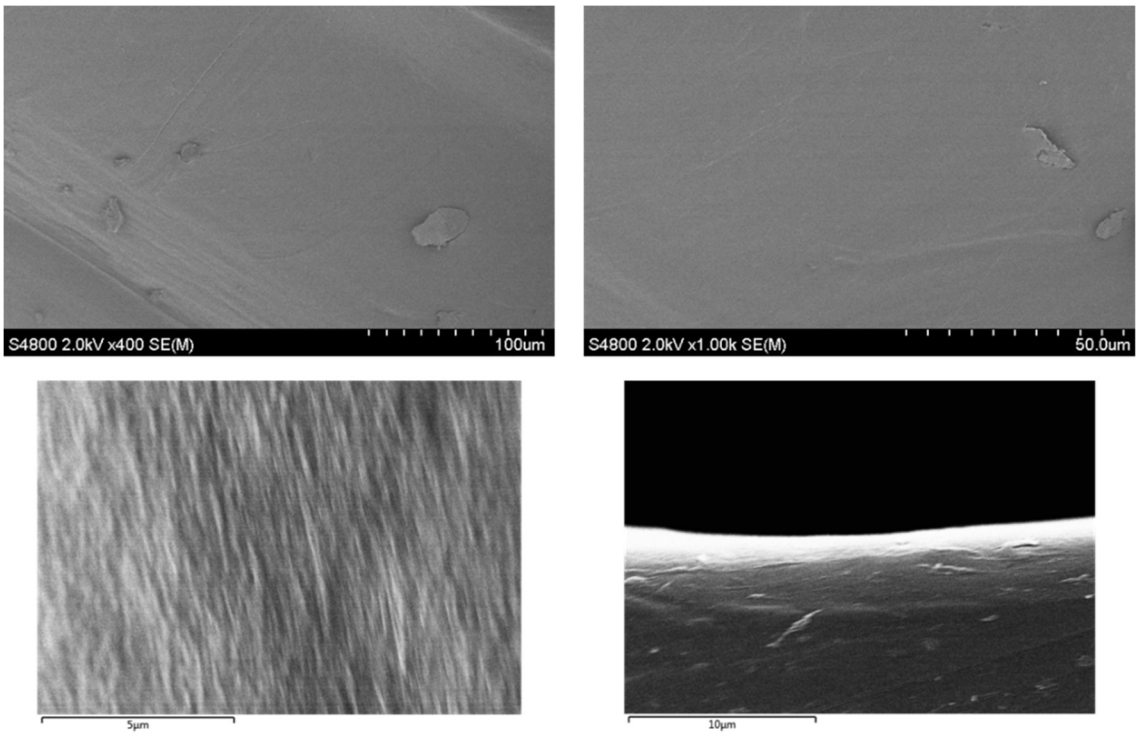

Figure 3.15 SEM imaging of raw (untreated) LDPE tubing. Top Left: 400x magnification showing macroscopic presentation of the polymer surface. Top Right: 1,000x magnification showing intermediate presentation of surface morphology. Bottom Left: 10,000x magnification showing microscopic surface morphology, including mild rippling/striations commonly observed on untreated surfaces. Bottom Right: Cross-sectional view of untreated polymer surface, showing a uniformly smooth surface (no significant protrusions/aspersions).

Throughout the course of this thesis work, numerous surface morphologies have been induced as a result of varied parameters related to the plasma discharge as well as electrode

grometry. However, the dominant surface feature that has become of interest, and the primary morphology type that has been observed, is a distribution of random aspersions, or protrusions, that have presented in a variety of shapes, sizes, densities, etc. In an effort to highlight pictographically the broad range of protrusion-specific morphologies that have been observed, SEM images of a few of the most common morphologies have been curated.

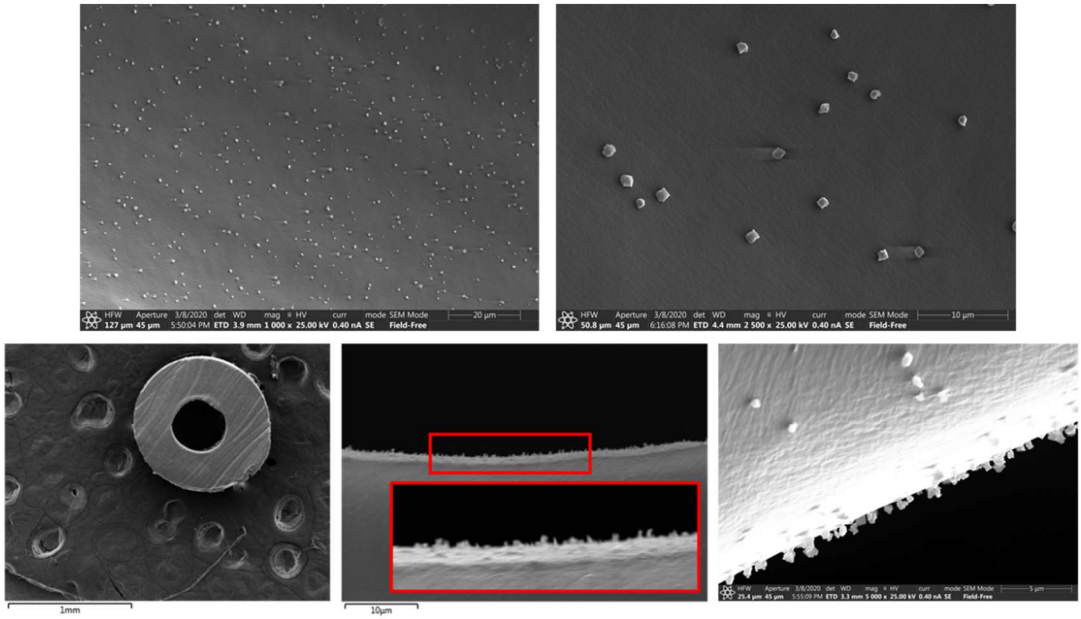

Figure 3.16 A common presentation of surface morphology induced by plasma treatment. Protrusions vary in density by orders of magnitude, and range in size from $0.1 - 1\ \mu m$. Samples were treated with arrangement A for 30 minutes at plasma powers estimated around 20-30 mW.

Figure 3.16 illustrates the most common morphology that has been observed from plasma treatment efforts. Here, protrusions present as random apparent emergences from the inner surface of the tubing. It is theorized that these protrusions are the result of local thermal events resulting from small defects on the surface of the tubing that can act to enhance the electric field about the defect. This local intensification of the electric field about the dielectric surface may act as a highly confined dielectric heating event, inducing a rapid change in the structure of the polymer leading to an eruption of material from the surface.

The resulting protrusions have been demonstrated to be repeatably induced by specific plasma treatment regimes and vary in density and size by orders of magnitude, dependent on numerous factors related to the plasma parameters and the electrode geometry. These protrusions are potentially capable of promoting surface adhesion through mechanical interlocking. Additionally, at certain densities there is potential for the promotion of certain desirable adhesion and wettability properties, including hyper-hydrophobicity and hydrophilicity.

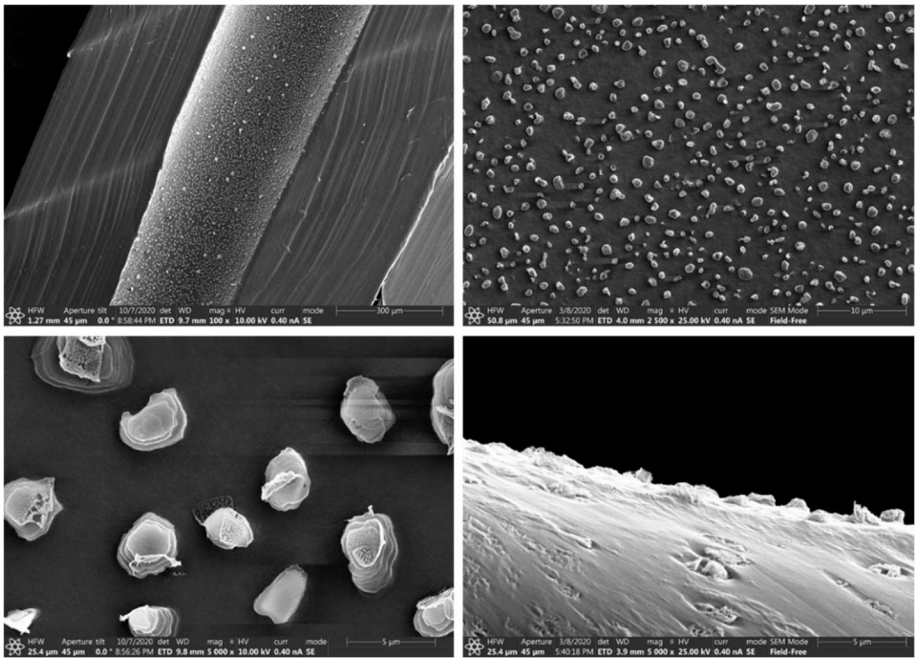

Figure 3.17 More extreme surface morphology of the same classification as discussed in Figure 3.16. This morphology is more regularly shaped with more stable connection with the surface of the LDPE tubing. Samples were treated with arrangement B for 30 minutes at plasma powers estimated around 20-30 mW.

The protrusions resulting from certain treatment profiles are irregularly shaped and often have a mushroom cap-like shape, having a large body that narrows to a thin neck at the surface. This necking has been observed to have strong connection to the surface or be extremely delicate. The delicacy of these protrusions was demonstrated with a simple flushing of the tubing with

deionized (DI) water, followed by SEM analysis of the sample after drying. In many cases, the protrusions were no longer evident, but rather small peaks were observed, evidently remnants from protrusions separated from the surface by fluid friction.

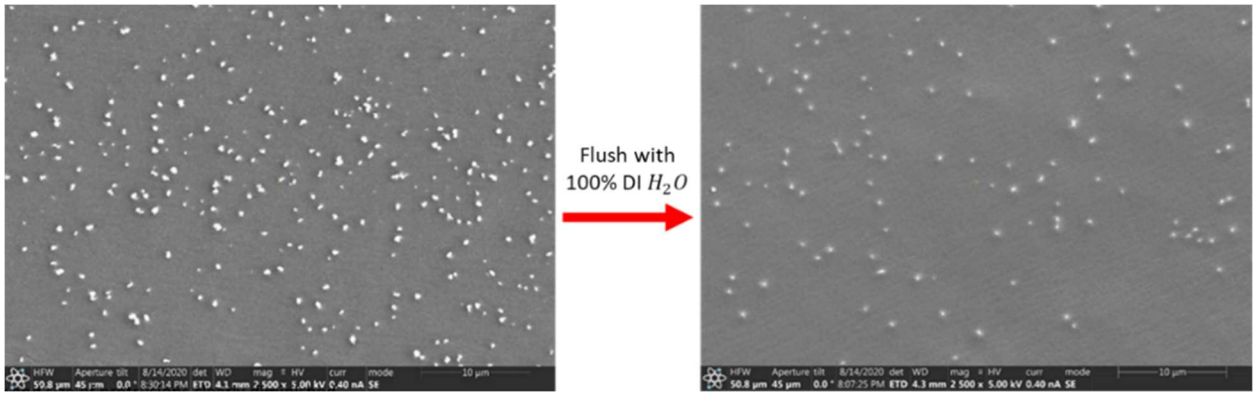

Figure 3.18 Left: Morphology of LDPE surface after plasma treatment. Right: Morphology of LDPE surface after plasma treatment and flush with DI water. Protrusions are clearly reduced in size and appear less bright, indicating a smoother surface. Samples were treated with arrangement A for 30 minutes at plasma powers estimated around 20-30 mW.

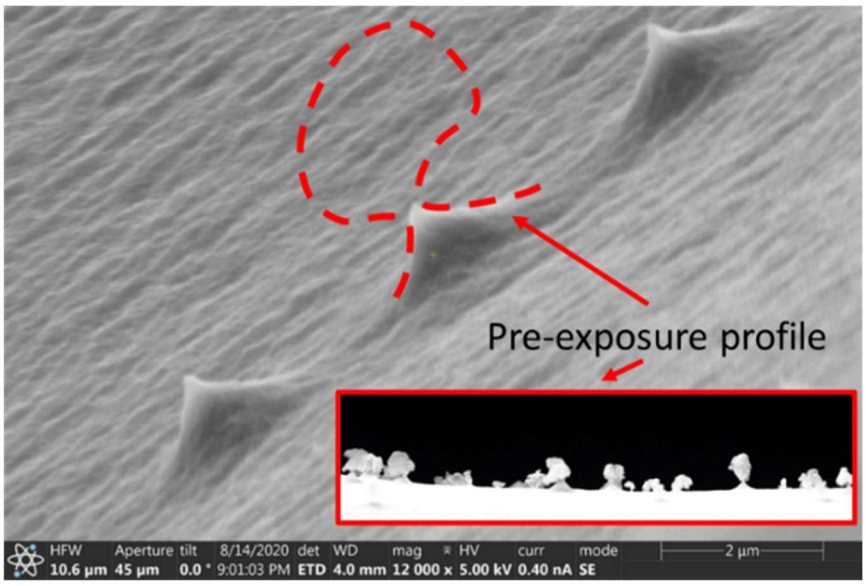

Figure 3.19 Side-on SEM image of protrusions after DI water flush, with cross-section of original surface boxed in red for comparison. It is evident by this comparison that a simple flush has removed the bulk of the protrusions as a result of the weak attachment of the protrusions to the surface.

A second morphology that has been observed on the surface of treated LDPE tubing is a more homogenously distributed and dense morphology. These surfaces are highly roughened. The means of generation of these morphologies is less clear; the morphologies are more likely the result of surface etching, but may be emergences, similar to the previously described morphologies. Additionally, these features are more limited in their size and densities, tending to consistently be $\sim 100\, nm$ in diameter with $\sim 1\, \mu m$ interstitial spacing. This morphology does not present with mushroom-cap bodies, but rather has more solid, sub-micron aspersions.

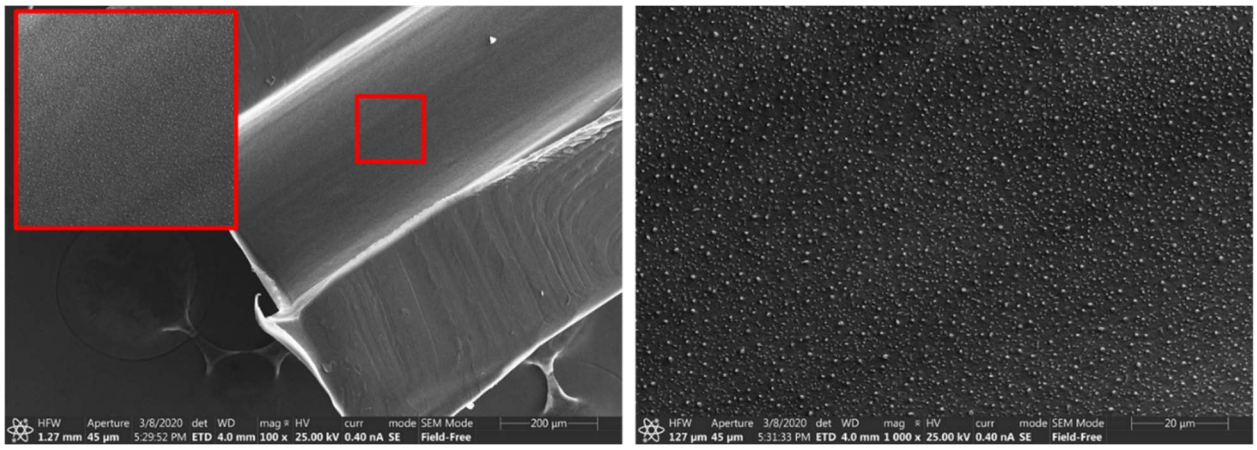

Figure 3.20 SEM imaging of surface morphologies of a second type induced by the atmospheric-pressure DBD plasma treatment apparatus. This morphology is more limited in size and density and is possibly a result of surface etching as opposed to emergences of other protrusions. Samples were treated with arrangement B on a continuous feed of 2 mm/min at plasma powers estimated around 20-30 mW.

In addition to morphologies formed at the micron scale, additional surface features were observed of substantially sub-micron ($\sim$10s of nanometers) size. These features were observed in two primary categories: a dappled, protrusion-like surface with surface striations visible between them, produced exclusively at very high plasma powers ($> 50\, mW$), and a latticed morphology with numerous crater formations separated by thin raised walls. The first of these two morphologies, pictured in Figure 3.21, may be explained similarly to the protrusion morphology

discussed at the micron scale, as a result of E-field concentration induced by surface imperfections in the dielectric material. It can be expected that smaller surface imperfections would be more densely distributed on the surface. These small imperfections would naturally generate less concentrated electric fields, and therefore, the resulting surface modification would occur at a smaller scale.

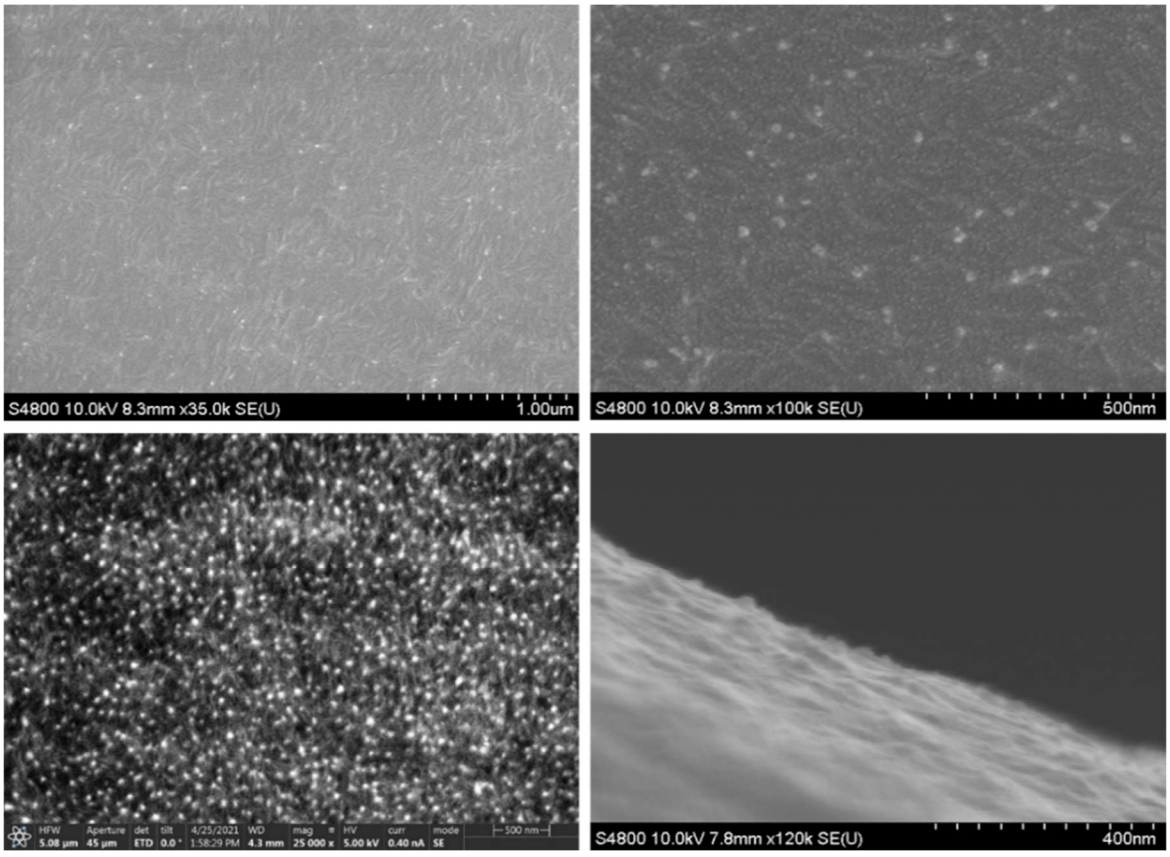

Figure 3.21 SEM imagery of nanometer scale surface protrusions induced by plasma treatment at very high plasma powers, $> 50\ mW$. Protrusions consistently have roughly proportional height to width ratios similar to the larger protrusions observed at the micron scale. Samples were treated with arrangement A for 30 minutes at plasma powers estimated around 20-30 mW.

The second nanometer scale morphology, shown in Figure 3.22, is more commonly observed, and occurs in most regions of the plasma discharge at low to moderate power ($10 - 50\ mw$), in the interstitial space between protrusions as well as in regions away from electrodes

where the plasma discharge has weaker interactions with the dielectric surface. This surface pattern is potentially a result of the formation of a cross-liking layer of polyethylene forming on top of the more regularly structured bulk material as a result of free radicals in the plasma medium interacting and restructuring the polymer on a molecular scale. Observations shown in Figure 3.22 are characteristic images of nanoscale morphology found on the inner surface of tubing throughout the overall length of the treated tubing, in the regions between the ground electrodes and the high voltage electrode.

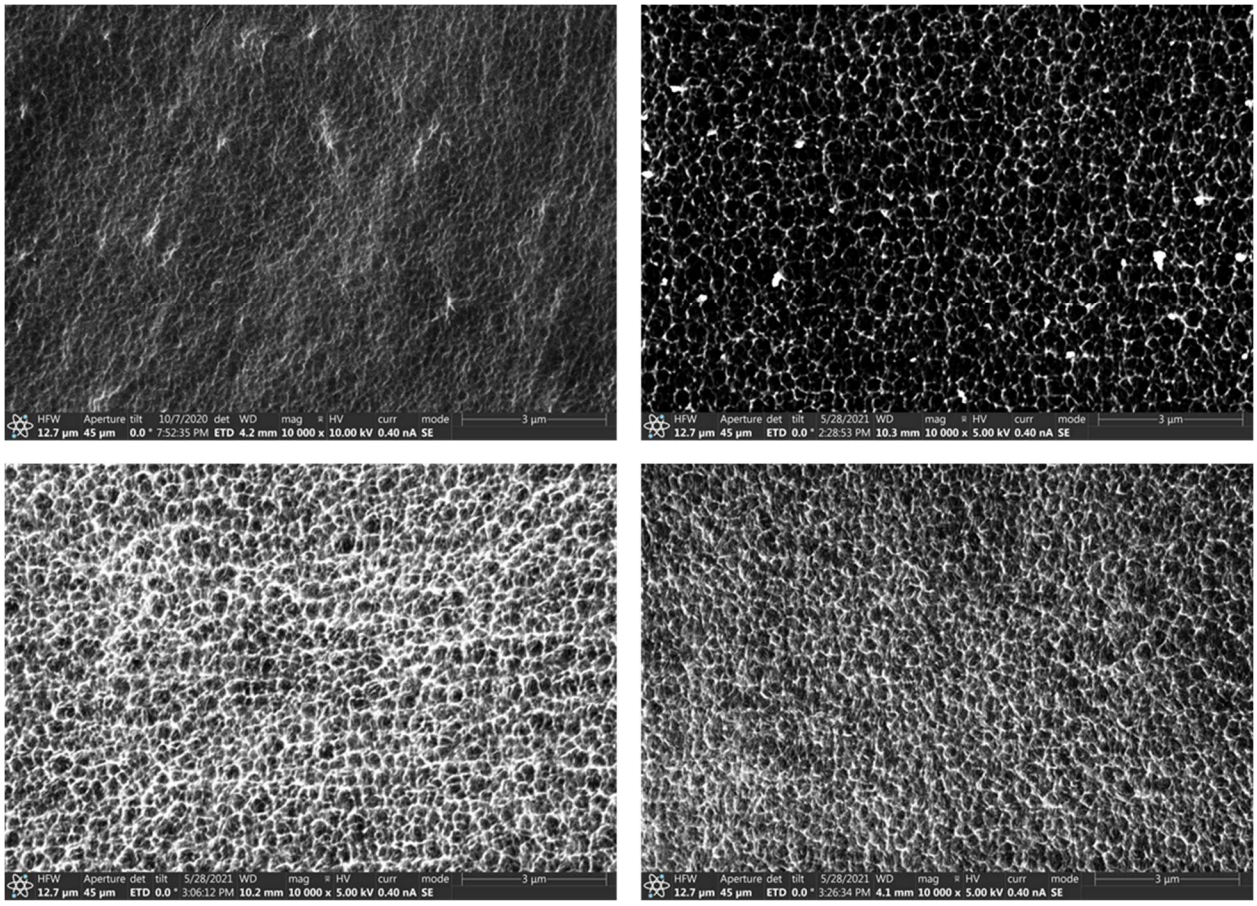

Figure 3.22 Common nanometer scale morphology induced on LDPE surfaces as a result of plasma treatment. These morphologies are potentially a result of cross-linking commonly induced by plasma treatment with neutral gasses. Samples were treated with arrangement A for 30 minutes at plasma powers estimated around 35-45 mW.

3.2.2 Impact of Exposure Time on Surface Morphology

LDPE tubing was treated in the Atmospheric Pressure DBD plasma treatment apparatus at a series of treatment times commensurate with times previously observed to produce interesting surface features, from $5 - 45$ minutes. Samples were treated using the arrangement "A" of the treatment apparatus. The tubing was kept stationary for the treatment, without any linear actuation. Samples were treated uniformly at a discharge power of $35\ mW$, a power level selected for its consistency in producing substantive protrusion morphologies across a broad range of exposure times.

After treatment, observations were made of the opacity changes induced on the tubing. For treatment times of 15, 30, and 45 minutes, significant opacity was observed in the regions on either side of the ground electrodes, with greater opacity observed on the sections of tube immediately on the outer edges of the ground electrode. Additionally, at 45 minutes, opacity was observed around the regions of the tube positioned around the high voltage electrode, though to a lesser degree.

Figure 3.23 shows SEM imaging of characteristic morphologies of tubing in regions of peak protrusion density. Surface morphology evolution as a function of time followed a dynamic pattern. Throughout the evolution of the surface morphology, there are two main phases: densification, followed by coalescence. The first phase follows similarly to the trends observed in the power study. From 5 to 15 minutes of treatment, protrusions become dramatically more dense. However, at 30 – 45 minutes, it is observed that protrusions begin to combine into larger formations. ImageJ analysis is therefore perhaps somewhat misleading without these observations.

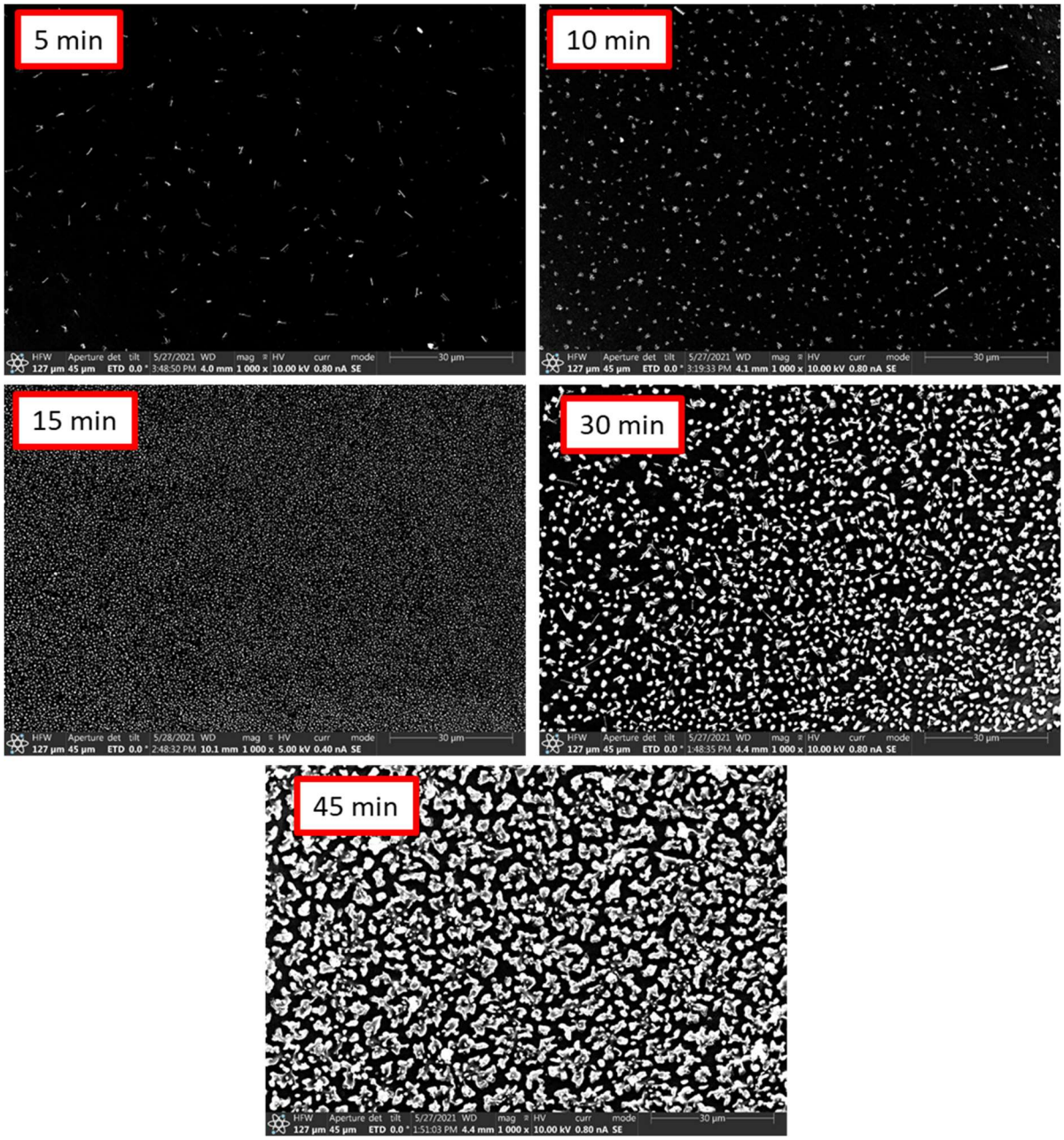

Figure 3.23 Characteristic images for peak morphological presentation at a selection of plasma treatment times for a fixed power level of 35 mW. Surface morphology evolution is more dynamic, showing a densification phase, and then a coalescence phase that begins at some point between 15 and 30 minutes.

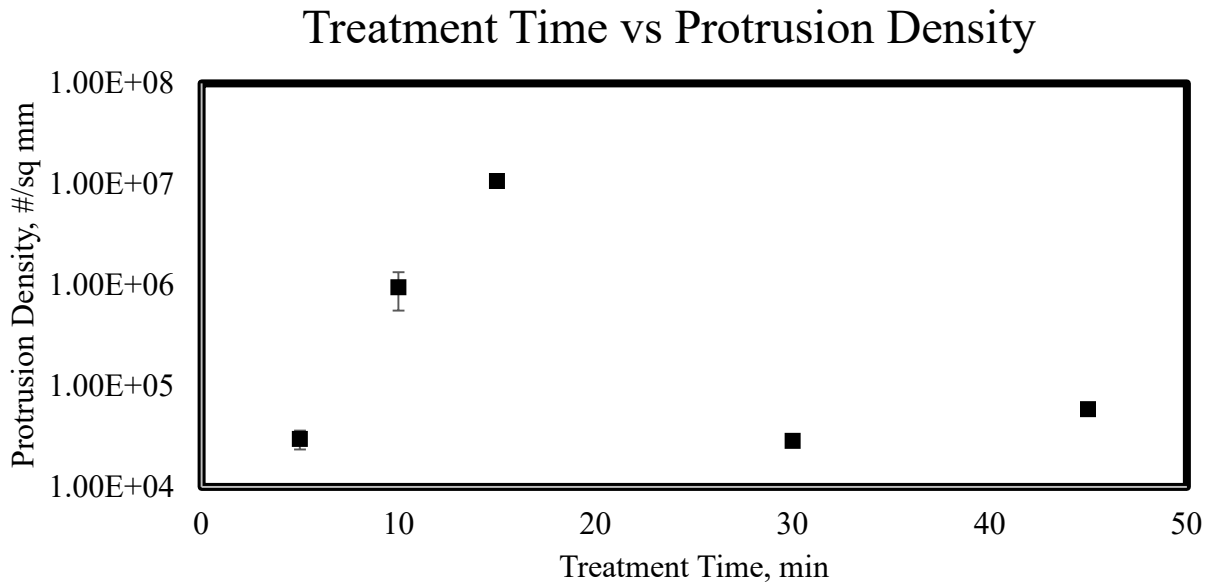

Figure 3.24 Trends of plasma treatment time impact on protrusion density at a fixed power level time of 35 mW. Protrusion density increases substantially during the first phase of morphology formation, with a shift downwards as protrusions coalesce.

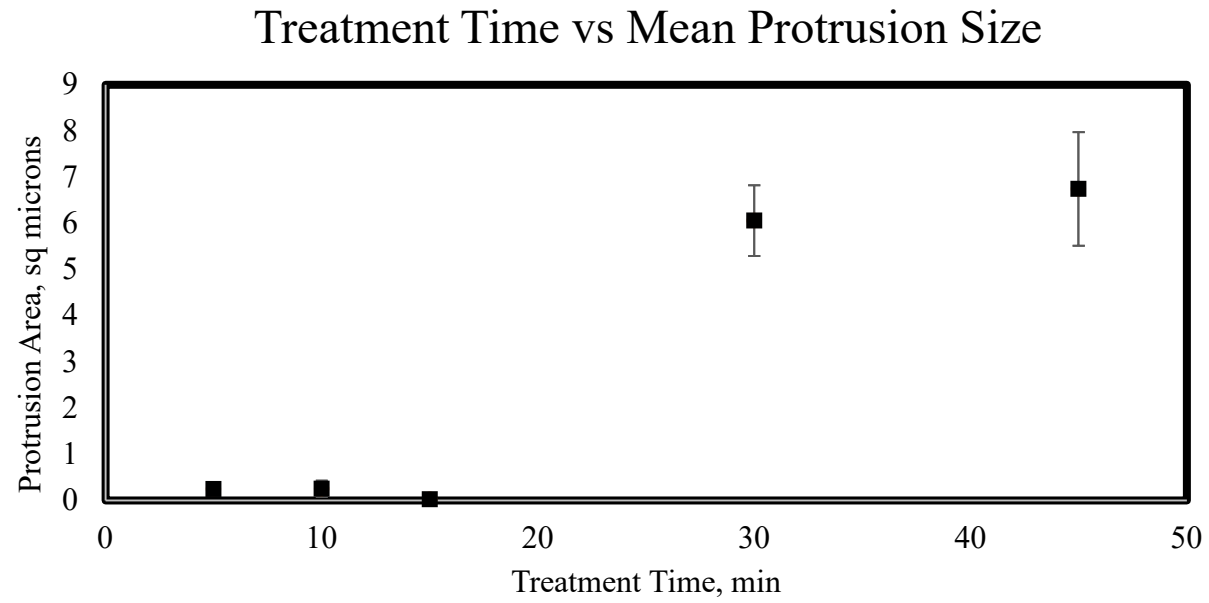

Figure 3.25 Trends of plasma treatment time impact on protrusion mean size at a fixed power level time of 35 mW. Protrusion size remains relatively constant as densification occurs during the first phase of morphology formation, with a significant shift upwards as protrusions coalesce.

Figure 3.26 shows the impact of treatment time on surface roughness parameter, R_a. As evidenced by visual inspection of the temporal evolution of surface morphology, R_a increases relatively linearly within the time scales observed. Observations of these three parameters of surface morphology for fixed time and power highlight the importance of using multiple metrics, as it is extremely challenging to capture the scope of morphology from a single parameter. Roughness values vary much more significantly as a factor of treatment time, swinging between values below ISO N1 roughness grade up to ISO N5.

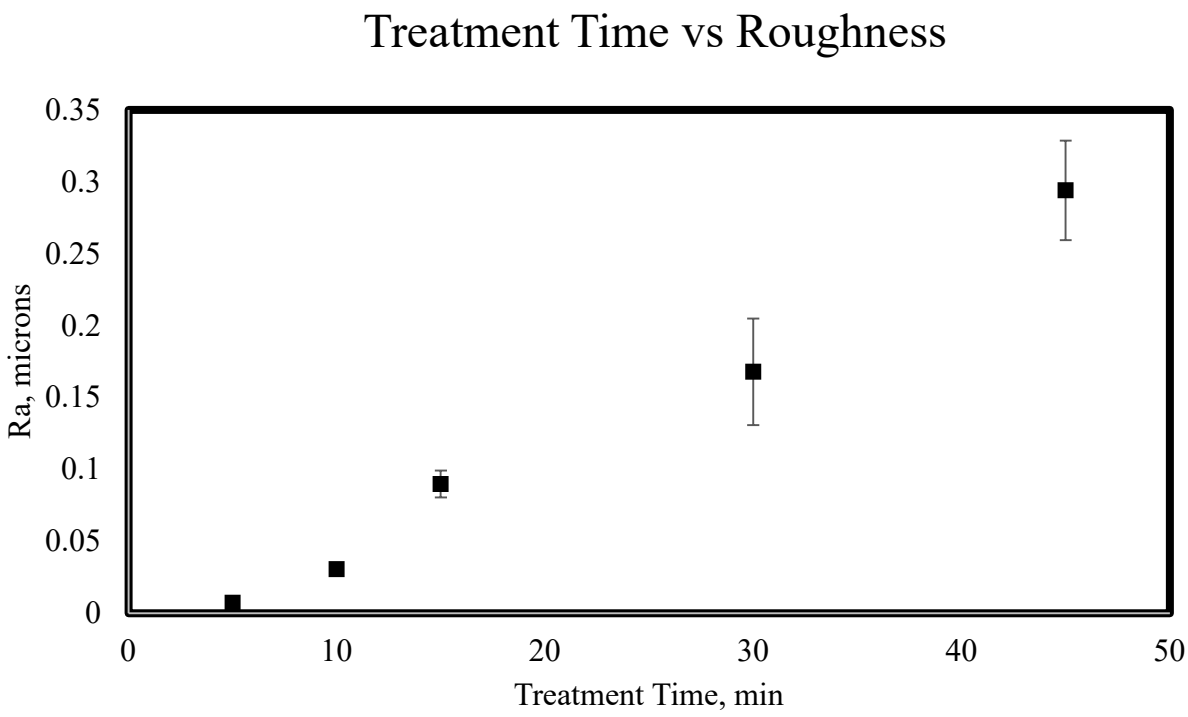

Figure 3.26 Trends of plasma treatment time impact on surface roughness factor, R_a, at a fixed power level time of 35 mW. The more dynamic evolution of protrusion morphology results in a trend of increasing roughness with time.

3.2.3 Impact of Discharge Power on Surface Morphology

LDPE tubing was treated in the Atmospheric Pressure DBD plasma treatment apparatus at a series of power levels within the range of treatment profiles that have been previously observed to be repeatable, from $9 - 45\ mW$. Samples were treated using the arrangement A. The tubing was kept stationary for the treatment, without any linear actuation. Samples were treated uniformly for 15 minutes, a time selected for its consistency in producing substantive protrusion morphologies across all plasma powers.

After treatment, observations were made of the opacity changes induced on the tubing. For all treatment profiles, significant opacity was observed in the regions on either side of the ground electrodes, with greater opacity observed on the sections of tube immediately on the outer edges of the ground electrode.

Figure 3.27 shows characteristic images of peak protrusion density for the plasma powers under investigation. It was generally observed that within the power levels treated, protrusion density increased substantially with an inverse trend in protrusion size. Quantitative analysis performed via ImageJ supported these observations. Data collected from image processing showed trends of surface morphology for varied plasma powers. Surprisingly, at lower plasma powers (9 mW being the minimum threshold for sustained plasma discharge), protrusions were observed to be substantially larger than at higher plasma powers. Not only were the surface features larger, but were also more densely clustered as a ratio of the surface area covered by protrusions to total surface area, with protrusions covering over 40% of the total observed surface in the most extreme cases, as compared to higher power profiles with coverages of $< 10\%$.

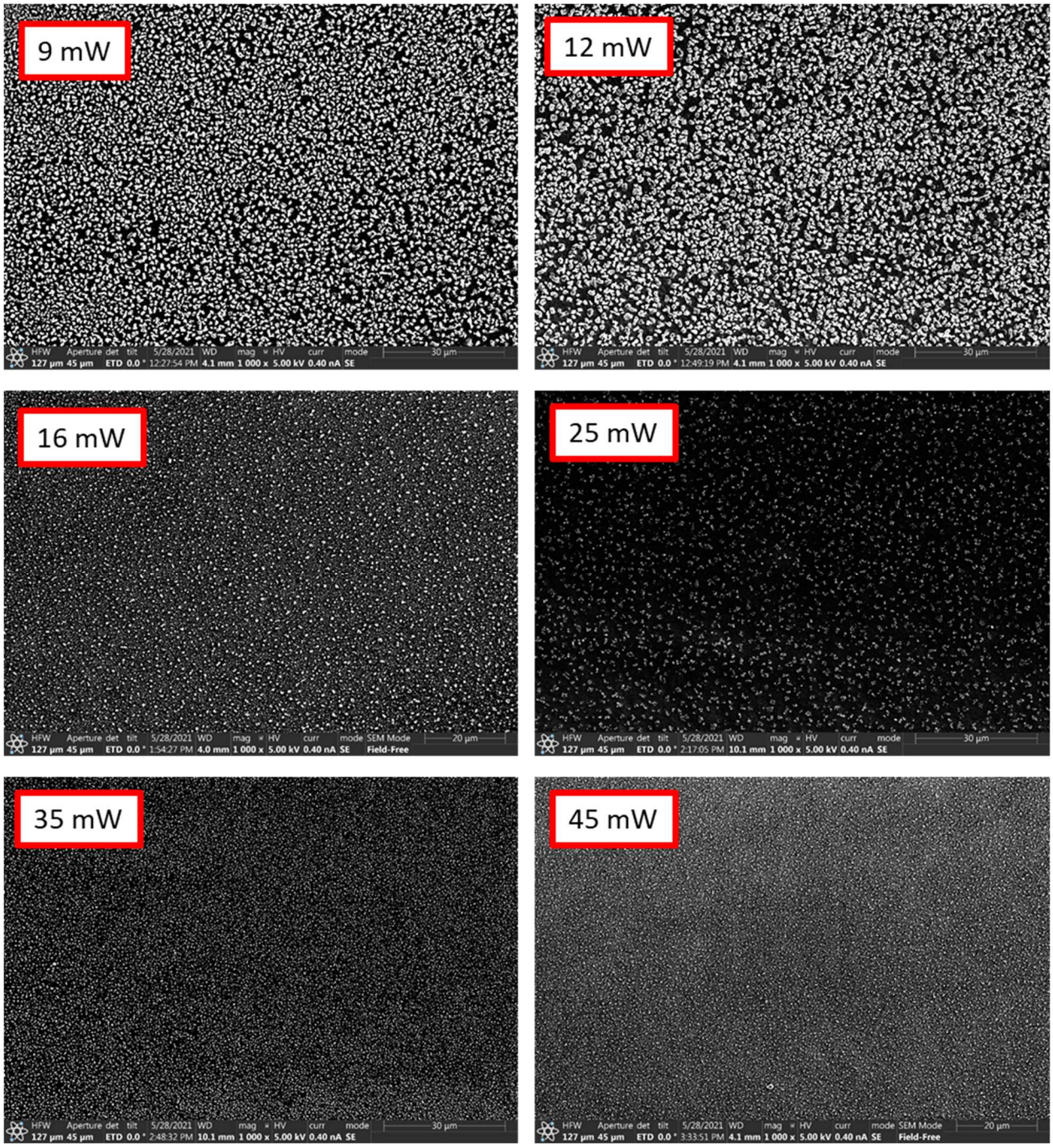

Figure 3.27 Characteristic images for peak morphological presentation at a selection of plasma powers for a fixed treatment time of 15 minutes. Protrusion size and density vary inversely with increasing power.

Figure 3.28 and Figure 3.29 show the trends of plasma power on protrusion density and protrusion mean size. As can be seen, Protrusion density increases dramatically, changing from

approximately $6 * 10^5 \frac{protrusions}{mm^2}$ to $2 * 10^7 \frac{protrusions}{mm^2}$ at power levels from $9 - 45\, mW$ The density saturated at power levels of 35 and 45 mW, with diminishing increases between power levels of $35\, mW$ and $45\, mW$. Similar inverse trends can be seen for protrusion size, with decreases in mean protrusion size from $.25\, \mu m^2 - 0.025\, \mu m^2$, with small increments of change observed at higher power levels.

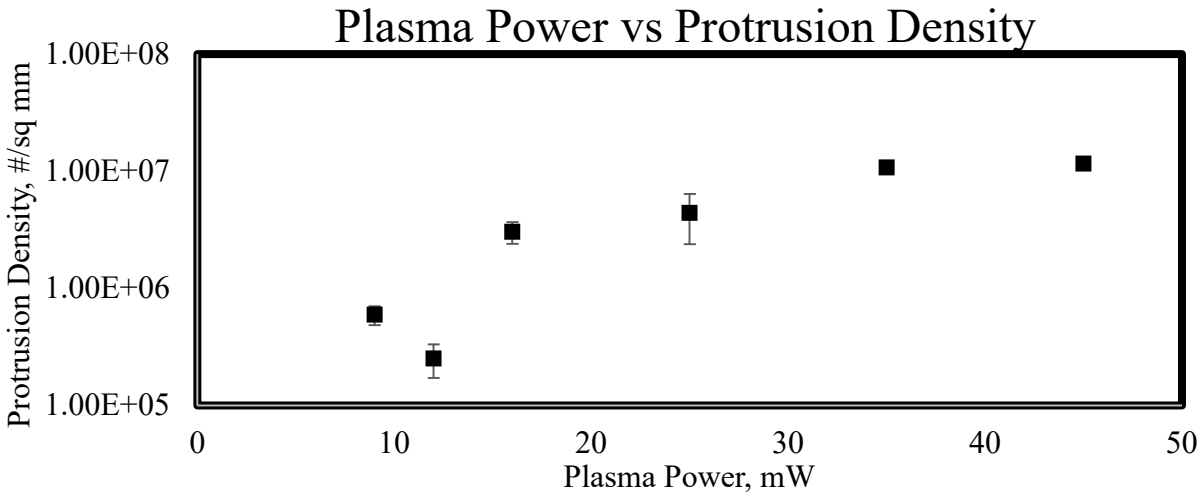

Figure 3.28 Trends of plasma power impact on protrusion density at a fixed treatment time of 15 minutes. Images were taken in regions of 25-27 mm from the centerline of the HV electrode. Protrusion density increases substantially with relatively small adjustments in plasma power, with changes of ~3 orders of magnitude across the plasma powers investigated.

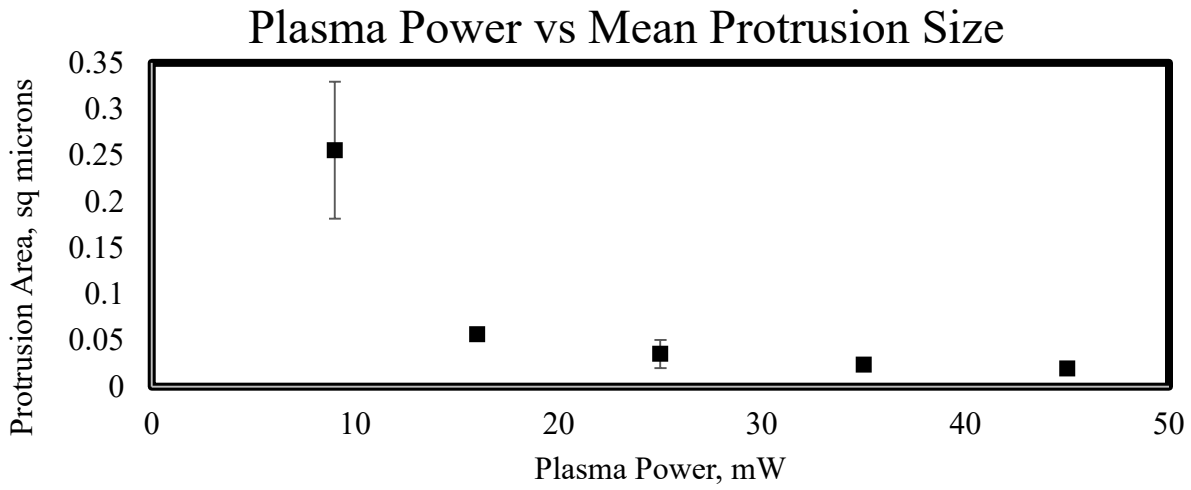

Figure 3.29 Trends of plasma power impact on protrusion mean size at a fixed treatment time of 15 minutes. Images were taken in regions of 25-27 mm from the centerline of the HV electrode. Protrusion mean size consistently trends inversely with density, with size decreasing by a factor of 10 across the plasma powers investigated.

Figure 3.30 shows the impact of varied plasma power against surface roughness. Interestingly, as a result of the inverse relationship of protrusion size and density with power, no great variation or trend was observed in the modified surface integral used to approximate R_a. R_a values vary from $0.04 - 0.1\ \mu m$ or, with respect to International Organization for Standardization (ISO) grade values for roughness, these values range from N1-N3.

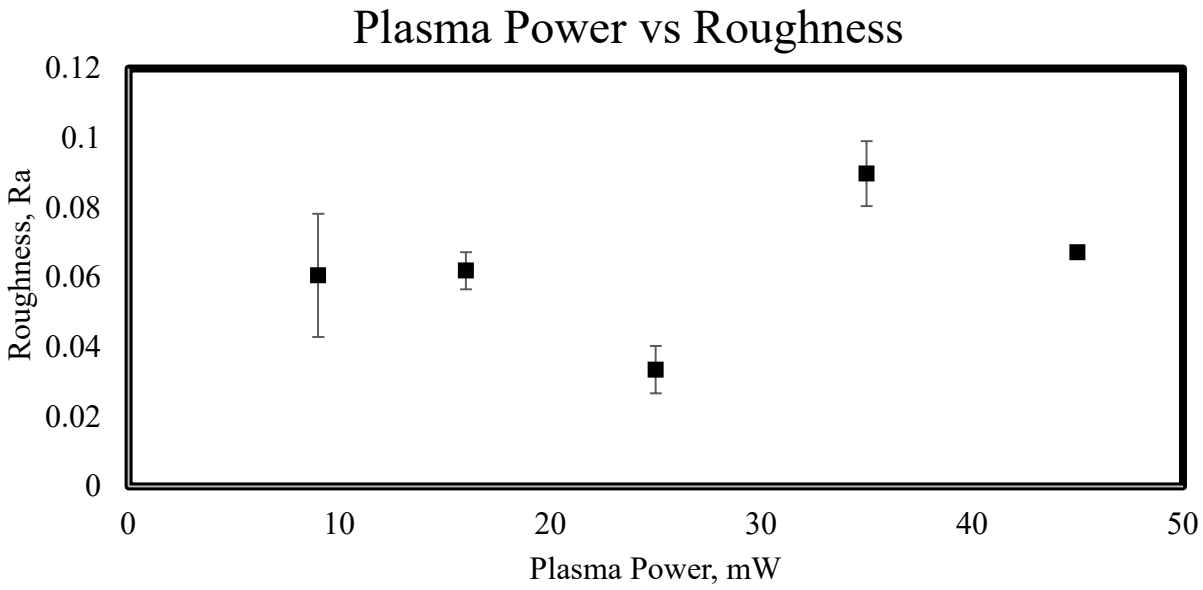

Figure 3.30 Trends of plasma power impact on roughness factor, R_a, at a fixed treatment time of 15 minutes. Images were taken in regions of 25-27 mm from the centerline of the HV electrode. Interestingly, as a result of the inverse correlation of size and density, surface roughness across these treatment profiles is somewhat constant: $0.04 > R_a > 0.09\ \mu m$.

3.2.4 Effect of Electrode Proximity on Surface Morphology

In the initial testing and characterization of the atmospheric pressure DBD plasma treatment apparatus, tubing remained stationary in with respect to the electrodes. As a result, highly heterogeneous morphologies were observed to form in regions proximal to the ground and high voltage electrode. Figure 3.31 illustrates typical variation of surface morphology change along short regions of plasma treated LDPE tubing over short ($4\ mm$) lengths in regions near to the electrodes. The sample was treated at a power level of approximately 40 mW for 30 minutes. Images were taken in increments of approximately 0.5 mm, in the regions from 30 – 26 mm from the centerline of the HV electrode. Generally, peaking points for morphology intensity has been observed in regions of tubing positioned immediately to the edges of the ground and high voltage

electrodes. This is unsurprising when considering the theory of morphology formation, as electric fields would be expected to be their most intense in these regions.

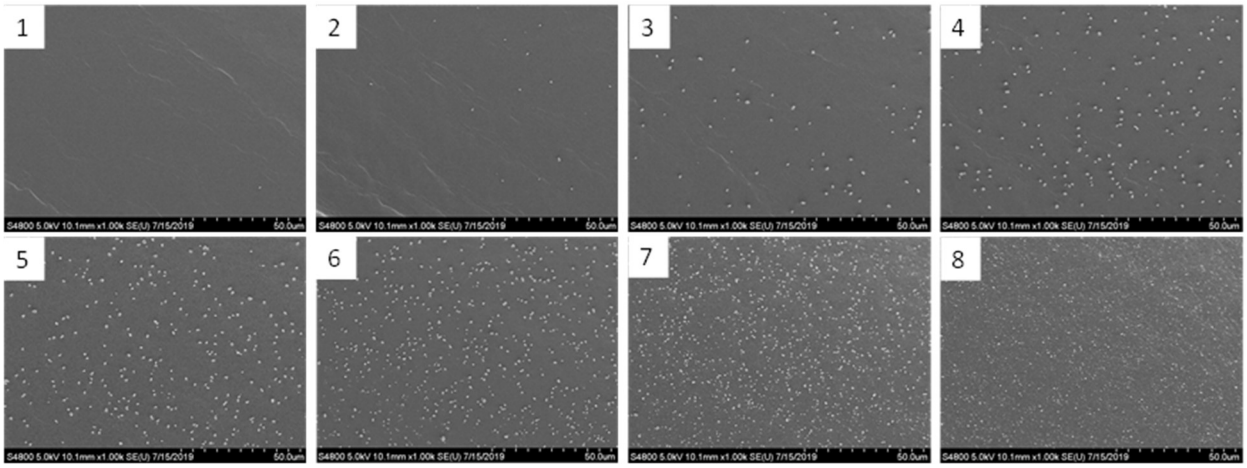

Figure 3.31 SEM images of surface morphology variation over 4 mm of LDPE tubing after stationary plasma treatment. Sample taken from tubing treated in immediate proximity to ground electrode. Protrusion density changes by several orders of magnitude in a very short region of tubing as a function of proximity to the electrodes.

To better understand the gradient of morphological formation with respect to electrode proximity, a series of samples were prepared at a range of power levels, with a fixed treatment time of 30 minutes. Samples were collected such that analysis could be performed on the region of tubing located between the outer edge of the high voltage electrode and the inner edge of one of the ground electrodes (the length of tubing between the red dotted line and black dotted line in Figure 3.32. Treated tubing was carefully marked to preserve reference points to allow for the imaged position of a given location in a tube to be correlated to its relative location with respect to the treatment apparatus. Samples were prepared and observed under SEM, and characteristic images were taken every $\frac{1}{2}$ mm along the length of the tubing.

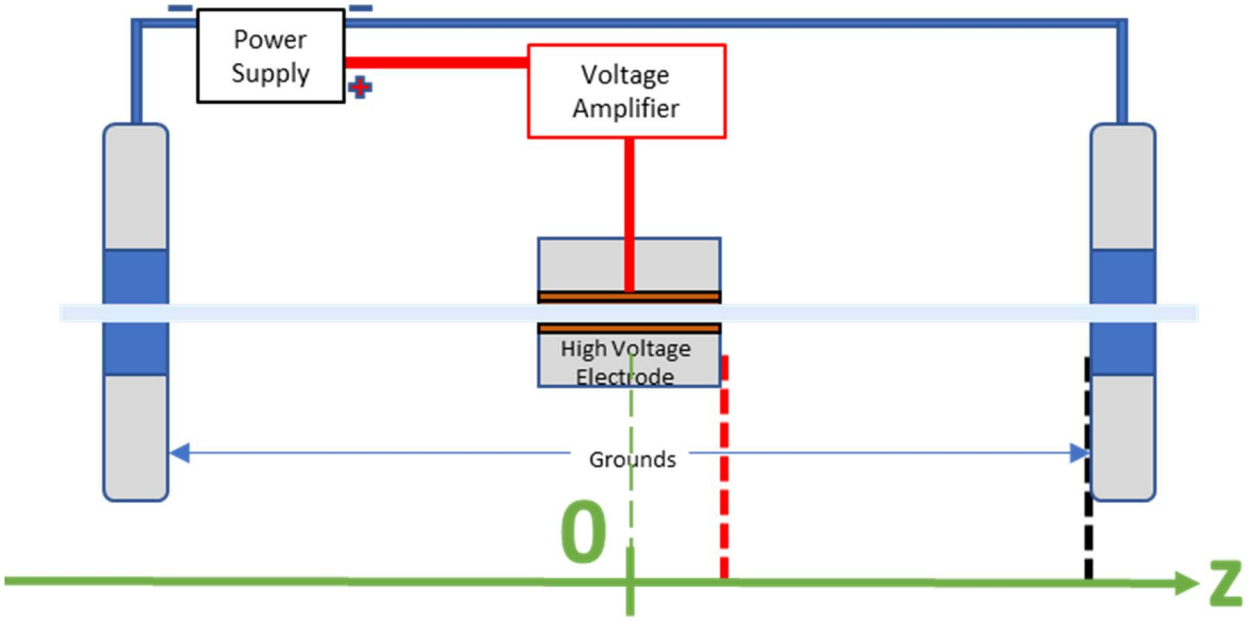

Figure 3.32 Diagram outlining the regions of interest investigated for the study of electrode proximity on protrusion density. The red dotted line indicates the edge of the high voltage electrode, and the black dotted line indicates the inner edge of the ground electrode. The dimensions of the electrodes in this image are not to scale.

After SEM analysis, ImageJ was used to quantify protrusion density along the length of the tubing under inspection. Generally, it was observed that the local regions around the edge of the electrodes displayed peak protrusion density. Figure 3.33 shows distribution of protrusion number density along z-axis for a sample treated at $10\,mW$. At this low power level, the lowest peak protrusion density was observed. Additionally, the smallest variance was observed in the regions where protrusions presented, with variation in order of magnitude of densities of $10^2 - 10^4$, with densities on the order of 10^2 being the lower threshold of densities that can be observed, as observation areas are generally smaller than $200\,x\,200\,\mu m$. As a result, observation of more than a few protrusions will result in densities of $100\,\frac{protrusions}{mm^2}$ or greater.

Similar trends of peak protrusion density to those observed in Figure 3.28 were observed in this study, with approximately an order of magnitude greater density observed at each power

level. 25 mW treatment profiles were observed to have peak densities on the order of 10^5, 40 mW densities peaking at magnitudes of 10^6, and peak densities for 50 mW samples around $5 * 10^7$. Additionally, consistent patterns were observed showing peaking in protrusion density oriented around the edge of the high voltage electrode, with a smaller peak clustered around the inner edge of the ground electrode, with dips in density being observed in regions between the edges.

Protrusion morphology rapidly diminishes to negligible degrees in regions more that a couple of millimeters inside of the high voltage electrode, likely due to the near negligible electric field that is expected to be present inside of the ground electrode. More morphologies have been observed in regions outside of these areas under inspection, but for the purposes of this study, these data highlight the strong dependence of electrode proximity on mechanical surface modification, and highlight the necessity for the development of techniques for homogenous treatment for consistent adhesive and wettability effects.

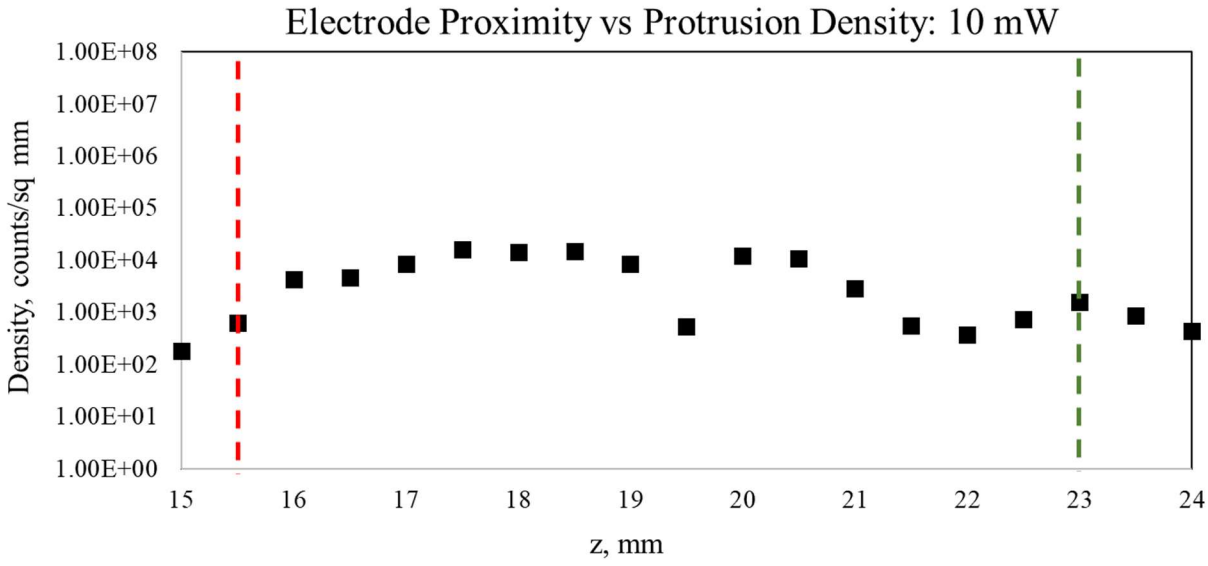

Figure 3.33 Effect of electrode proximity on protrusion density at a power level of 10 mW

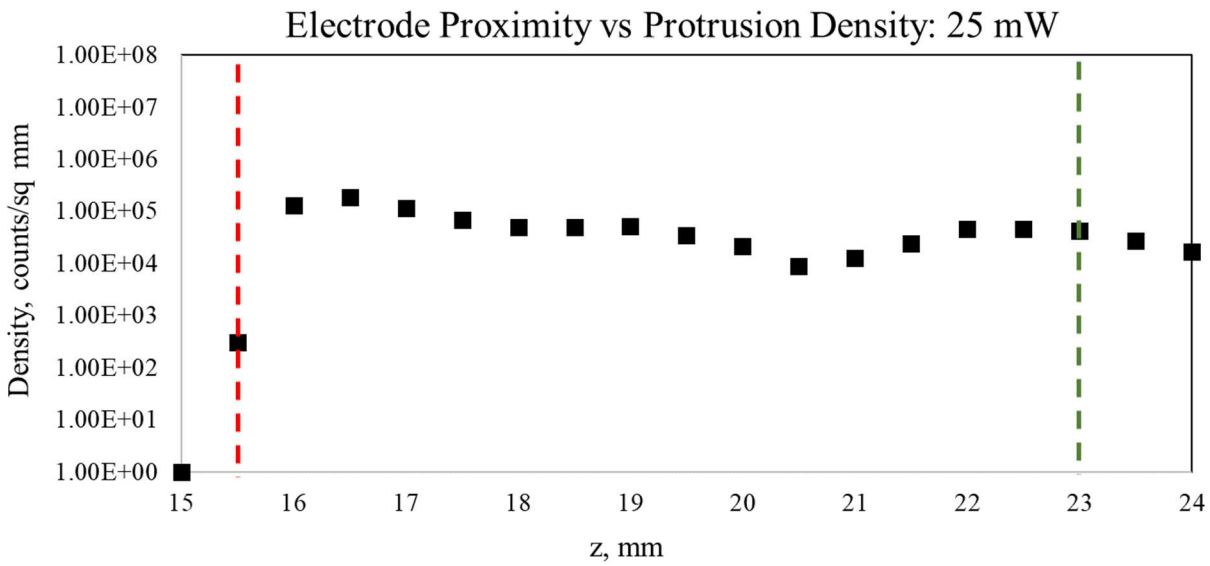

Figure 3.34 Effect of electrode proximity on protrusion density at a power level of 25 mW

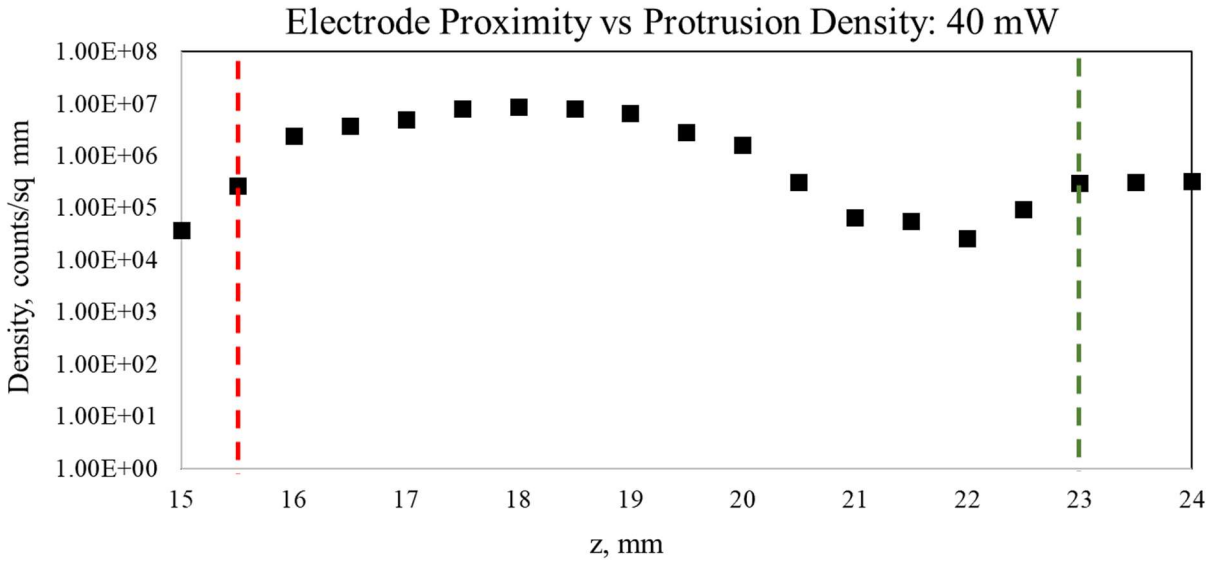

Figure 3.35 Effect of electrode proximity on protrusion density at a power level of 40 mW

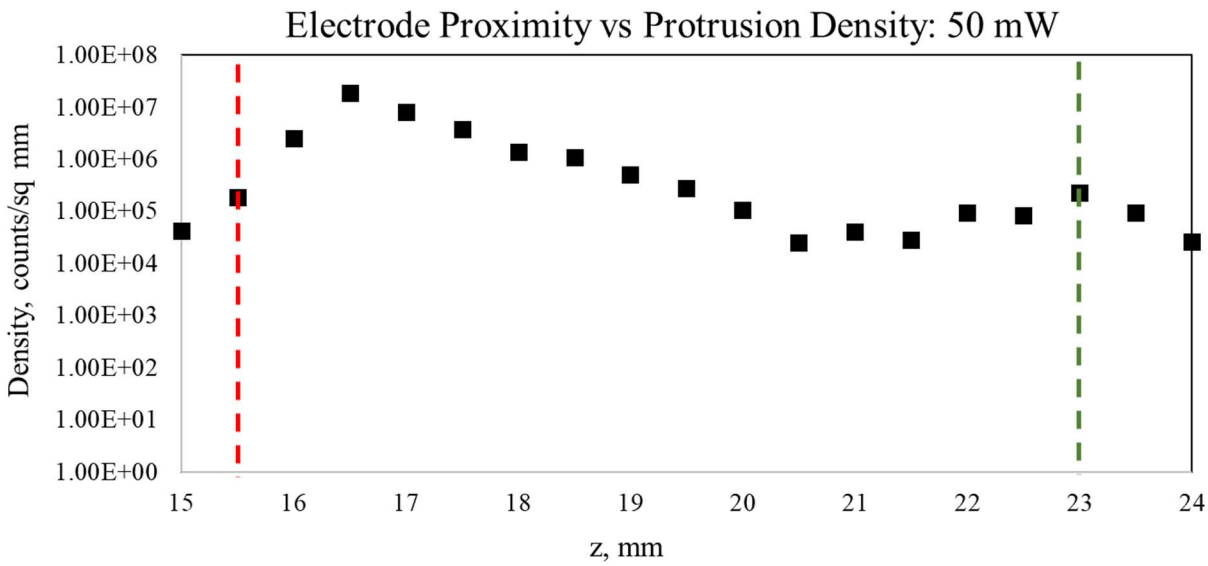

Figure 3.36 Effect of electrode proximity on protrusion density at a power level of 50 mW

3.2.5 Qualitative Observations of Surface Adhesion

In addition to observation on surface morphology, an investigation was performed to analyze the impacts of surface morphology changes induced by plasma treatment on the adhesion of a polymer. After plasma treatment, poly(lactic-co-glycolic acid) (PLGA) was coated on the surface of the tubing via a simple solvent exchange procedure, in which PLGA powder was dissolved in a cosolvent and, after direct injection into the tubing and an incubation process, precipitated on the LDPE surface by the introduction of a non-solvent. After the polymer was coated on the surface, the sample was prepared and analyzed under SEM.

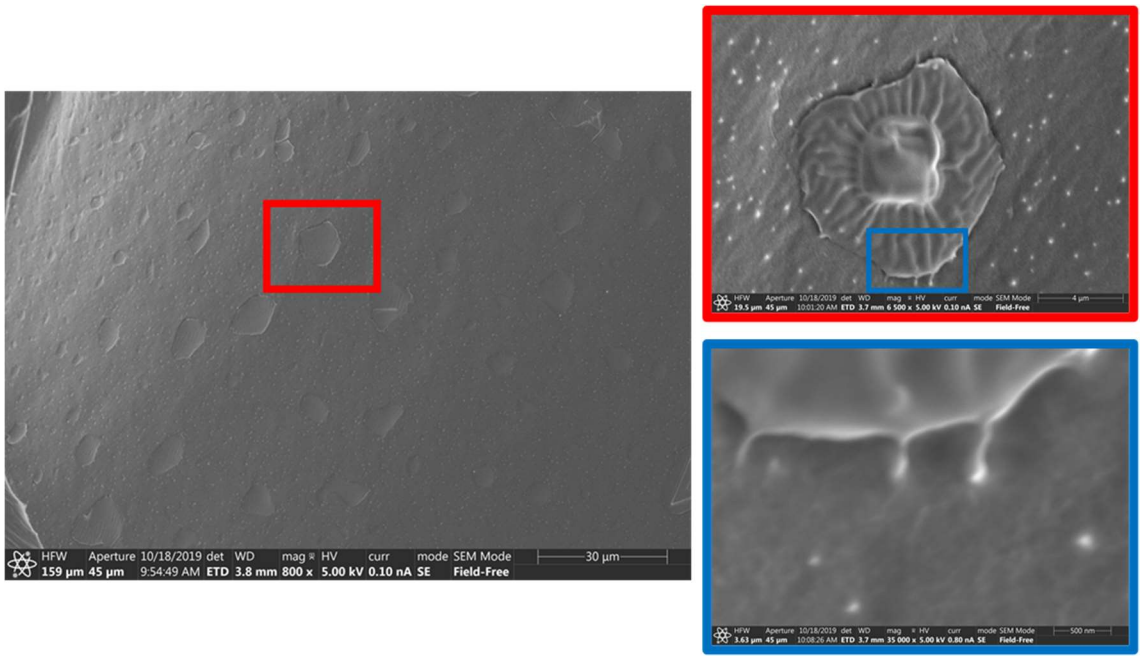

Figure 3.37 SEM imaging showing adhesion of PLGA to the surface of treated LDPE tubing. Adhesion is likely induced through multiple mechanisms, but mechanical interlocking is readily visible at the outer edges of the PLGA mound after retraction induced by heating from the electron beam.

Under SEM analysis, islands of PLGA were observed on the inner surface of the LDPE tubing. Islands of PLGA were observed to be more densely populous and generally larger in regions with greater concentrations of protrusions. On closer inspection, PLGA was observed to be directly adhering to surface protrusions at the outer edges of the islands. When the voltage of the electron beam of the SEM was increased moderately, the PLGA islands contracted, and at the points of contact where the protrusions were observed to adhere to the coating polymer, a clear retention of the adherence to the tubing was observed. In addition to observations made of adhesion at the micron scale, several observations were also made of surface adhesion of PLGA on the nanometer scale. These observations demonstrate the evident capacity of protrusions induced by the atmospheric pressure DBD plasma treatment to enable surface adhesion via mechanical interlocking.

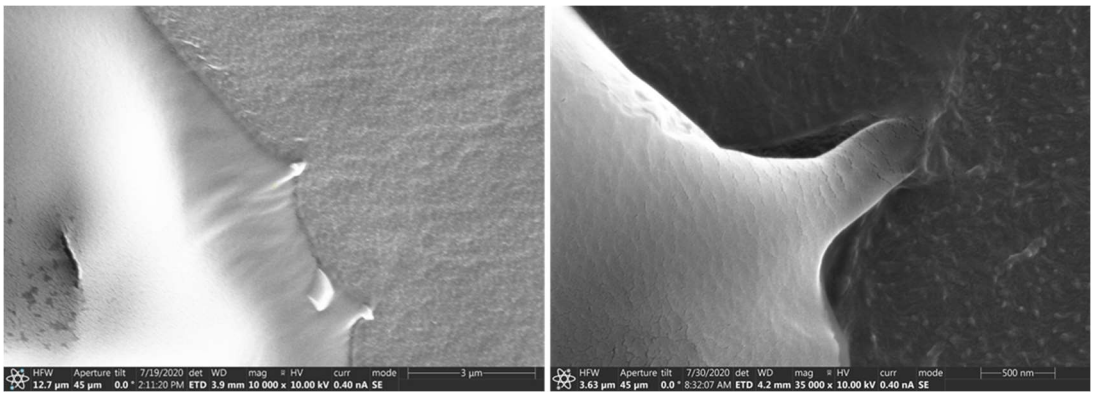

Figure 3.38 Additional SEM imaging showing mechanical interlocking of PLGA on both micron-scale protrusions as well as smaller nano-scale surface roughening

3.2.6 Initial Observations of Continuous Spool-Fed Treatment

While initial observations of surface morphology were performed in a "stationary" treatment profile, the heterogeneity of surface treatments was clearly incompatible with potentials for industrial applications. To improve the uniformity and scalability of surface treatments, modifications were made to the plasma treatment apparatus to enable linear actuation for semi-continuous treatment of lengths of tubing in increments of 30 cm. The modifications included the implementation of a stepper motor mounted to a worm gear and stage that could be attached to the tubing and enable discreet linear movement of tubing in increments of $\frac{1}{2}mm$. In addition to the addition of actuation, the ground electrodes were replaced with thin, tight electrodes to enhance surface treatment effects induced by the treatment process and enhance the rate at which treatment could be performed to induce equivalent morphologies.

An initial set of samples was prepared at a feed rate of 2 mm per minute, a speed selected to allow for any local point of tubing to be exposed to the plasma environment, from ground electrode to ground electrode, for approximately 30 minutes. After the treatment of the samples, SEM

analysis was performed. When compared to the highly heterogeneous morphology induced by stationary treatment, as can be seen in Figure 3.39, the morphology induced in the actuated system demonstrated vastly improved homogeneity. Samples treated in lengths of upwards of 30 cm were found to display consistent morphologies at any random point selected along the length of the tubing, corresponding to local observations of samples treated at 15-30 min at 20-45 mW, with only small variation (5-10%) observed from point to point.

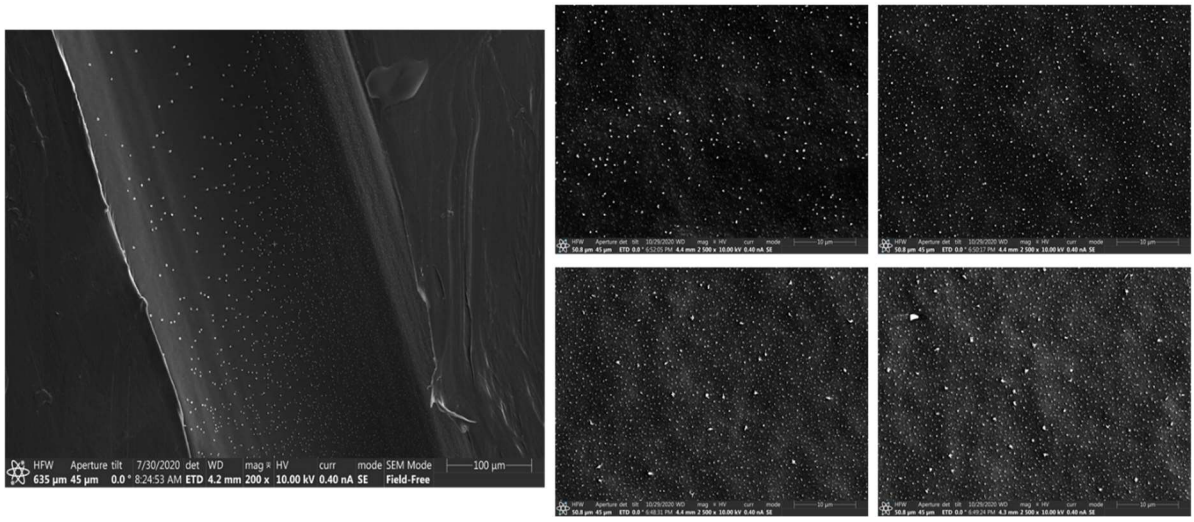

Figure 3.39 Left: SEM imaging emphasizing the high variability of surface morphologies induced by stationary plasma treatment. Right: 4 SEM images taken at random locations along a 30 cm treated sample. Linear actuation successfully and substantially improved the homogeneity of surface morphologies induced by plasma treatment.

After demonstrations of the homogeneity of the treatment apparatus, additional treatments were performed at 1, 2, 5 and 10 mm/min to examine their impact of surface treatment at a fixed power of 15 mW. Figure 3.40 shows the surface morphology characteristics resulting from varied feed rates of 1 – 10 mm/min. Unsurprisingly, as feed rate was decreased, analogous to increased treatment time in stationary treatment profiles, surface morphology was more dynamically changed relative to an untreated sample. The lower threshold for treatment at which morphological

changes were observed was 10 mm/minute, with more extreme morphologies induced at slower feed rates.

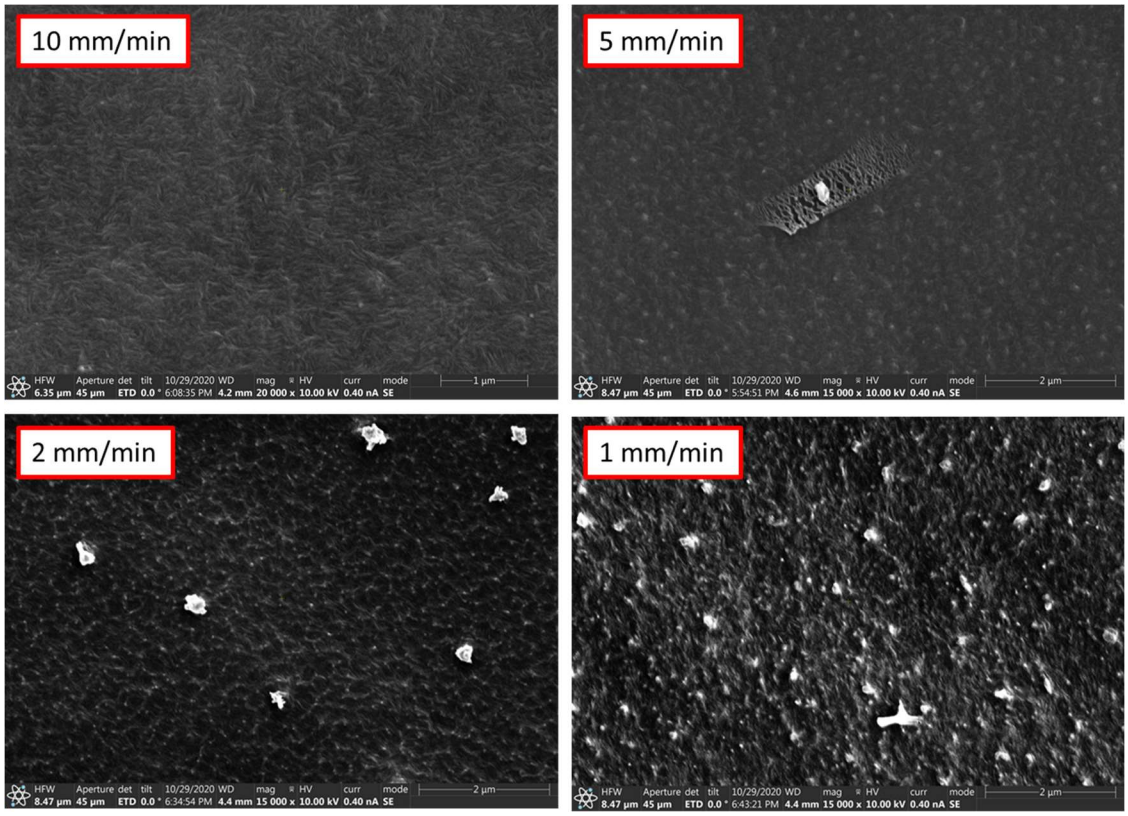

Figure 3.40 Surface morphology presentation of several feed rates at a fixed power level. Surface morphology becomes more extreme as feed rates are reduced. Feed rates of 10 mm/min were generally the threshold for visibility of surface morphology changes relative to an untreated sample.

3.2.7 Discussion of Surface Morphology Results

In investigating surface morphologies, it was observed that the unique design of this system enabled plasma treatments that produced surface profiles of characteristics not found in contemporary literature. Surface morphologies similar to those observed in Figure 3.21 and Figure 3.22 have been cited in contemporary literature, though not identical. Through the use of selective films and plasma etching, Piliyalil et al and others were able to generate interesting surface morphologies similar to those we have observed at the nanoscale [22], [54]. Additionally, similar

surfaces were observed to be produced by RF plasma treatment on PMMA, PEEK, and PTFE [55], [56]. Beyond these observations of nanoscale surface roughening, no examples have been identified of direct surface roughening by plasma treatment that have been able to generate surfaces with such extreme morphologies, some of which are comparable in regularity and size to pattern transferred surfaces.

The morphologies generated on the surfaces of the LDPE tubing was demonstrated to be heavily impacted by small variations in plasma parameters, and a clear factor in the production of the surface features was the electrode geometry. Seemingly as a result of the unique electric field patterns generated by the ring electrode geometry, these protrusions are forming in those regions where electric fields are more focused, around the edges of the ring electrodes. One potential explanation centers around well studied effects of surfaces in the presence of strong electric fields. Micro and nano-scale surface defects in the presence of an electric field can act to focus and intensify local electric fields about those defects [57]. These local fields may act to alter the local structure of the surface of the polymer by highly local heating, inducing reordering of the polymer material and inducing a sudden reduction in the density, leading to an emergence. Little literature into the effects of single polymer block materials has been performed to investigate electric field effects on orientation and alignment outside of thermodynamic effects. The physical parameters that influence the dynamic evolution of the polymer surface are likely complex and multi-faceted, warranting in-depth investigation. Further, more work needs to be done to explore the microfluidics, adhesive properties, etc. of these surface features, but the wide variety of surface morphologies that have been repeatably produced by this single plasma system lays a foundation for a broad range of applications, including biocompatibility, biomimetics, antibiofouling, wettability modification, and so on.

Additionally, it was extremely interesting and promising for the capabilities of the protrusion morphology formed from the plasma treatment process to demonstrate evidence for mechanical interlocking of PLGA. This evidence directly demonstrates the adhesion properties that can be embedded on polymer surfaces by this treatment process. Aside from the mechanical adhesion, it is commonly understood that radicals produced in the plasma treatment process produce functional groups that also promote adhesion. Further, simple addition of seed gasses like O_2 could potentially enhance functionalization for specific purposes.

3.3 Investigation of Plasma Treatment on Wetting

3.3.1 Qualitative Observations of Surface Wetting

The earliest efforts at investigation of surface wettability changes induced by plasma treatment was a simple droplet test. For this test, a section of untreated tubing, in addition to a section of tubing treated at 25 mW for 30 minutes, were bisected, and a small droplet of water was introduced to the inner surface of the tubing. The untreated tubing formed a substantial droplet when DI water was introduced and remained in place without substantial dissipation into the channel. The treated sample was immediately wetted by the droplet of DI water, and readily spread out in the channel. Attempts at direct measurement of contact angle proved extremely challenging, as water droplets of sufficiently small size were functionally impossible to repeatably produce with equipment available, and water in the channel of the treated sample spread out quickly, causing the water layer to thin out rapidly in a few seconds.

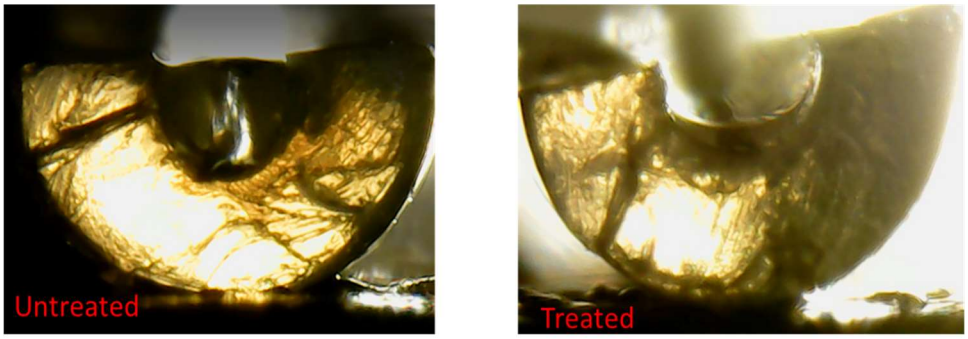

Figure 3.41 Initial observations of wettability from a droplet test performed on the inner surface of a cross-sectioned untreated and treated LDPE sample, demonstrating improved hydrophilicity induced by plasma treatment.

After modifications to the experimental procedure, methodology was developed to measure the contact angle of the meniscus formed on the inner surface of the tubing. DI water was introduced to a section of tubing mounted to a test stand, with a digital microscope mounted perpendicular to the tubing with a backlight used to refine the features of the meniscus. Efforts to image water contact angle using this methodology proved extremely successful, with very little variability in contact angle measurements collected via image processing.

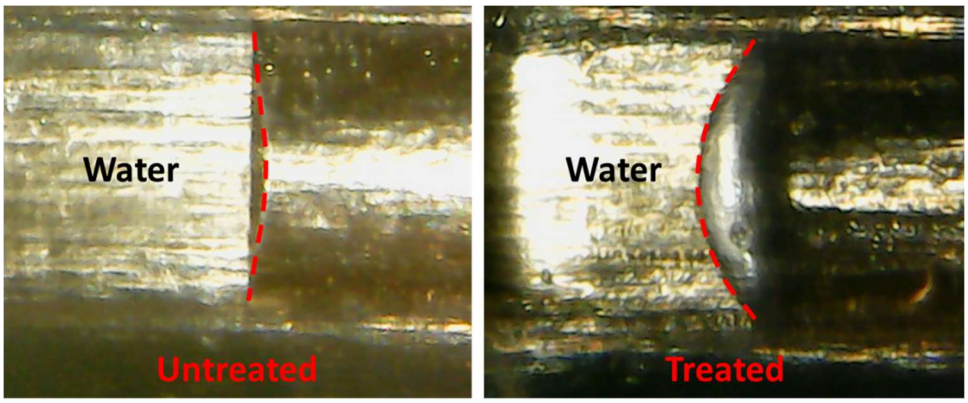

Figure 3.42 Microscopic imaging of meniscus formation on the inner surface of treated and untreated tubing, highlighting the significant shift in water contact angle used to measure wettability effects induced by plasma treatment.

3.3.2 Time Decay of Wettability Effects

An important factor in surface modification is the retention of wettability effects as a function of time. To explore these effects, a series of tests were performed. A 24-hour study was necessary to identify with fineness the temporal dynamics of wettability after plasma treatment. To accomplish this, two tests were performed, one 16- hour study, and one 24 hour study. For this study, as with previous wettability studies, triplicate samples were prepared for each time step to eliminate the wetting factor on contact angle measurements.

Figure 3.43 and Figure 3.44 shows the dynamic wetting trends revealed from these studies. In the 16-hour study, nonlinear behavior was observed in the first 8 hours of the study, with an initial drop in contact angle, indicating that there is an initial increase in wettability in the first few hours after treatment. After this drop, contact angle measurements rose to roughly 15^o above the initial contact angle, reaching a steady-state similar to those made in previous longer-term studies.

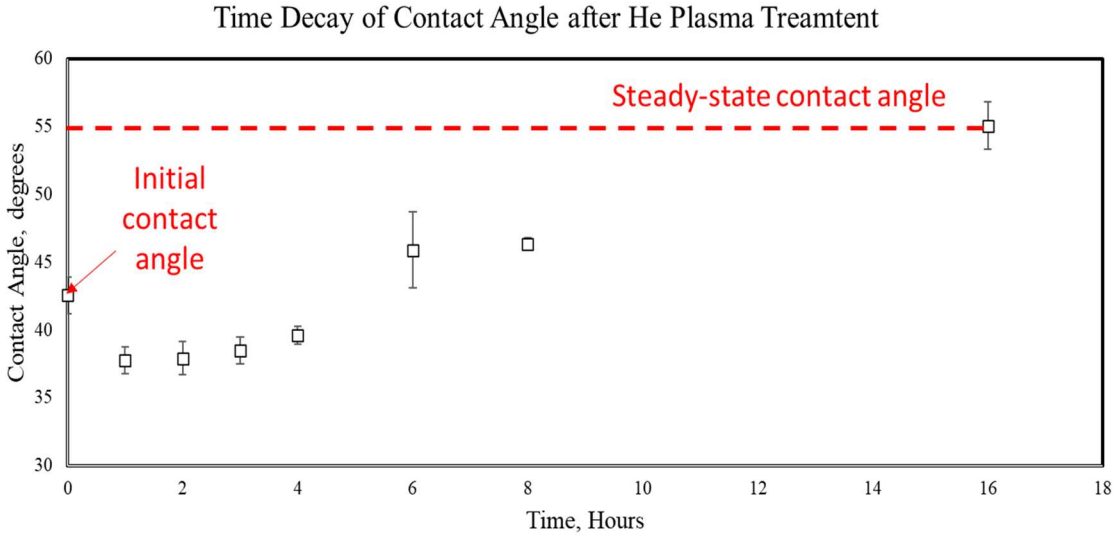

Figure 3.43 Time decay of wettability via water contact angle measurements from a plasma treated sample for the first 16 hours after treatment. Trends indicate an interesting nonlinearity in wettability in the first several hours after treatment, with an initial drop in contact angle before increasing to a steady-state.

The second study involved the production of a substantially larger set of samples, enabling a longer time study with more refined time steps. Int this study, the same trends were observed, with an initial increase in wetting characteristics in the first several hours after treatment, followed by a return to a steady-state contact angle of roughly 15^o above the initial contact angle after 12 hours. Observations from these two studies reveal two key wettability features of the plasma treatment process: contact angle change follows a nonlinear trend, with an initial increase in wettability in the first few hours after treatment, and transient wettability features fade nearly completely after 12 hours post-treatment.

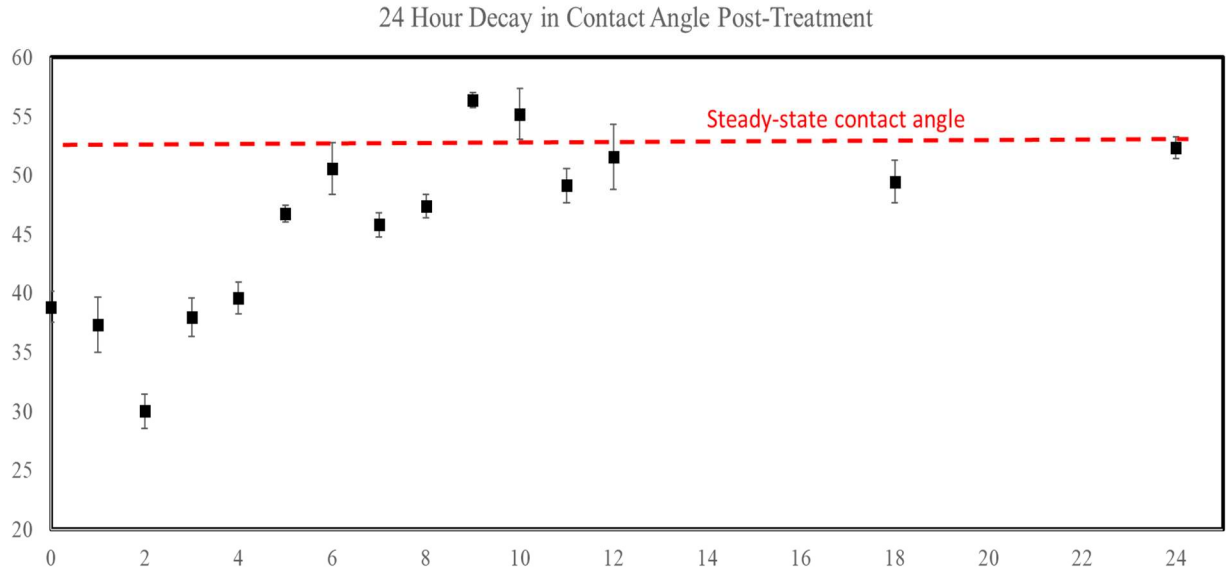

Figure 3.44 Time decay of wettability via water contact angle measurements from a plasma treated sample for the first 24 hours after treatment. Trends continue to demonstrate nonlinearity in wettability in the first several hours after treatment and show that a steady-state is reached in the first 12 hours after treatment.

Observations were made through the process of these studies that a significant shift in contact angle occurred after the surface of tubing was wetted. Two theories were posited to explain this phenomenon: wettability decay occurs in a time scale shorter than 24 hours, or the process of wetting removes transient wetting effects, such as functional groups or surface charging. To test

the first theory, triplicate samples were prepared on the actuated treatment system. After treatment, samples were wetted, and then subsequently dried using neutral helium gas, and then wetted again. Measurements of contact angle were taken after each wetting, with less than 10 minutes passing between each measurement. Data taken from this test, illustrated in Figure 3.45, showed a near-identical shift in contact angle as observed between the first two time steps in the first time decay study. This observation clearly indicates that wetting the surface has a significant impact on the wettability of the tubing surface.

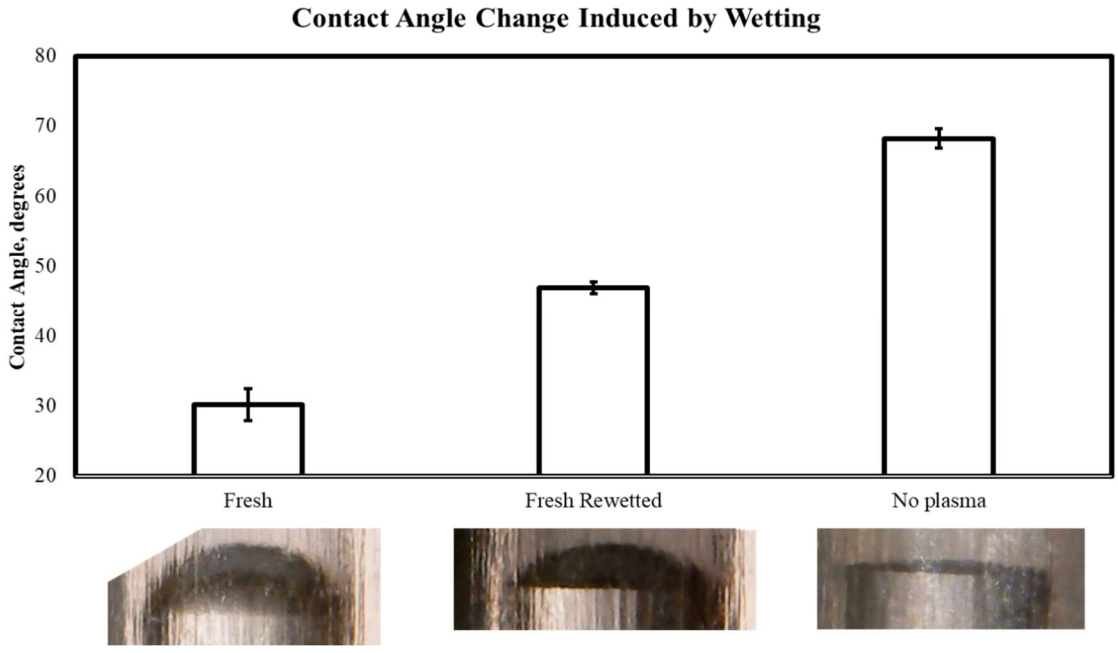

Figure 3.45 Investigation into shift of contact angle for a plasma treatment after a first and second wetting, compared to an untreated sample. Samples were treated at 15 mW at a feed rate of 2 mm/min

Identical samples were produced to compare the contact angle shift of temporal decay relative to the contact angle shift induced by wetting. For this study, a large population of plasma treated samples were produced at identical conditions such that samples were not reused. After 24 hours, well after the 10 hour time frame necessary to reach steady-state, a nearly identical shift in

wettability was observed as compared the contact angle shift induced by a first wetting. For assurance, additional data points were taken at 2 and 4 days to ensure no significant variance in contact angle from additional decay was occurring. These observations enabled the development of an experimental protocol to use a first wetting as a means of artificially inducing steady-state wetting characteristics. For studies performed in section 3.3.3, these methods were applied to investigate both initial contact angle, θ_o, and steady-state contact angle, θ_{SS}, without waiting for steady-state to be reached through natural decay.

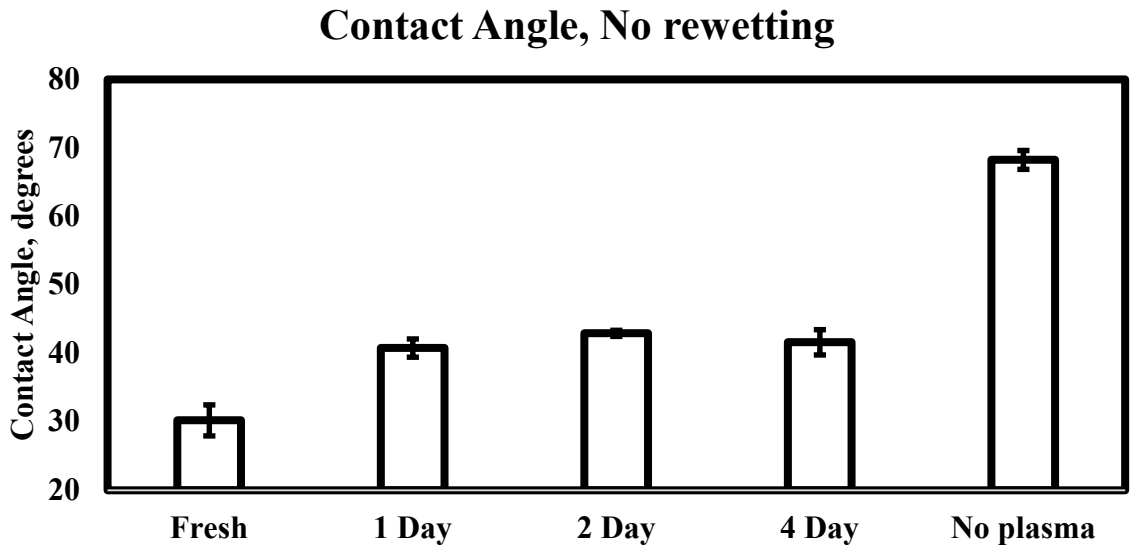

Figure 3.46 Time decay of wettability via water contact angle measurements from a plasma treated sample. No samples were re-used in this study. Again, no substantial change in wettability was observed after the first 24 hours.

3.3.3 Impact of Discharge Power and Feed Rate on Wettability

In addition to studies in the time decay of wettability induced by the plasma treatment process, additional tests were performed on the effect of discharge power and feed rate on wettability. By taking advantage of previously observed phenomena of the removal of transient

wettability effects by an initial wetting, measurements were made for initial contact angle as well as the steady-state contact angle.

For the investigation of plasma power on wettability, power levels of 7 to 40 mW were selected, accounting for the general range of previously observed power levels, from the minimum sustainable discharge power up to the upper limit of useful plasma discharge. For all power levels, samples were fed through the apparatus at a fixed feed rate of 2 mm/min with a step size of $\frac{1}{2}\ mm$. Figure 3.47 shows the results of the effects of the power study. Initial contact angle measurements showed little variation in the initial wetting effect of the plasma treatment process, with average contact angles of $\sim 20^o - 26^o$, with no statistically significant difference observed. However, measurements of the steady-state contact angle indicated an interesting pattern.

At low power levels, steady state contact angles returned to values approaching those of an untreated sample, while greater power level regimes showed increased degrees of retention of wettability effects. This is likely due to the duality of transient vs permanent wettability. Permanent wetting features in this treatment profile are likely dominated by surface morphology. Very likely, treatment profiles at higher power levels are generating favorable surfaces for wetting, while lower power profiles are either generating no significant surface changes, or the surface changes induced are comparably hydrophobic to an untreated sample. The combination of transient and permanent wetting effects may be approaching the upper threshold of contact angle achievable in the channel where surface energy of the fluid-surface interface are no longer significant enough to drive a greater radius of curvature in the confined volume. However, these results do highlight the tunability of surface wettability and wetting retention post-treatment, up to and including full hydrophobic recovery to untreated wetting characteristics.

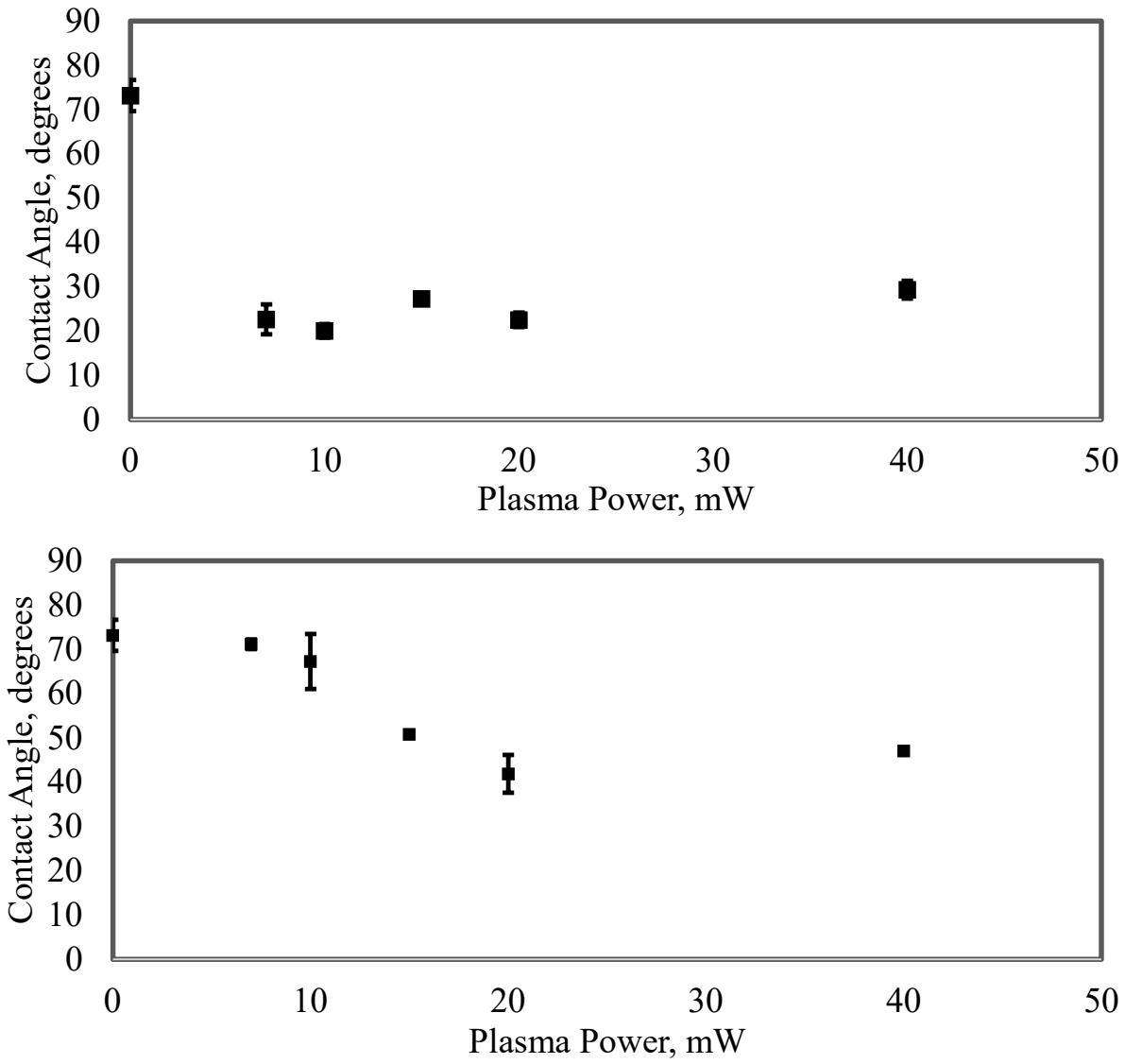

Figure 3.47 Impact of discharge power on wettability at a constant linear feed rate of 2 mm/min via surface contact angle for initial contact angle, θ_o (Top) as well as steady-state contact angle, θ_{SS} (Bottom). While no significant variance is observed in the initial contact angle, there is a significant retention in wettability effects at higher power levels.

3.3.4 Discussion of Wettability Results

While early attempts to perform tubing ID wettability tests comparable to those performed by Chen et al [58] ultimately proved unsuccessful, alternative measurements of meniscus geometry proved to be a consistent means of measuring wetting characteristics, with consistent

measurements between triplicate samples. One key observation from these wettability studies is the nonlinear wetting behavior in the first several hours after treatment. Behavior like this has not been observed in literature, though wetting decay studies on an hour-by-hour basis have rarely been seen. This temporary increasing in wetting perhaps indicates a more complex surface chemistry that evolves as it mixes with air before eventually decaying. It would be of interest to perform additional studies into the surface chemistry of the treated tubing at a few key time steps after treatment.

In addition to the nonlinear development of wetting characteristics, another interesting observation was the dependence of surface treatment on the retention of wettability effects. It is evident that this treatment process has capability to control to some degree the amount of surface wettability that is retained by the LDPE tubing, up to and including a full reversibility of wetting characteristics at low power levels. This too, like the broad range of surface morphologies produced by tuning plasma parameters and electrode geometries, potentially has extensive industrial applications. θ_0

4. CONCLUSION AND FUTURE WORK

4.1 Summary and Conclusion

The body of this thesis outlines the development, design iterations, and characterization of a novel atmospheric-pressure DBD plasma treatment apparatus for the isolated treatment of inner surfaces of polymer tubing. In the characterization process, numerous factors related to electrode geometry and plasma parameters are outlined as critical factors influencing the morphology generated as well as the adhesive and wetting properties of the surface.

Section 3.1 covers the development and design iterations of the atmospheric-pressure DBD plasma treatment apparatus, including the characterization of the system electrically, and improvements made to enhance the development of morphologies of interest as well as reduce the time required to perform said treatments. The section concludes with a detailed overview of the apparatus' key functional arrangements and provides definitions for these arrangements for reference further in the work.

Section 3.2 details the works in surface morphology characterization for the system, beginning with a qualitative overview of morphologies observed. The section then details results from cross-sectional studies of plasma power and treatment time on protrusion density, mean protrusion size, and roughness. For fixed power, it was observed that protrusion density increased dramatically from 5-15 minutes, and then began to coalesce from 30-45 minutes. For fixed treatment time, and inverse relationship was observed between density and size, with density increasing with increasing power. Roughness values of ISO standard N1 to N5 were observed across the samples under investigation. Then, this section covers the relationship between electrode proximity and protrusion density. Protrusion density was observed to be significantly higher in regions proximal to the edges of the ground and high voltage electrode. Finally, the

section covers some qualitative observations of adhesion of PLGA on the inner surface of the tubing, and observations are shown from characterization efforts for a spool-fed linear actuation of the LDPE tubing. PLGA adhesion is demonstrated through mechanical interlocking between the PLGA matrix and protrusions induced on the surface of the tubing. It is finally demonstrated that an actuated, spool fed system is capable of performing plasma treatments with highly homogenous surface morphologies comparable to local morphologies achieved in the stationary treatment profiles.

Section 3.3 covers characterization of surface wetting induced by plasma treatment. The first observations were to characterize the temporal decay of surface wetting. It was observed that wettability increased dynamically in the first few hours after treatment, and then rapidly reduced to a steady state at 10 hours. Lastly, observations of the impact of plasma power on wettability was presented. No significant difference was observed in meniscus contact angle with increasing power for initial contact angle measurements. It was observed that at low powers, less than 10 mW, wettability nearly completely returned to the untreated hydrophobic wetting state, and at higher powers, significant retention of wettability was observed after steady-state was reached.

4.2 Future Work

4.2.1 Analytical Techniques

As a logical progression of research into scalable plasma treatment in confined dielectric volumes, several analytical approaches are proposed for future work for completeness and scientific interest. In the interest of understanding the species in the plasma medium, it is important to perform emission spectroscopy at a variety of discharge power levels, as well as with a variety

of gas mixtures of interest, potentially including O_2, N_2, atmospheric air, ammonia, CH_4, CF_4, and so on as seed gasses in Helium.

For the improved understanding of surface modification, both mechanically and chemically induced by plasma treatment, several procedures are recommended. Atomic Force Microscopy (AFM) should be performed to enable more refined measurements of the topography of the surfaces generated by plasma treatment, allowing for the presentation of 3D models of surfaces as well as more precise calculations of surface roughness parameters, and enabling the calculation of more complex roughness parameters. Additionally, X-ray Photoelectron Spectroscopy (XPS) should be employed for analysis of functional groups generated as a result of plasma treatment for a variety of treatment profiles, gas compositions, etc.

Investigation of wetting, adhesion and roughness effects can be further expanded to include additional mechanical analyses. For the investigation of surface roughness on adhesion, axial and translational pull-tests can be performed on treated surfaces coated with an adhesive polymer. Fluid dynamics tests (Darcy friction factor) should be performed to characterize the hydrodynamic roughness induced by different treatment profiles and how those factors impact volumetric flow rate for fixed fluid pressures. Wetting can be further characterized with contact angle behavior of additional solvents of interest, and further tests investigating capillary rise and its relationship to contact angle can be performed.

4.2.2 Improvements to Treatment Apparatus

A variety of changes to the plasma treatment apparatus have been recommended to improve performance factors such as scalability, homogeneity, plasma discharge control, and variability of application. A first simple modification that has been suggested is the introduction of an arbitrary number of alternating ring electrodes (GND/HV/GND/HV…/GND) to increase the total active

length of the treatment apparatus, and thereby improving the time necessary to treat longer lengths of tubing. Figure 4.1 shows an early concept demonstration of a multiple alternating electrode concept, allowing for simultaneous exposure of 30 cm of tubing to the plasma environment.

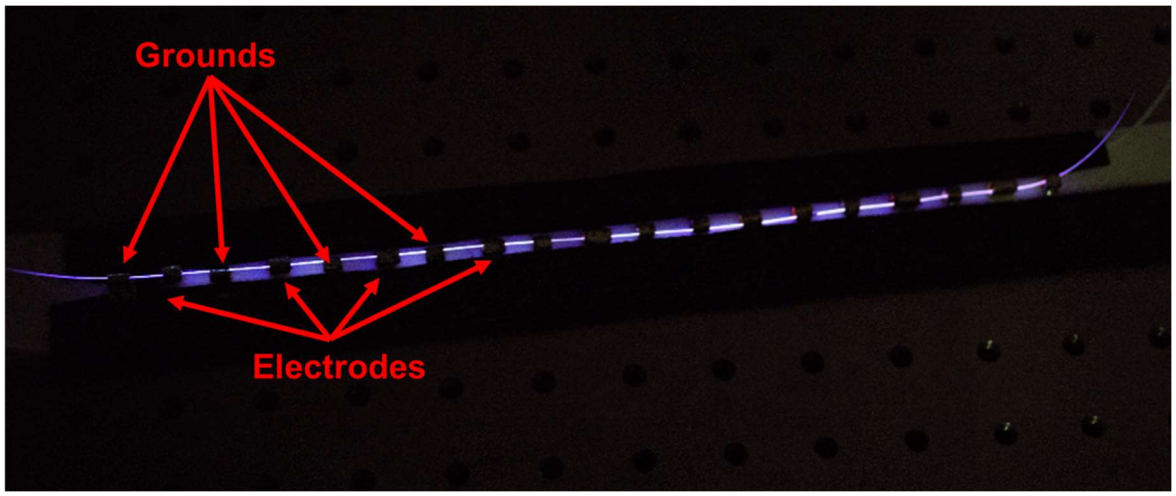

Figure 4.1 Early prototype of alternating ring electrode atmospheric-pressure DBD plasma treatment apparatus, with 30 cm of total treatment length.

To improve the dynamic capability of the treatment apparatus to operate with a more dynamic range of tubing materials and sizes, adaptions to the system are being applied to replace the ground and high voltage electrodes with conductive variable diameter apertures, with aperture sizes ranging from $0 - 1\ in$. This will enable consistent analysis of treatment with a tight fitted aperture for a wider range of tubing, however, due to the mechanical complexity of the apertures, concerns have surfaced regarding potential issues with corona discharges and internal reflections, and further work is needed to fully enable this capability.

Figure 4.2 Example of a variable aperture similar to those proposed for implementation in future iterations of the atmospheric pressure DBD plasma treatment apparatus.

To improve the repeatability and reliability of the linear actuation of the plasma treatment system, a more refined, spool-fed actuated mechanism s proposed. It has been noted that traditional stepper-motor driven spooling systems are generally unable to drive feed rates at levels low enough to replicate experimental processes currently being performed. As an alternative, a capstan-driven servo motor spooler system is proposed to enable ultra-low feed rates as slow as 1 mm/min, as well as more rapid feed rates as work is performed to enable higher feed rates with desirable modification results.

Figure 4.3 Capstan-driven servo motor proposed for improved control and repeatability of ultra-low feed rates necessary for the plasma treatment profiles under investigation.

Finally, to improve the controllability and repeatability of the plasma discharge, it is proposed to replace the current high voltage power supply with a new power supply capable of generating pulses with rise times faster than the time scale of the plasma discharge, with either a nanosecond pulse discharge or a square wave power supply. Currently, the system uses a 10 kHz power supply with a sinusoidal waveform. However, the plasma discharge occurs on a timescale of $\sim 100\ ns$. As a result, discharge events are uncontrolled at higher voltages, and do not occur at the peak voltage in the waveform. To improve this and to enable "overvoltage" of the plasma discharge, these new power supplies are proposed.

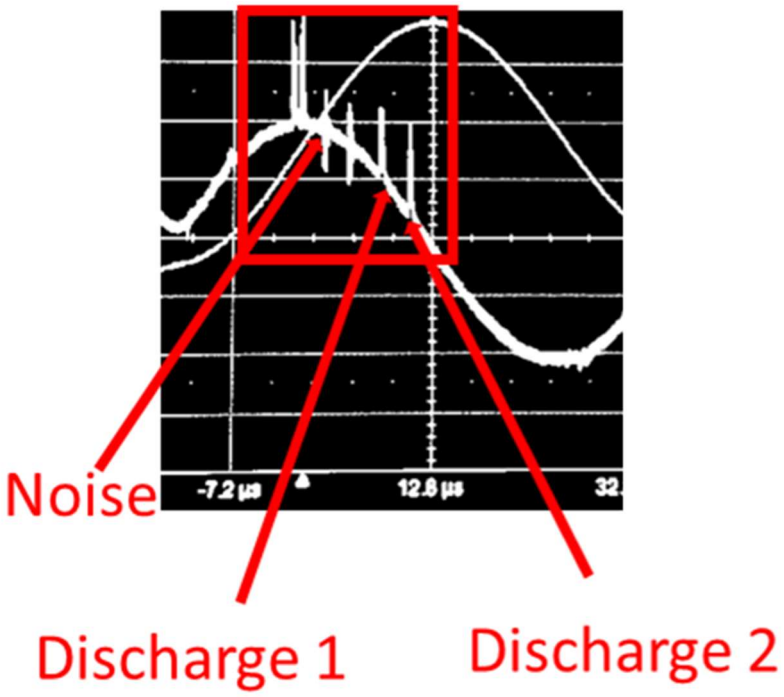

Figure 4.4 Oscilloscope readout of a plasma discharge event using conventional 10 kHz sinusoidal power supply at high voltages. Discharge events can be readily seed to be occurring before peak voltage is reached.

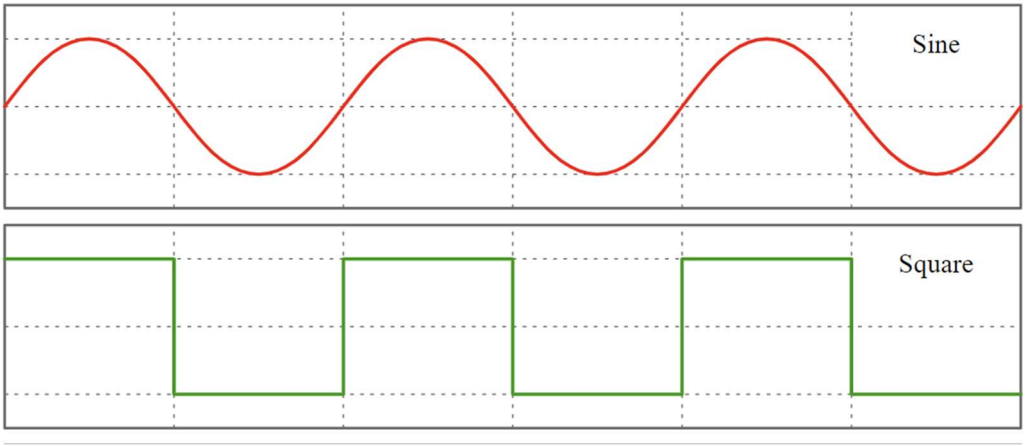

Figure 4.5 Examples of a sine vs a square wave. By taking advantage of ultra-fast, nanosecond rise times of a square wave power supply, voltage levels of discharge events can be directly controlled, even at voltages in excess of the threshold for discharge.

4.2.3 Additional work

In addition to comprehensive continuation of the characterization of the current plasma treatment process, and further improvements to the system for enhanced performance of the

developed plasma treatment process, further expansions to the system are proposed to widen its capabilities beyond what has already been demonstrated. A simple first proposal is the introduction of seed gasses of interest in the helium plasma to investigate potential effects. Of particular interest is the introduction of O_2 in small quantity to explore the impact of functionalization and increased surface wetting capabilities, as observed in other works [24], [29], [55], [59], [60]. Also of potential interest could be the introduction of more exotic gasses such as SF_6 or CF_4, which have been demonstrated as agents for enhanced hydrophobization of polymer surfaces vie the introduction of fluorinated functional groups [23], [61]–[63].

Finally, it is proposed to further enhance the capability of the plasma treatment system to enable the deposition of polymer films by means of monomer precursors. The application of these films can enable many interesting capabilities, including enhanced surface adhesion, wettability, biocompatibility, and drug loading [26], [50], [51], [64], [65].

REFERENCES

[1] S. Kumar, R. Singh, T. P. Singh, and B. L. Sethi, "Surface modification by electrical discharge machining: A review," *J. Mater. Process. Technol.*, vol. 209, no. 8, pp. 3675–3687, Apr. 2009, doi: 10.1016/j.jmatprotec.2008.09.032.

[2] H. Chouirfa, H. Bouloussa, V. Migonney, and C. Falentin-Daudré, "Review of titanium surface modification techniques and coatings for antibacterial applications," *Acta Biomater.*, vol. 83, pp. 37–54, Jan. 2019, doi: 10.1016/j.actbio.2018.10.036.

[3] J. Cruz and R. Fangueiro, "Surface Modification of Natural Fibers: A Review," *Procedia Eng.*, vol. 155, pp. 285–288, 2016, doi: 10.1016/j.proeng.2016.08.030.

[4] H. Namazi, "Polymers in our daily life," *BioImpacts*, vol. 7, no. 2, pp. 73–74, Jun. 2017, doi: 10.15171/bi.2017.09.

[5] "Timeline - Overview for polymer AND sur... in Publications - Dimensions." https://app.dimensions.ai/analytics/publication/overview/timeline?search_mode=content&search_text=polymer%20AND%20surface%20modification&search_type=kws&search_field=full_search&year_from=1990&year_to=2020 (accessed Jun. 15, 2021).

[6] S. K. Nemani *et al.*, "Surface Modification of Polymers: Methods and Applications," *Adv. Mater. Interfaces*, vol. 5, no. 24, p. 1801247, Dec. 2018, doi: 10.1002/admi.201801247.

[7] X.-M. Li, D. Reinhoudt, and M. Crego-Calama, "What do we need for a superhydrophobic surface? A review on the recent progress in the preparation of superhydrophobic surfaces," *Chem. Soc. Rev.*, vol. 36, no. 8, p. 1350, 2007, doi: 10.1039/b602486f.

[8] P. Fabbri and M. Messori, "Surface Modification of Polymers," in *Modification of Polymer Properties*, Elsevier, 2017, pp. 109–130. doi: 10.1016/B978-0-323-44353-1.00005-1.

[9] H. Y. Zheng, Y. C. Guan, K. Liu, Z. K. Wang, and S. M. Yuan, "Other Methods of Polymer Surface Modifications," in *Printing on Polymers*, Elsevier, 2016, pp. 161–178. doi: 10.1016/B978-0-323-37468-2.00010-5.

[10] N. Okulova, P. Johansen, L. Christensen, and R. Taboryski, "Replication of micro-sized pillars in polypropylene using the extrusion coating process," *Microelectron. Eng.*, vol. 176, pp. 54–57, May 2017, doi: 10.1016/j.mee.2017.01.027.

[11] A.-F. Chen and H.-X. Huang, "Rapid Fabrication of T-Shaped Micropillars on Polypropylene Surfaces with Robust Cassie–Baxter State for Quantitative Droplet Collection," *J. Phys. Chem. C*, vol. 120, no. 3, pp. 1556–1561, Jan. 2016, doi: 10.1021/acs.jpcc.5b10079.

[12] H. Sojoudi, M. Wang, N. D. Boscher, G. H. McKinley, and K. K. Gleason, "Durable and scalable icephobic surfaces: similarities and distinctions from superhydrophobic surfaces," *Soft Matter*, vol. 12, no. 7, pp. 1938–1963, 2016, doi: 10.1039/C5SM02295A.

[13] F.-G. Chizoba Ekezie, D.-W. Sun, and J.-H. Cheng, "A review on recent advances in cold plasma technology for the food industry: Current applications and future trends," *Trends Food Sci. Technol.*, vol. 69, pp. 46–58, Nov. 2017, doi: 10.1016/j.tifs.2017.08.007.

[14] J. N. Bardsley, "Industrial applications of low temperature plasmas," in *AIP Conference Proceedings*, Gaithersburg, Maryland (USA), 1998, pp. 333–376. doi: 10.1063/1.56165.

[15] J. Friedrich, *The plasma chemistry of polymer surfaces: advanced techniques for surface design*. Weinheim: Wiley-VCH, 2012.

[16] *Introduction to plasma physics and controlled fusion*. New York, NY: Springer Science+Business Media, 2015.

[17] B. D. Ratner, A. Chilkoti, and G. P. Lopez, “Plasma Deposition and Treatment for Biomaterial Applications,” in *Plasma Deposition, Treatment, and Etching of Polymers*, Elsevier, 1990, pp. 463–516. doi: 10.1016/B978-0-12-200430-8.50013-0.
[18] T. Desmet, R. Morent, N. De Geyter, C. Leys, E. Schacht, and P. Dubruel, “Nonthermal Plasma Technology as a Versatile Strategy for Polymeric Biomaterials Surface Modification: A Review,” *Biomacromolecules*, vol. 10, no. 9, pp. 2351–2378, Sep. 2009, doi: 10.1021/bm900186s.
[19] E. M. Liston, L. Martinu, and M. R. Wertheimer, “Plasma surface modification of polymers for improved adhesion: a critical review,” *J. Adhes. Sci. Technol.*, vol. 7, no. 10, pp. 1091–1127, Jan. 1993, doi: 10.1163/156856193X00600.
[20] M. Iqbal, D. K. Dinh, Q. Abbas, M. Imran, H. Sattar, and A. Ul Ahmad, “Controlled Surface Wettability by Plasma Polymer Surface Modification,” *Surfaces*, vol. 2, no. 2, pp. 349–371, May 2019, doi: 10.3390/surfaces2020026.
[21] M.-E. Vlachopoulou, G. Kokkoris, C. Cardinaud, E. Gogolides, and A. Tserepi, “Plasma Etching of Poly(dimethylsiloxane): Roughness Formation, Mechanism, Control, and Application in the Fabrication of Microfluidic Structures,” *Plasma Process. Polym.*, vol. 10, no. 1, pp. 29–40, Jan. 2013, doi: 10.1002/ppap.201200008.
[22] H. Puliyalil and U. Cvelbar, “Selective Plasma Etching of Polymeric Substrates for Advanced Applications,” *Nanomaterials*, vol. 6, no. 6, p. 108, Jun. 2016, doi: 10.3390/nano6060108.
[23] S. G. Walton *et al.*, “Study of plasma-polyethylene interactions using electron beam-generated plasmas produced in Ar/SF6 mixtures,” *J. Appl. Polym. Sci.*, p. n/a-n/a, 2010, doi: 10.1002/app.32249.
[24] Y. P. Li, S. Y. Li, W. Shi, and M. K. Lei, “Hydrophobic over-recovery during aging of polyethylene modified by oxygen capacitively coupled radio frequency plasma: A new approach for stable superhydrophobic surface with high water adhesion,” *Surf. Coat. Technol.*, vol. 206, no. 23, pp. 4952–4958, Jul. 2012, doi: 10.1016/j.surfcoat.2012.05.120.
[25] M. Ito, J.-S. Oh, T. Ohta, M. Shiratani, and M. Hori, “Current status and future prospects of agricultural applications using atmospheric-pressure plasma technologies,” *Plasma Process. Polym.*, vol. 15, no. 2, p. 1700073, Feb. 2018, doi: 10.1002/ppap.201700073.
[26] S. Cheruthazhekatt, M. Černák, P. Slavíček, and J. Havel, “Gas plasmas and plasma modified materials in medicine,” *J. Appl. Biomed.*, vol. 8, no. 2, pp. 55–66, Jul. 2010, doi: 10.2478/v10136-009-0013-9.
[27] L. Yang, J. Chen, Y. Guo, and Z. Zhang, “Surface modification of a biomedical polyethylene terephthalate (PET) by air plasma,” *Appl. Surf. Sci.*, vol. 255, no. 8, pp. 4446–4451, Feb. 2009, doi: 10.1016/j.apsusc.2008.11.048.
[28] C. Wang, J. Chen, and R. Li, “Studies on surface modification of poly(tetrafluoroethylene) film by remote and direct Ar plasma,” *Appl. Surf. Sci.*, vol. 254, no. 9, pp. 2882–2888, Feb. 2008, doi: 10.1016/j.apsusc.2007.10.029.
[29] S. Park, J. Kim, and C. H. Park, “Influence of micro and nano-scale roughness on hydrophobicity of a plasma-treated woven fabric,” *Text. Res. J.*, vol. 87, no. 2, pp. 193–207, Jan. 2017, doi: 10.1177/0040517515627169.
[30] K. Haji, Y. Zhu, M. Otsubo, and C. Honda, “Surface Modification of Silicone Rubber After Corona Exposure,” *Plasma Process. Polym.*, vol. 4, no. S1, pp. S1075–S1080, Apr. 2007, doi: 10.1002/ppap.200732408.

[31] J. F. Friedrich, R. Mix, R. Schulze, A. Meyer-Plath, R. Joshi, and S. Wettmarshausen, "New Plasma Techniques for Polymer Surface Modification with Monotype Functional Groups," *Plasma Process. Polym.*, vol. 5, no. 5, pp. 407–423, Jul. 2008, doi: 10.1002/ppap.200700145.

[32] I. Novák, V. Pollák, and I. Chodák, "Study of Surface Properties of Polyolefins Modified by Corona Discharge Plasma," *Plasma Process. Polym.*, vol. 3, no. 4–5, pp. 355–364, Jul. 2006, doi: 10.1002/ppap.200500163.

[33] R. Foerch, J. Izawa, and G. Spears, "A comparative study of the effects of remote nitrogen plasma, remote oxygen plasma, and corona discharge treatments on the surface properties of polyethylene," *J. Adhes. Sci. Technol.*, vol. 5, no. 7, pp. 549–564, Jan. 1991, doi: 10.1163/156856191X00747.

[34] M. Pascual, R. Sanchis, L. Sánchez, D. García, and R. Balart, "Surface Modification of Low Density Polyethylene (LDPE) Film Using Corona Discharge Plasma for Technological Applications," *J. Adhes. Sci. Technol.*, vol. 22, no. 13, pp. 1425–1442, Jan. 2008, doi: 10.1163/156856108X305723.

[35] A. Popelka, P. N. Khanam, and M. A. AlMaadeed, "Surface modification of polyethylene/graphene composite using corona discharge," *J. Phys. Appl. Phys.*, vol. 51, no. 10, p. 105302, Mar. 2018, doi: 10.1088/1361-6463/aaa9d6.

[36] O. V. Penkov, M. Khadem, W.-S. Lim, and D.-E. Kim, "A review of recent applications of atmospheric pressure plasma jets for materials processing," *J. Coat. Technol. Res.*, vol. 12, no. 2, pp. 225–235, Mar. 2015, doi: 10.1007/s11998-014-9638-z.

[37] M. Laroussi, "Low-Temperature Plasma Jet for Biomedical Applications: A Review," *IEEE Trans. Plasma Sci.*, vol. 43, no. 3, pp. 703–712, Mar. 2015, doi: 10.1109/TPS.2015.2403307.

[38] C. Cheng, Z. Liye, and R.-J. Zhan, "Surface modification of polymer fibre by the new atmospheric pressure cold plasma jet," *Surf. Coat. Technol.*, vol. 200, no. 24, pp. 6659–6665, Aug. 2006, doi: 10.1016/j.surfcoat.2005.09.033.

[39] J. Toshifuji, T. Katsumata, H. Takikawa, T. Sakakibara, and I. Shimizu, "Cold arc-plasma jet under atmospheric pressure for surface modification," *Surf. Coat. Technol.*, vol. 171, no. 1–3, pp. 302–306, Jul. 2003, doi: 10.1016/S0257-8972(03)00290-1.

[40] I. Onyshchenko, N. De Geyter, A. Y. Nikiforov, and R. Morent, "Atmospheric Pressure Plasma Penetration inside Flexible Polymeric Tubes: Atmospheric Pressure Plasma Penetration…," *Plasma Process. Polym.*, vol. 12, no. 3, pp. 271–284, Mar. 2015, doi: 10.1002/ppap.201400190.

[41] K. G. Kostov, M. Machida, V. Prysiazhnyi, and R. Y. Honda, "Transfer of a cold atmospheric pressure plasma jet through a long flexible plastic tube," *Plasma Sources Sci. Technol.*, vol. 24, no. 2, p. 025038, Apr. 2015, doi: 10.1088/0963-0252/24/2/025038.

[42] M. Kuchenbecker, N. Bibinov, A. Kaemlimg, D. Wandke, P. Awakowicz, and W. Viöl, "Characterization of DBD plasma source for biomedical applications," *J. Phys. Appl. Phys.*, vol. 42, no. 4, p. 045212, Feb. 2009, doi: 10.1088/0022-3727/42/4/045212.

[43] C. Z. Liu *et al.*, "Comparative study on the effect of RF and DBD plasma treatment on PTFE surface modification," *Mater. Chem. Phys.*, vol. 85, no. 2–3, pp. 340–346, Jun. 2004, doi: 10.1016/j.matchemphys.2004.01.026.

[44] C.-S. Ren, K. Wang, Q.-Y. Nie, D.-Z. Wang, and S.-H. Guo, "Surface modification of PE film by DBD plasma in air," *Appl. Surf. Sci.*, vol. 255, no. 5, pp. 3421–3425, Dec. 2008, doi: 10.1016/j.apsusc.2008.09.064.

[45] T. Shao *et al.*, "Surface modification of polyimide films using unipolar nanosecond-pulse DBD in atmospheric air," *Appl. Surf. Sci.*, vol. 256, no. 12, pp. 3888–3894, Apr. 2010, doi: 10.1016/j.apsusc.2010.01.045.
[46] Z. Fang, X. Xie, J. Li, H. Yang, Y. Qiu, and E. Kuffel, "Comparison of surface modification of polypropylene film by filamentary DBD at atmospheric pressure and homogeneous DBD at medium pressure in air," *J. Phys. Appl. Phys.*, vol. 42, no. 8, p. 085204, Apr. 2009, doi: 10.1088/0022-3727/42/8/085204.
[47] A. Mercado-Cabrera *et al.*, "Surface modification of polypropylene fiber for hydrophilicity enhancement aided by DBD plasma," *Prog. Org. Coat.*, vol. 76, no. 12, pp. 1858–1862, Dec. 2013, doi: 10.1016/j.porgcoat.2013.05.029.
[48] T. Jacobs, N. De Geyter, R. Morent, T. Desmet, P. Dubruel, and C. Leys, "Plasma treatment of polycaprolactone at medium pressure," *Surf. Coat. Technol.*, vol. 205, pp. S543–S547, Jul. 2011, doi: 10.1016/j.surfcoat.2011.02.012.
[49] F. Palumbo *et al.*, "Plasma-Deposited Nanocapsules Containing Coatings for Drug Delivery Applications," *ACS Appl. Mater. Interfaces*, vol. 10, no. 41, pp. 35516–35525, Oct. 2018, doi: 10.1021/acsami.8b11504.
[50] M. Bashir, J. M. Rees, and W. B. Zimmerman, "Plasma polymerization in a microcapillary using an atmospheric pressure dielectric barrier discharge," *Surf. Coat. Technol.*, vol. 234, pp. 82–91, Nov. 2013, doi: 10.1016/j.surfcoat.2013.01.041.
[51] P. Heyse *et al.*, "Dielectric Barrier Discharge at Atmospheric Pressure as a Tool to Deposit Versatile Organic Coatings at Moderate Power Input," *Plasma Process. Polym.*, vol. 4, no. 2, pp. 145–157, Feb. 2007, doi: 10.1002/ppap.200600087.
[52] P. Dimitrakellis and E. Gogolides, "Atmospheric plasma etching of polymers: A palette of applications in cleaning/ashing, pattern formation, nanotexturing and superhydrophobic surface fabrication," *Microelectron. Eng.*, vol. 194, pp. 109–115, Jul. 2018, doi: 10.1016/j.mee.2018.03.017.
[53] "Complete Guide to Surface Finish Symbols, Charts, RA, RZ, Measurements, and Callouts." [Online]. Available: https://www.cnccookbook.com/surface-finish-chart-symbols-measure-calculators/
[54] L. Phan, S. Yoon, and M.-W. Moon, "Plasma-Based Nanostructuring of Polymers: A Review," *Polymers*, vol. 9, no. 12, p. 417, Sep. 2017, doi: 10.3390/polym9090417.
[55] K. Tsougeni, N. Vourdas, A. Tserepi, E. Gogolides, and C. Cardinaud, "Mechanisms of Oxygen Plasma Nanotexturing of Organic Polymer Surfaces: From Stable Super Hydrophilic to Super Hydrophobic Surfaces," *Langmuir*, vol. 25, no. 19, pp. 11748–11759, Oct. 2009, doi: 10.1021/la901072z.
[56] T. Dufour *et al.*, "PTFE Surface Etching in the Post-discharge of a Scanning RF Plasma Torch: Evidence of Ejected Fluorinated Species: Evidence of Ejected Fluorinated Species," *Plasma Process. Polym.*, vol. 9, no. 8, pp. 820–829, Aug. 2012, doi: 10.1002/ppap.201100209.
[57] K. F. Ferris and S. M. Risser, "Effects of Surface Defects on the Local Electric Field in Inhomogeneous Media," *MRS Proc.*, vol. 291, p. 521, Jan. 1992, doi: 10.1557/PROC-291-521.
[58] F. Chen *et al.*, "Surface modification of tube inner wall by transferred atmospheric pressure plasma," *Appl. Surf. Sci.*, vol. 389, pp. 967–976, Dec. 2016, doi: 10.1016/j.apsusc.2016.08.024.

[59] K. Fatyeyeva *et al.*, “Effect of cold plasma treatment on surface properties and gas permeability of polyimide films,” *RSC Adv*, vol. 4, no. 59, pp. 31036–31046, 2014, doi: 10.1039/C4RA03741C.

[60] R. Di Mundo, F. Bottiglione, M. Notarnicola, F. Palumbo, and G. Pascazio, “Plasma-Textured Teflon: Repulsion in Air of Water Droplets and Drag Reduction Underwater,” *Biomimetics*, vol. 2, no. 4, p. 1, Jan. 2017, doi: 10.3390/biomimetics2010001.

[61] M. Resnik, R. Zaplotnik, M. Mozetic, and A. Vesel, “Comparison of SF6 and CF4 Plasma Treatment for Surface Hydrophobization of PET Polymer,” *Materials*, vol. 11, no. 2, p. 311, Feb. 2018, doi: 10.3390/ma11020311.

[62] R. Y. Korotkov, T. Goff, and P. Ricou, “Fluorination of polymethylmethacrylate with SF6 and hexafluoropropylene using dielectric barrier discharge system at atmospheric pressure,” *Surf. Coat. Technol.*, vol. 201, no. 16–17, pp. 7207–7215, May 2007, doi: 10.1016/j.surfcoat.2007.01.028.

[63] R. Di Mundo, F. Palumbo, and R. d’Agostino, “Nanotexturing of Polystyrene Surface in Fluorocarbon Plasmas: From Sticky to Slippery Superhydrophobicity,” *Langmuir*, vol. 24, no. 9, pp. 5044–5051, May 2008, doi: 10.1021/la800059a.

[64] K. G. Doherty *et al.*, “Plasma polymerization using helium atmospheric-pressure plasma jet with heptylamine monomer,” *Plasma Process. Polym.*, vol. 16, no. 4, p. e1800185, Apr. 2019, doi: 10.1002/ppap.201800185.

[65] C. Oehr, “Plasma surface modification of polymers for biomedical use,” *Nucl. Instrum. Methods Phys. Res. Sect. B Beam Interact. Mater. At.*, vol. 208, pp. 40–47, Aug. 2003, doi: 10.1016/S0168-583X(03)00650-5.

DISCLOSURES

This thesis work was supported in part by Eli Lilly and Company as part of a research partnership with Purdue University.

VITA

Professional Experience

Graduate Technical Intern

The Aerospace Corporation
iLabs, June 2020 – August 2020

- Led two teams on independent projects for the iLabs department, leading meetings, providing critical input, delegating tasks, and presenting designs and findings.
- Project 1:
  - Conducted in-depth literature review to understand the state of understanding of reentry debris on the stratosphere, identifying key areas where there is a gap in research.
  - Developed a more in depth understanding of nanoparticles and their effect on climate.
  - Generated interest in studies related to reentry with state-of-the-art climate models, focusing on debris inserting into the stratosphere from reentering satellites.
  - Investigated heating kinetics during reentry, and compared this information to reaction kinetics of aluminum, and its boiling point and reactivity in stratospheric pressure.
  - Proposed experimental procedures to enhance the understanding of reentry physics.
  - Submitted an abstract to preset at the Fall 2020 AGU conference, and compiled an extensive internal white paper reviewing the findings of the project.
- Project 2:
  - Proposed unique design concepts for a modular cubesat form factor for rapid assembly and launch of payloads.
  - Performed individual CAD modelling work to visualize modularity concepts.
  - Worked as the systems integrator, working with individual interns to adjust designs and integrate them into the larger system.

Microelectronics Technology Department, May 2019 – August 2019

- Characterized the properties and performance parameters of carbon nanotube (CNT) memristor for applications in neuromorphic computing
- Developed sophisticated systems and techniques for performing pulse programming for precise control of switching mechanisms, on the order of picosecond and nanosecond time scale
- Developed current amplifier and feedback system for reactively detecting changes in CNT memristor state for quick and accurate controls, as well as high resolution detection of current state, as low as 100 nanoamps.

Graduate Research Assistant

Purdue University | Department of Aerospace and Astronautical Engineering | January 2019 - Present

- Investigated the use of DC/AC dielectric barrier discharge (DBD) plasmas to induce surface morphology changes on inner surfaces of medical tubing to promote adhesion of drug compounds and generally enhance wettability of surfaces.
- Study and development of roll-to-roll plasma chemical vapor deposition (CVD) for synthesis of 2D materials and surface functionalization.
- Work with nanosecond repetitive pulse discharges in atmospheric pressure for flow control (10-100 ns, up to 40 kV and 50 A).

- Worked as Entrepreneurial Lead on NSF Innovation Corps team, performing customer discovery for plasma-based technology developed in the lab.

Graduate Teaching Assistant *Purdue University | Department of Aerospace and Astronautical Engineering | August 2018 – May 2019*

- Supervised and instructed sessions for fluid mechanics and aerodynamics laboratory.
- Aided and advised students regarding laboratory procedure and physical theory behind experiments.
- Graded lab reports and provided feedback for students to improve their laboratory report writing skills.

Undergraduate Research Assistant

Virginia Tech | Department of Aerospace and Ocean Engineering, CREATe | June 2017 – August 2018

- Led a three-person team to design and implement the construction of a new wind tunnel based off old designs. Not only replicated, but drastically improved upon the tunnel both in terms of functionality and aesthetics using skills developed both in class and on the job.
- Due to the quality of the first tunnel, was hired to design and construct from scratch a brand-new anechoic open jet wind tunnel (30 x 30 inch test section cross-section) in the same laboratory facility.
- Due to the small team environment, developed experience in every stage of development of a substantial engineering project, including research, design, material acquisition, communication with technicians, hands-on construction, optimization, and calibration.

Quality Engineering Intern

Continental Automotive | March 2016 – July 2019

- Performed teardowns on fuel injector/fuel pump components returned from the line or customer and returned complete failure root cause analysis reports for warranty returns.
- Worked extensively on a SEM/EDS (Scanning Electron Microscope with X-Ray Microanalysis) for particle analysis in failures from the production line and field.
- Worked with a team of engineers to complete various quality projects in manufacturing, including developing metal pickling methods and press force failure analysis to resolve high pressure pump leak issues.
- Successfully completed several coding projects using Visual Basic and Excel that have had lasting impacts on the functionality and methodology of SEM/EDS analysis and the general operation of the Materials Lab.

Master Tutor

Thomas Nelson Community College | January 2014 – May 2015

- Provided one-on-one assistance to students in STEM related classes.
- Successfully aided students in coursework ranging from remedial math to advanced science and arithmetic.

Educational Qualification

Purdue University

Beginning PhD in Aerospace Engineering, Currently Enrolled, Beginning Fall 2021
3.4/4.0 GPA

Purdue University

Completing MS in Aerospace Engineering, Currently Enrolled, Summer 2021
3.4/4.0 GPA

Virginia Tech

Bachelor of Science in Aerospace Engineering, May 2018
3.6/4.0 GPA
Dean's List with Distinction, Spring 2017, Fall 2017, Spring 2018; Significant Aerospace-related project experience; Member of Sigma Gamma Tau, National Aerospace Honor Society

Thomas Nelson Community College

Associate of Science in Mechanical Engineering, May 2015
Academic Merit List

Additional Skills/Awards/Achievements

Proficient skills
Microsoft Office, Soldering, Python, SolidWorks, Visual Basic, Mathematica, MATLAB, SEM/EDX microscopy, FIB microscopy

Entry skills
AutoCAD, C++, Microelectronics analysis, RF/Microwave Experimentation, Circuit Design, Plasma analysis

Dean's List with Distinction | Eagle Scout | National Youth Leadership Training

Publications

Austin W. Kleinfelter, Russell Repasky, Nandita Hari, Stefan Letica, Vidya Vishwanathan, Lee Organski, Jon Schwaner, William N. Alexander, and William J. Devenport. "Development and Calibration of a new Anechoic Wall Jet Wind Tunnel", AIAA Scitech 2019 Forum, AIAA SciTech Forum, (AIAA 2019-1936) https://doi.org/10.2514/6.2019-1936